

OPTIMUM TOPOLOGICAL DESIGN OF GEOMETRICALLY
NONLINEAR SINGLE LAYER LAMELLA DOMES USING
HARMONY SEARCH METHOD

A THESIS SUBMITTED TO
THE GRADUATE SCHOOL OF NATURAL AND APPLIED SCIENCES
OF
MIDDLE EAST TECHNICAL UNIVERSITY

BY

SERDAR ÇARBAŞ

IN PARTIAL FULFILLMENT OF THE REQUIREMENTS
FOR
THE DEGREE OF MASTER OF SCIENCE
IN
ENGINEERING SCIENCES

JULY 2008

Approval of the thesis:

**OPTIMUM TOPOLOGICAL DESIGN OF GEOMETRICALLY
NONLINEAR SINGLE LAYER LAMELLA DOMES USING
HARMONY SEARCH METHOD**

Submitted by **SERDAR ÇARBAŞ** in partial fulfillment of the requirements for the degree of **Master of Science in Engineering Sciences Department, Middle East Technical University** by,

Prof. Dr. Canan Özgen
Dean, Graduate School of **Natural and Applied Sciences**

Prof. Dr. Turgut Tokdemir
Head of Department, **Engineering Sciences**

Prof. Dr. Mehmet Polat Saka
Supervisor, **Engineering Sciences Dept., METU**

Examining Committee Members:

Prof. Dr. Mehmet Polat Saka
Engineering Sciences Dept., METU

Prof. Dr. Gülin Ayşe Birlik
Engineering Sciences Dept., METU

Assoc. Prof. Dr. Murat Dicleli
Engineering Sciences Dept., METU

Assist. Prof. Dr. Oğuzhan Hasańeıbi
Civil Engineering Dept., METU

Assist. Prof. Dr. M. Tolga Yılmaz
Engineering Sciences Dept., METU

Date: July 03, 2008

I hereby declare that all information in this document has been obtained and presented in accordance with academic rules and ethical conduct. I also declare that, as required by these rules and conduct, I have fully cited and referenced all material and results that are not original to this work.

Name, Last name : Serdar arbaş

Signature :

ABSTRACT

OPTIMUM TOPOLOGICAL DESIGN OF GEOMETRICALLY NONLINEAR SINGLE LAYER LAMELLA DOMES USING HARMONY SEARCH METHOD

Çarbaş, Serdar

M.S., Department of Engineering Sciences

Supervisor: Prof. Dr. Mehmet Polat Saka

July 2008, 118 pages

Harmony search method based optimum topology design algorithm is presented for single layer lamella domes. The harmony search method is a numerical optimization technique developed recently that imitates the musical performance process which takes place when a musician searches for a better state of harmony. Jazz improvisation seeks to find musically pleasing harmony similar to the optimum design process which seeks to find the optimum solution. The optimum design algorithm developed imposes the behavioral and performance constraints in accordance with LRFD-AISC. The optimum number of rings, the height of the crown and the tubular cross-sectional designations for dome members are treated as design variables. The member grouping is allowed so that the same section can be adopted for each group. The design algorithm developed has a routine that build the data for the geometry of the dome automatically that covers the numbering of joints, and member incidences, and the computation of the coordinates of joints. Due to the slenderness and the presence of imperfections in dome structures it is necessary to consider the geometric nonlinearity in the prediction of their response under the external loading. Design examples are considered to demonstrate the efficiency of the algorithm presented.

Keywords: Optimum Structural Design, Harmony Search Algorithm, Minimum Weight, Stochastic Search Technique, Lamella Domes.

ÖZ

HARMONİ ARAMA YÖNTEMİ KULLANILARAK GEOMETRİK YÖNDEN DOĞRUSAL OLMAYAN TEK KATMANLI YAPRAKSI KUBBELERİN OPTİMUM TOPOLOJİ BOYUTLANDIRMASI

Çarbaş, Serdar

Yüksek Lisans, Mühendislik Bilimleri Bölümü

Tez Yöneticisi: Prof. Dr. Mehmet Polat Saka

Temmuz 2008, 118 sayfa

Tek katmanlı yapraksı kubbeler için harmoni arama yöntemine dayalı optimum topoloji tasarım algoritması sunulmaktadır. Bir müzisyenin daha iyi bir müzikal sunum arayışı içinde uygulamaya çalıştığı müzikal performans sürecine benzetilen harmoni arama yöntemi yakın geçmişte geliştirilen bir sayısal optimizasyon tekniğidir. Caz doğaçlaması, optimum çözüme ulaşmaya çalışan optimum tasarım sürecine benzer şekilde, müzikal açıdan tatmin edici uyumu bulmaya çabalar. Geliştirilen optimum tasarım algoritması, LRFD-AISC (Load and Resistance Factor Design-American Institute of Steel Construction)'ye uygun olan davranış ve performans sınırlayıcılarını uygular. Optimum halka sayısı, tepe yüksekliği ve boru şeklindeki kesitler kubbe için tasarım değişkenleridir. Her grupta aynı kesitlerin seçilebilmesi için eleman gruplandırmasına izin verilmiştir. Geliştirilen tasarım algoritması, bağlantı noktalarının ve eleman numaralandırılmalarının ve bağlantı noktalarının koordinat hesaplarının otomatik olarak yapılmasını kapsayan, kubbenin geometrik verilerini oluşturan bir yordama sahiptir. Kubbe yapılarında,

narinlikten ve kusurların var olmasından dolayı bu yapıların dış yükler altında vereceği tepkiyi tahmin ederken geometrik doğrusalsızlığı göz önüne almak gerekmektedir. Dikkate alınan tasarım örnekleri sunulan algoritmanın etkinliğini göstermeyi amaçlamaktadır.

Anahtar Kelimeler: Optimum Yapısal Tasarım, Harmoni Arama Yöntemi, Minimum Ağırlık, Stokastik Arama Tekniđi, Yapırsı Kubbeler.

To My Family,
For your endless support and love

ACKNOWLEDGEMENTS

I wish to offer my sincere thanks and appreciation to my supervisor Prof. Dr. Mehmet Polat Saka for his precious help, invaluable suggestions, continuous support, guidance, criticisms, encouragements and patience throughout this study.

Secondly, I would like to thank Prof. Dr. M. Ruşen Geçit for his helpful advices and avuncular humanity to me during my work life at Department of Engineering Sciences.

My special thanks are due to Prof. Dr. Temel Yetimođlu from Atatürk University Engineering Faculty Civil Engineering Department for his great encouragement in performing this research.

I should remark that without the sincere friendship of my roommate Semih Erhan, this work would not have been realized. I strongly thank him for his amity. And many thanks to Ferhat Erdal, Erkan Dođan, Alper Akın, and İbrahim Aydođdu for their excellent understanding and no end of aid at every stage of my thesis study.

I would also like to thank to my friends, especially Hakan Bayrak, Refik Burak Taymuş, Fuat Korkut, Hüseyin Çelik and Kaveh Hassanzehtap for their friendship and encouragement during this study.

I owe thanks to most special person in my life Buket Bezgin and her housemate Yasemin Çetin for their boundless moral support giving me joy of living.

Last but not least, I can hardly find words to express my feelings about my parents Süreyya and Hayriye Çarbaş, and my unique elder sister Ayşegül for their lifetime support to compensate all the disadvantages in my life. I will always be indebted to their compassion and humanism no matter how hard I try to give back what they have given to me. They have priceless meaning for me. I feel very lucky to have such a family.

TABLE OF CONTENTS

ABSTRACT	iv
ÖZ.....	vi
ACKNOWLEDGEMENTS.....	ix
TABLE OF CONTENTS.....	xi
LIST OF FIGURES.....	xiv
LIST OF TABLES	xvi
1.INTRODUCTION.....	1
1.1 Domes.....	1
1.1.1 Types of Braced Domes	4
1.2 Optimization in Engineering	6
1.3 Structural Optimization	8
1.3.1 Mathematical Modeling of Structural Optimization Problems	9
1.3.2 Methods of Structural Optimization	10
1.3.2.1 Analytical Methods.....	11
1.3.2.2 Numerical Methods	11
1.4 Stochastic Optimization Techniques	13
1.4.1 Genetic Algorithms	14
1.4.2 Evolutionary Strategies	15
1.4.3 Simulated Annealing.....	15
1.4.4 Particle Swarm Optimization.....	16
1.4.5 Ant Colony Optimization	17
1.4.6 Tabu Search	18
1.4.7 Harmony Search Optimization	19

1.5 Literature Survey on the Optimum Design of Dome Structures.....	20
1.6 The Scope of This Study.....	26
2.ELASTIC-CRITICAL LOAD ANALYSIS OF SPATIAL STRUCTURES	28
2.1 Definition of Elastic Critical Load Analysis.....	28
2.2 Calculation of Elastic Critical Load Factor	29
2.3 Stiffness Matrix of a Space Member	30
2.4 Derivation of a Nonlinear Stiffness Matrix Using Stability Functions	33
2.4.1 Stability Functions	34
2.4.1.1 Effect of Flexure on Axial Stiffness	35
2.4.1.2 Effect of Axial Force on Flexural Stiffness	41
2.4.1.2.1 Bending in <i>X-Y</i> Plane	41
2.4.1.2.2 Bending in <i>X-Z</i> Plane	42
2.4.1.3 Effect of Axial Force on Stiffness Against Translation.....	43
2.4.1.3.1 Translation in <i>X-Y</i> Plane.....	43
2.4.1.3.2 Translation in <i>X-Z</i> Plane.....	46
2.5 Geometric Nonlinearity	49
2.5.1 Construction of Overall Stiffness Matrix	49
2.6 Elastic Critical Load Analysis.....	59
3.OPTIMUM DESIGN OF LAMELLA DOMES	63
3.1 Morphology of Lamella Domes	63
3.2 Optimum Topology Design of Lamella Domes.....	68
3.3 Mathematical Model of Optimum Design Problem of Lamella Domes According to LRFD-AISC.....	71

4.HARMONY SEARCH METHOD BASED OPTIMUM DESIGN ALGORITHM.....	75
4.1 General Concept of Harmony Search Algorithm.....	75
4.2 A Harmony Search Algorithm Based Optimum Design Method For Single Layer Lamella Domes	81
5.DESIGN EXAMPLES	88
5.1 CASE 1 (P)	90
5.2 CASE 2 (D + P).....	96
5.3 CASE 3 (D + P + W).....	100
5.3.1 Load Combinations	105
5.3.1.1 D + P + W (internal pressure coefficient is taken as positive)..	105
5.3.1.2 D + P + W (internal pressure coefficient is taken as negative).	108
6.CONCLUSIONS.....	112
REFERENCES	114

LIST OF FIGURES

Figure 1.1 Astrodome, Sport Hall, Houston – USA	2
Figure 1.2 Nagoya dome, Sport Hall, Nagoya - Japan.....	2
Figure 1.3 Georgia World Congress Center, Atlanta - Usa.....	3
Figure 1.4 Gasometer Container, Vienna – Austria.....	3
Figure 1.5 The Spruce Goose Storage Hall in Long Beach, California - USA ..	3
Figure 1.6 Terzibaba Mosque, Erzincan - Turkey	4
Figure 1.7 Panora Shopping Hall, Ankara - Turkey	4
Figure 1.8 Dome Types	5
Figure 1.9 Harmony search optimization procedure.....	20
Figure 2.1 A Typical Space Member with Displacements and Rotations.....	30
Figure 2.2 A Typical Space Member with Forces and Moments.	31
Figure 2.3 Stiffness matrix of a space member in local coordinate system.	32
Figure 2.4 Effect of Flexure on Axial Stiffness:	35
(a) Bending in X-Y plane	35
(b) Bending in X-Z plane	35
Figure 2.5 Effect of Axial Force on Stiffness Against Translation	43
Figure 2.6 Nonlinear stiffness matrix for three-dimensional beam-column element in local coordinate system.	48
Figure 2.7 Rotation α about y-axis.....	51
Figure 2.8 Rotation β about z-axis	52
Figure 2.9 Final rotation γ of the member about yz plane.....	53
Figure 2.10 Nonlinear response of a structure obtained through successive elastic linear analysis.	56
Figure 2.11 A single layer lamella dome with 3 rings subjected to different concentrated loads on its crown.	57
Figure 2.12 Linear and nonlinear Y-displacements of joint 1 of the lamella dome.	58

Figure 2.13 Flowchart for the determination of nonlinear elastic critical load	60
.....	60
Figure 3.1 Lamella Dome.	64
Figure 3.2 Automated computation of joint coordinates in a lamella dome. ...	65
Figure 3.3 (a) Lamella Dome with Two Different Member Groups.	69
Figure 3.3 (b) Lamella Dome with Eight Different Member Groups.	71
Figure 4.1 Improvisation of a new harmony memory vector.	80
Figure 4.2 Flowchart of Harmony Search method based optimum design of algorithm.	87
Figure 5.1 3D view of optimum single layer lamella dome.	91
Figure 5.2 Side view of optimum single layer lamella dome.	91
Figure 5.3 3D view of optimum single layer lamella dome with 4 rings.	93
Figure 5.4 Side view of optimum single layer lamella dome with 4 rings.	93
Figure 5.5 3D view of optimum single layer lamella dome with 5 rings.	94
Figure 5.6 Side view of optimum single layer lamella dome with 5 rings.	94
Figure 5.7 Load Case 2 (Dead Load + Equipment Load).	96
Figure 5.8 3D view of optimum single layer lamella dome for Case 2.	99
Figure 5.9 Side view of optimum single layer lamella dome for Case 2.	99
Figure 5.10 Pieces of single layer lamella dome with 3 rings.	104
Figure 5.11 Load Case 3.1.1 (Dead Load + Equipment Load + Wind Load (internal pressure coefficient is taken as positive)).	105
Figure 5.12 Load Case 3.1.2 (Dead Load + Equipment Load + Wind Load (internal pressure coefficient is taken as negative)).	108
Figure 5.13 (a) and (b) Load Case 1 (P).	111
Figure 5.14 Load Case 2 (D+P)	111
Figure 5.15	111
(a) Load Case 3 (D+P+W (internal pressure coefficient is taken as positive))	111
.....	111
(b) Load Case 3 (D+P+W (internal pressure coefficient is taken as negative))	111
.....	111

LIST OF TABLES

Table 1 Y-displacement values of the joint 1 of the dome under different external loads.	57
Table 2 Determinant values of the stiffness matrix of the dome.	62
Table 4.1 Discrete Set of Height Values.	82
Table 4.2 Dimensions and Properties of Steel Pipe Sections.	83
Table 4.3 A harmony set of a designed dome.....	86
Table 4.4 New harmony set of a designed dome.	86
Table 5.1 Displacement restrictions of the single layer lamella dome.....	88
Table 5.2 The effect of Harmony Search algorithm parameters.....	89
Table 5.3 Optimum design for the single layer lamella dome for load case 1.	90
Table 5.4 Elastic Critical Load Factor Iterations for optimum designed dome for Case 1.....	92
Table 5.5 Optimum design of single layer lamella dome with 3 rings according to different support conditions.	95
Table 5.6 Loads Acting on Joints for Case 2 (D + P).	97
Table 5.7 Optimum design of single layer lamella dome with 3 rings for load Case 2.	97
Table 5.8 Elastic Critical Load Factor Iterations for optimum design of Case 2	98
Table 5.9 Schematic display of the pieces of the dome with 3 rings.	105
Table 5.10 Optimum design obtained for dome with 3 rings for the case D + P + W (internal pressure coefficient is taken as positive).	107
Table 5.11 Elastic Critical Load Factor Iterations for optimum design of loading case D+P+W (internal pressure coefficient is taken as positive). ...	107
Table 5.12 Optimum design for dome with 3 rings for D + P + W (internal pressure coefficient is taken as negative)	109
Table 5.13 Elastic Critical Load Factor Iterations for optimum design of loading case D+P+W (internal pressure coefficient is taken as positive)	110

CHAPTER 1

INTRODUCTION

1.1 Domes

Engineering is the activity through which designs for material objects are produced. The engineering design communicates to the agency of manufacture of construction not only the creative product of the designer, but the results of all scientific deductions and judgmental decisions which were rendered in developing design. The majority of engineering tasks have as their ultimate goal the production of an engineering design or the provision of a means or aid to designing.

Engineers and designers have been trying to find some new ways to cover large spans, such as exhibition halls, stadiums, concert halls, shopping centers and swimming pools, economically and to produce elegant structures from past to now. Domes supply unimpeded wide spaces and they encompass a maximum amount of areas with a minimum surface. They are also exceptionally suitable structures for covering places where minimum interference from internal supports are required. These specifications of domes make them very economical structures when they are compared with the classical structure types in terms of consumption of constructional materials.

Domes are structural systems which include one or more layers of elements that are arched in all directions. The surface of a dome may be a part of a single surface such as a sphere or paraboloid, or it may consist of a patchwork of different surfaces. Besides, domes are either formed by using curved members

forming a surface of revolution or by straight members meeting at joints which lie on the surface. The spherical structure of a dome does not only provide elegant appearance but also offers one of the most efficient interior atmospheres for human residence because air and energy are allowed to circulate without obstruction.

Braced steel dome structures have been widely used all over the world during the last three decades in many engineering applications. Some examples of braced domes in the world are shown in Figures 1.1 through 1.7.

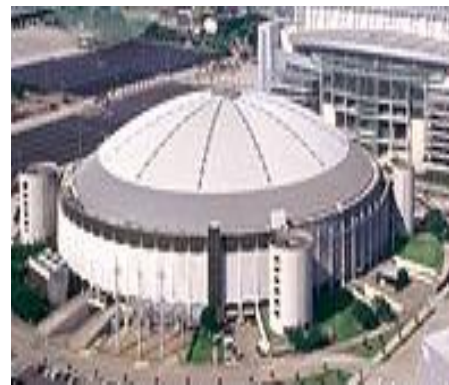


Figure 1.1 Astrodome, Sport Hall, Houston – USA



Figure 1.2 Nagoya dome, Sport Hall, Nagoya - Japan



Figure 1.3 Georgia World Congress Center, Atlanta - USA

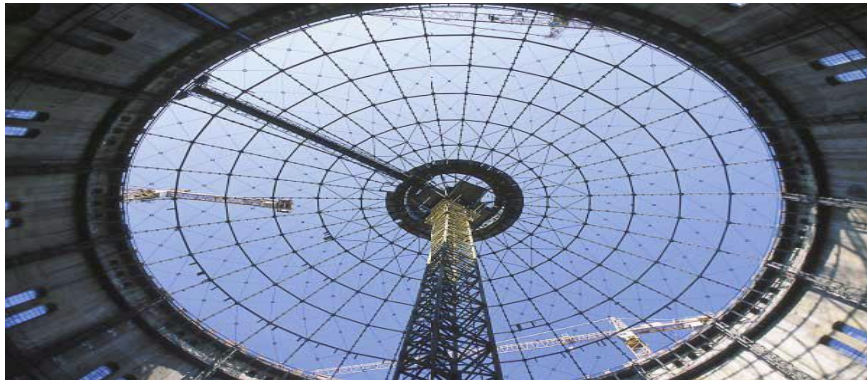


Figure 1.4 Gasometer Container, Vienna – Austria

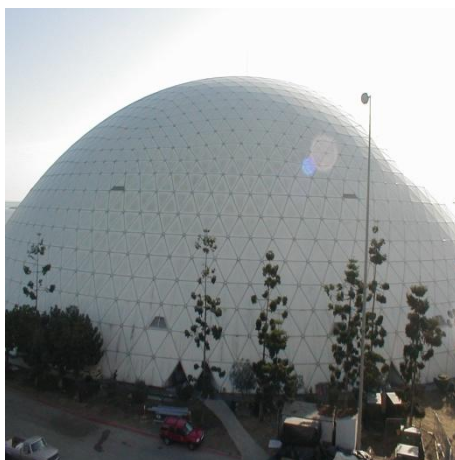


Figure 1.5 The Spruce Goose Storage Hall in Long Beach, California - USA



Figure 1.6 Terzibaba Mosque, Erzincan - Turkey



Figure 1.7 Panora Shopping Hall, Ankara - Turkey

1.1.1 Types of Braced Domes

There are many types of braced domes, some of which are used very often, while others have limited applications. The eight types of domes maybe listed below as [1]:

1. The Scwedler Dome
2. The Ribbed Dome
3. The Lamella Dome
4. The Grid Dome
5. The Geodesic Dome
6. The Stiff-jointed Framed Dome
7. The Plate Type Dome
8. The Zimmermann Dome

Mostly used dome types are demonstrated in Figure 1.8

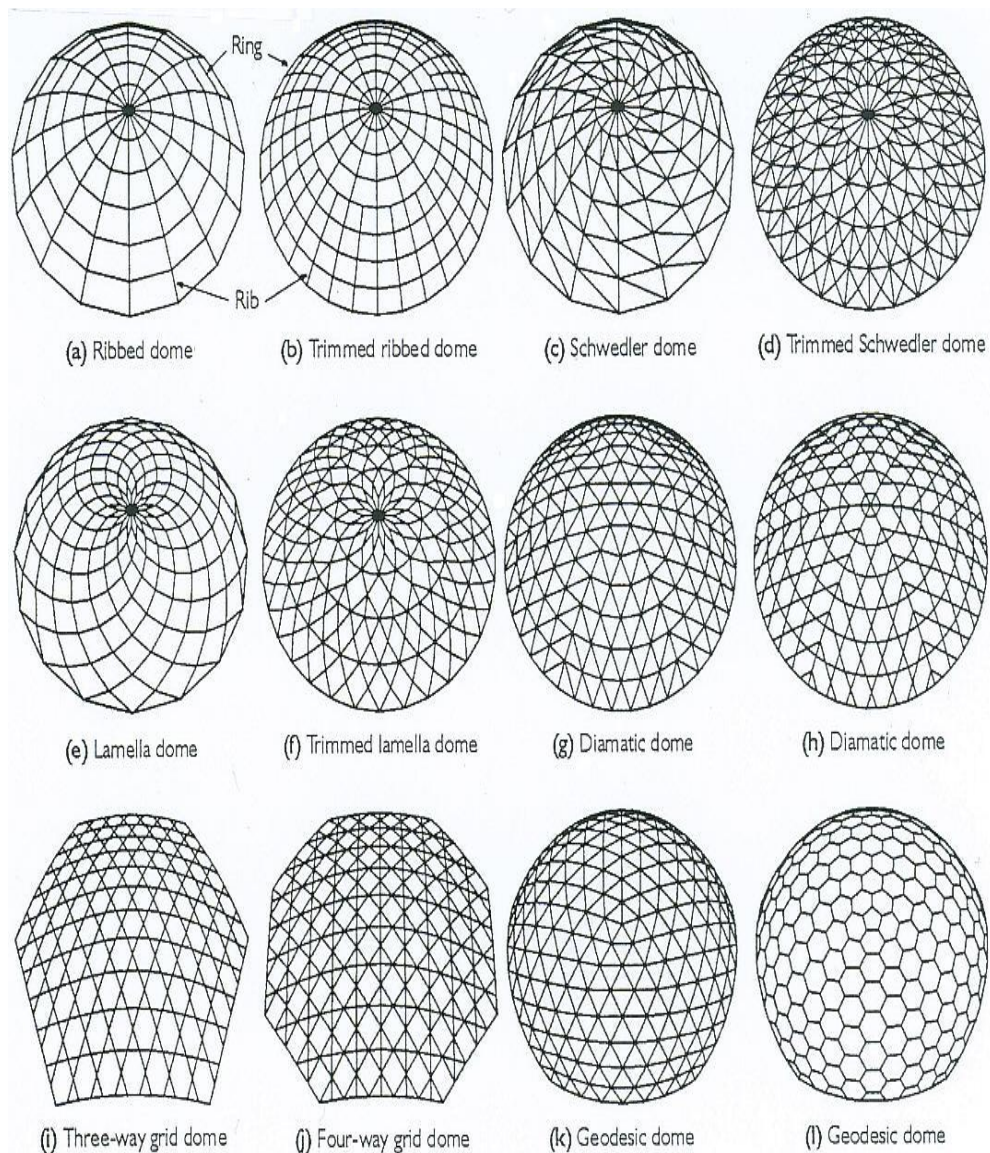


Figure 1.8 Dome Types

Whilst the early domes were all masonry ones, modern domes construction have kept abreast with the times, being entirely in concrete, steel and aluminum. Steel is generally used for construction of braced domes. However, occasionally aluminum and glass fibers can also be used. Among the latter materials, aluminum is the most ideal to make up braced domes due to its light weight and ease of fabrication.

Braced domes can be classified into two main groups about their construction places as single layer systems and double layer systems. Single layer systems are appropriate for smaller spans of about 40 m while double layer systems can cover more than 200 m span lengths. These systems can be designed as rigidly-jointed systems or pin-connected systems. Semi-rigid connected systems are also used owing to impracticality of perfect pin connection.

1.2 Optimization in Engineering

A goal of every designer is to design the best (optimum) systems. The increasing demand on engineers to lower production costs to withstand competition has prompted engineers to look for rigorous methods of decision making, such as optimization methods, to design and produce products both economically and efficiently.

Optimization is the act of obtaining the best result under given circumstances. In design, construction, and maintenance of any engineering system, engineers have to take many technological and managerial decisions at several stages. The ultimate goal of all such decisions is either to minimize the effort required or to maximize the desired benefit. Since the effort required or the benefit desired in any practical situation can be expressed as a function of certain decision variables, optimization can be defined as the process of finding the conditions that give the maximum or minimum value of a function.

Common problems faced in the optimization field are static and dynamic response, shape optimization of structural systems, reliability-based design and optimum control of systems. Any optimization problem requires proper identification of objective function, design variables and constraints at problem formulation state. Depending on the class of problems and needs, several types of design variables and objective functions can be identified. Constraints

usually involve physical limitations, material failure, buckling load and other response quantities.

An optimization or a mathematical programming problem can be stated as follows [2];

$$\text{Find } \mathbf{X} = \begin{Bmatrix} X_1 \\ X_2 \\ \vdots \\ X_n \end{Bmatrix} \text{ which minimizes } f(\mathbf{X}) \quad (1.1)$$

subject to the constraints:

$$g_j(\mathbf{X}) \leq 0, j = 1, 2, \dots, m \quad (1.2)$$

$$l_j(\mathbf{X}) = 0, j = 1, 2, \dots, p \quad (1.3)$$

where \mathbf{X} is an n -dimensional vector called the design vector, $f(\mathbf{X})$ is termed the objective function, and $g_j(\mathbf{X})$ and $l_j(\mathbf{X})$ are known as inequality and equality constraints, respectively. The number of variables n and the number of constraints m and/or p need not be related in any way. This kind of problem is called constrained optimization problem. Some optimization problems do not involve any constraints and can be stated as;

$$\text{Find } \mathbf{X} = \begin{Bmatrix} X_1 \\ X_2 \\ \vdots \\ X_n \end{Bmatrix} \text{ which minimizes } f(\mathbf{X}) \quad (1.4)$$

such problems are called unconstrained optimization problems.

Optimization techniques, having reached a degree of maturity over the past several years, are being used in a wide spectrum of industries, including aerospace, automotive, chemical, electrical, and manufacturing industries. With rapidly advancing computer technology, computers are becoming more powerful, and correspondingly, the size and the complexity of the problems being solved using optimization techniques are also increasing. Optimization methods, coupled with modern tools of computer-aided design, are also being used to enhance the creative process of conceptual and detailed design of engineering systems.

1.3 Structural Optimization

The demand for economical and reliable structures in virtually all fields of endeavor has provided the impetus for the development of rapid, convergent and effective structural algorithms. Structural optimization (or optimal design) deals with the problem of designing a mechanical structure in an efficient way with respect to some criterion, such as minimum weight which is related to cost, maximum stiffness, minimum displacement at specific structural points and minimum structural strain energy, subject to design restrictions.

Structural optimization when first emerged has attracted a widespread attention among designers. It has provided a systematic solution to age-old structural design problems which were handled by using trial-error methods or engineering intuition or both. Application of mathematical programming methods to structural design problems has paved the way in obtaining a design procedure which was capable of producing structures with cross-sectional dimensions. The development of computer programs enabled the engineers to simulate and experiment many different designs without actually building them. In that way it is easier today for design engineers to create an optimum design which performs the intended task within the design limits.

The logic in the optimization process is to build the model parametrically so that the sizes of the model can be changed through iterations and to find the most efficient design by changing those variables. First of all, the design should be able to do the task required. For example in case of a beam, the beam should carry the required load, which it is designed for. An optimum design should satisfy all the design criteria determined. Those criteria are defined by constraints in the optimization problem. The maximum normal stress in a beam may be a constraint for an optimization problem and can be limited to a certain value like yield stress. In structural optimization, usually the objective is to minimize the weight of the structure. Thus, an optimum design is usually the one with least amount of material. Also, to minimize the production cost can be the objective of the optimization in some cases.

1.3.1 Mathematical Modeling of Structural Optimization Problems

A general mathematical model for the optimum design problem of a pin-jointed structure has the following form [3];

Find cross-sectional area vectors that are selected as design variables,

$$\mathbf{A}^T = [A_1, A_2, \dots, A_{N_m}] \in S \quad (1.5)$$

to minimize;

$$W(\mathbf{A}) = \sum_{i=1}^{N_m} \rho_i \cdot A_i \cdot L_i \quad (1.6)$$

subject to;

$$g_i(\mathbf{A}) = |\sigma_i| - |\sigma_i^a| \leq 0 \quad i = 1, \dots, N_m \quad (1.7)$$

$$h_i(\mathbf{A}) = |H_i| - |H_i^a| \leq 0 \quad i = 1, \dots, N_m \quad (1.8)$$

$$u_{j,k}(\mathbf{A}) = |u_{j,k}| - |u_{j,k}^a| \leq 0 \quad j = 1, \dots, N_m \quad (1.9)$$

where;

\mathbf{A} : a vector of cross-sectional areas,

S : available list,

$W(\mathbf{A})$: objective function (weight of the structure),

ρ_i : unit weight of i-th member,

L_i : length of i-th member,

A_i : cross-sectional area of i-th member,

N_m : total number of structural members,

$g_i(\mathbf{A})$: stress constraint of i-th member,

$h_i(\mathbf{A})$: stability constraint of i-th member,

$u_{j,k}(\mathbf{A})$: displacement constraint at the j-th node in the k-th direction,

σ_i : stress in the i-th member,

σ_i^a : allowable stress in the i-th member,

H_i : slenderness ratio in i-th member,

H_i^a : allowable slenderness ratio in the i-th member,

$u_{j,k}$: displacement at the j-th node in the k-th direction,

$u_{j,k}^a$: allowable displacement at the j-th node in the k-th direction.

1.3.2 Methods of Structural Optimization

There is no single method available for solving all structural optimization problems efficiently. A number of optimization methods have been developed for solving different types of structural optimization problems. Methods of optimization have been studied and developed over the last 35 years. These methods have matured to the point where they are beginning to be utilized in the design of realistic engineering systems. Although the methods are currently being used primarily by large systems, they will undoubtedly be developed further so that even small design systems will have access to this new

technology. Optimization methods offer a designer the flexibility of studying many alternatives in a relatively short time, thus producing better and cost effective designs more efficiently. The purpose of this section is to describe the structural optimization methods briefly.

1.3.2.1 Analytical Methods

Analytical methods usually employ the mathematical theory of calculus and variational methods, in studies of optimal layouts or geometrical forms of structural elements, such as columns, beams and plates. These analytical methods are most convenient for fundamental studies of single structural components, and they are not intended to handle larger structural systems. The structural design is represented by a number of unknown functions and the goal is to find the form of these functions. The optimal design is theoretically found exactly through the solution of a system of equations expressing the conditions for optimality.

Applications based on analytical methods though they sometimes omit the practical aspects of realistic structures, are still of certain value. Analytical solutions provide valuable insight and theoretical lower bound optimum against which more practical designs may be judged. Problems solved by analytical methods are called continuous problems or distributed parameter optimization problems.

1.3.2.2 Numerical Methods

Closed form analytical solutions for practical optimization problems are difficult to obtain if the number of design variables is more than two and the constraint expressions are complex. Therefore numerical methods and computers must be used to solve most of the optimization problems. In these methods, an initial design for the system is selected which is iteratively

improved until no further improvements are possible without violating any of the constraints [4].

One of the advantages of using numerical optimization methods and associated programs is that once the problem has been properly formulated and defined for the program, it is quite easy to solve it for a variety of conditions and requirements. In most practical applications, the design variables cannot have arbitrary values due to manufacturing and fabrication limitations. For example, the plate thickness and width must be selected from the available ones, the number of bolts used must be an integer, the number of rebars must be an integer and their size must be selected from those available, and so on. Design problems with such variables are called discrete variable optimization problems in contrast to the continuous variable problems where design variables can have any value within the specified limits. To solve discrete variable problems, the optimization software must have the capability to obtain a final design for which values of the variables have been selected from a specified set [4].

Mathematical programming techniques are useful in finding the minimum of a function of several variables under prescribed set of constraints. The various techniques available for the solution of different types of optimization problems are given under the heading of mathematical programming techniques, such as calculus methods, calculus of variations, linear programming, nonlinear programming, geometric programming, quadratic programming, dynamic programming, integer programming, stochastic programming, separable programming, and multiobjective programming [5].

The desire to optimize more than one objective or goal while satisfying the physical limitations led to the development of multiobjective programming methods. Goal programming is a well-known technique for solving specific types of multiobjective optimization problems. Game theory technique applied

to solve several mathematical economics and military problems when it was firstly developed, but during the last decade game theory has been applied to solve engineering design problems. Simulated annealing, genetic algorithms, evolution strategies, tabu search, harmony search, ant colony and particle swarm represent a new class of mathematical programming techniques that have come into prominence during last decade.

Another numerical optimization method is Optimality Criteria based on the derivation of an appropriate criterion for specialized design conditions and developing an iterative procedure to find the optimum design [6]. Its principal attraction was that the method was easily programmed for the computer, was relatively independent of problem size, and usually provided a near-optimum design with a few structural analyses. This last feature represented a remarkable improvement over the number of analyses required in mathematical programming methods to reach an optimum solution. The optimality criteria methods were originally developed for discrete systems. The methods were first presented for linear elastic structures with stress and displacement constraints and later extended to problems with other types of constraints.

1.4 Stochastic Optimization Techniques

In most of the various engineering practices, including structural optimization, Mathematical Programming and Optimality Criteria Methods, known as classical optimization methods, have been used up to recent years. However, differential mathematical solution algorithms, which depend on the acceptance of continuous design variables of these methods, bring about some difficulties for the application of methods to large structural systems and do not produce ideal solutions for engineering structures requiring a design process according to previously identified discrete profile lists. Stochastic search is a class of search methods which includes heuristics and an element of nondeterminism in traversing the search space. Unlike the search algorithms introduced so far, a

stochastic search algorithm moves from one point to another in the search space in a nondeterministic manner, guided by heuristics. The next move is partly determined by the outcome of the previous move. Stochastic search techniques deal with situations where some or all of the parameters of the optimization problem are described by random or probabilistic variables rather than by deterministic quantities. The source of random variables may be several, depending on the nature and the type of problem.

1.4.1 Genetic Algorithms

Genetic algorithms (GAs) are adaptive heuristic search algorithm based on the evolutionary ideas of natural selection and genetics. They represent an intelligent exploitation of a random search used to solve optimization problems. Although randomized, genetic algorithms are by no means random, instead they exploit historical information to direct the search into the regions of better performance within the search space. The basic techniques of the genetic algorithms are designed to simulate processes in natural systems necessary for evolution, especially those following the first laid down by Charles Darwin of survival of the fittest [7].

Genetic algorithms have been applied to optimization problems in many fields, such as optimal control problems, job scheduling, transportation problems, pattern recognition, machine-learning [7-8], etc. Genetic algorithms have been extremely successful in solving unconstrained optimization problems. Several methods have been proposed to handle constraints in construction with genetic algorithms for numerical optimization problems.

1.4.2 Evolutionary Strategies

Evolution strategies (ES) were developed by Rechenberg [9] and Schwefel [10] in Germany. This method is conceptually similar to Genetic Algorithms, but originally did not use crossover operators. Evolution strategies have very complex mutation and replacement functions. Mutation is the main operator while recombination is the secondary in evolution strategies. In this technique, selection is a deterministic operator.

Evolution strategies work with vectors of real numbers for representation of designs and optimization parameters. Mutation and adaptation of mutation rates are important working mechanisms in this method. Each new design point is created by adding random noise to the current one. If the new point is better than the former one search proceeds from this new point, if not the older point is retained. Historically evolution strategies search only one point at a time but recently they use a population of designs like GAs [11]. The main difference between evolution strategies and genetic algorithms is that only the best fit individuals are allowed to reproduce (elitist selection) in the former.

Evolution strategies are often used for empirical experiments and it is based on principal of strong causality, that is, small changes have small effects.

1.4.3 Simulated Annealing

Simulated annealing (SA) is the classical algorithm in thermodynamics for finding low-energy or even optimum configurations for complex physical problems that cannot be solved analytically. It simulates the cooling process of a physical system, taking advantage of the fact that if this cooling procedure is performed slowly enough, the system will end up in the optimum state (e.g., a flawless crystal). On the other hand, it only reaches a less desirable local minimum in the energy landscape (e.g., a crystal with many defects), if the

system is rapidly cooled down. Therefore, starting at a very high temperature, a series of temperatures steps is performed such that the temperature is slowly reduced between the steps. With decreasing temperature, the system undergoes a transition from a high-energy, unordered regime to a relatively low-energy, at least partially ordered regime. The optimization process ends when the system is frozen in an optimum state at a low temperature [12].

1.4.4 Particle Swarm Optimization

Particle swarm optimization (PSO) is a population based stochastic optimization technique inspired by social behavior of bird flocking or fish schooling.

Particle swarm optimization shares many similarities with evolutionary computation techniques such as genetic algorithms (GAs). The system is initialized with a population of random solutions and searches for optimum result by updating generations. However, unlike genetic algorithms, particle swarm optimization has no evolution operators such as crossover and mutation. In particle swarm optimization, the potential solutions, called particles, fly through the problem space by following the current optimum particles.

In the past several years, particle swarm optimization has been successfully applied in many research and application areas. It is demonstrated that particle swarm optimization gets better results in a faster and cheaper way compared with other methods.

Another reason why particle swarm optimization is attractive is that there are few parameters to adjust. One version, with slight variations, works well in a wide variety of applications. Particle swarm optimization has been used for approaches that can be used across a wide range of applications, as well as for specific applications focused on a specific requirement.

1.4.5 Ant Colony Optimization

The fundamental theory in an ant colony optimization (ACO) algorithm is the simulation of the positive feedback process exhibited by a colony of ants. This process is modeled by utilizing a virtual substance called “trail” inspired by real ants. Each ant colony optimization algorithm follows a basic computational structure. An ant begins at a randomly selected point and must decide which of the available paths to travel. This decision is based upon the intensity of trail present upon each path leading to the adjacent points. The path with the most trail has a higher probability of being selected. If no trail is present upon a path, there is zero probability that the ant will choose that path. If all paths have an equal amount of trail, then the ant has an equal probability of choosing each path, and its decision is random. An ant chooses a path using a decision mechanism and travels along it to another point. Some ant colony optimization algorithms now apply a local update to the trail. This process reduces the intensity of trail on the path chosen by the ant. The idea is that when subsequent ants arrive at this point, they will have a slightly smaller probability of choosing the same path as other ants before them. This mechanism is intended to promote exploration among the ants, and helps to prevent early stagnation of the search and premature convergence of the solution. The amount of this trail reduction should not be great enough to prevent overall solution convergence. The ant continues to choose paths to travel between points, visiting each point, until all points have been visited and it arrives back at its point of origin. When it returns to its starting point, the ant has completed a tour. The combination of paths an ant chooses to complete a tour is a solution to the problem, and is analyzed to determine how well it solves the problem. The intensity of trail upon each path in the tour is then adjusted through a global update process. The magnitude of the trail adjustment reflects how well the solution produced by an ant’s tour solves the problem. The paths that make up the tours that best solve the problem receive more trail

than those paths that make up poor solutions. In this way, when the ant begins the next tour, there is a greater probability that an ant will choose a path that was the part of the tour that performed well in the past. When all the ants have completed a tour and all of the tours have been analyzed and the trail levels on the paths have been updated, an ant colony optimization cycle is complete. A new cycle now begins and the entire process is repeated. Eventually almost all of the ants will make the same tour on every cycle and converge to a solution. Stopping criteria are typically based on comparing the best solution from the last cycle to the best global solution. If the comparison shows that the algorithm is no longer improving the solution, then the criteria are reached [13].

1.4.6 Tabu Search

Tabu search (TS) is a metaheuristic technique proposed by Glover [14] as a strategy for solving combinatorial optimization problems. Tabu search is an iterative improvement method based on neighborhood search methods and on memories to guide the search. A tabu search algorithm uses a function called move which transforms a current solution into another solution until certain conditions to stop the process are met. The algorithm starts with an initial solution. In scheduling optimization problems this solution can be generated by a priority rule. A subset of candidate moves is defined for this solution, and for each move a subset of solutions called the neighborhood is generated. At each iteration the best neighbor of each move is selected, and similarly the best of all moves is chosen to lead the current solution to a new solution. The inverse of this move is stored in a short term memory of fixed size, called tabu list. The list prevents the process cycling, and guide the search to good regions in the search space. When a move is in the tabu list, this move is tabu or forbidden for a fixed number of iterations. However, if a tabu move is attractive according to an aspiration criterion, then this move is allowed. One aspiration criterion is to do a tabu move if their solution improves the best solution found to date. To

further improve the search, an intensification strategy can be used to concentrate the search in a localized region, and a diversification strategy can be used to direct the search to unexplored regions. Finally the algorithm iterates from a solution to another solution until a set of stopping conditions are satisfied [15].

1.4.7 Harmony Search Optimization

The new HS meta-heuristic algorithm was derived by adopting the idea that existing meta-heuristic algorithms are found in the paradigm of natural phenomena. The algorithm was based on natural musical performance processes that occur when a musician searches for a better state of harmony, such as during jazz improvisation [16]. Jazz improvisation seeks to find musically pleasing harmony (a perfect state) as determined by an aesthetic standard, just as the optimization process seeks to find a global solution (a perfect state) as determined by an objective function. The pitch of each musical instrument determines the aesthetic quality, just as the objective function value is determined by the set of values assigned to each decision variable [17]. Figure 1.9 shows the harmony search optimization procedure.

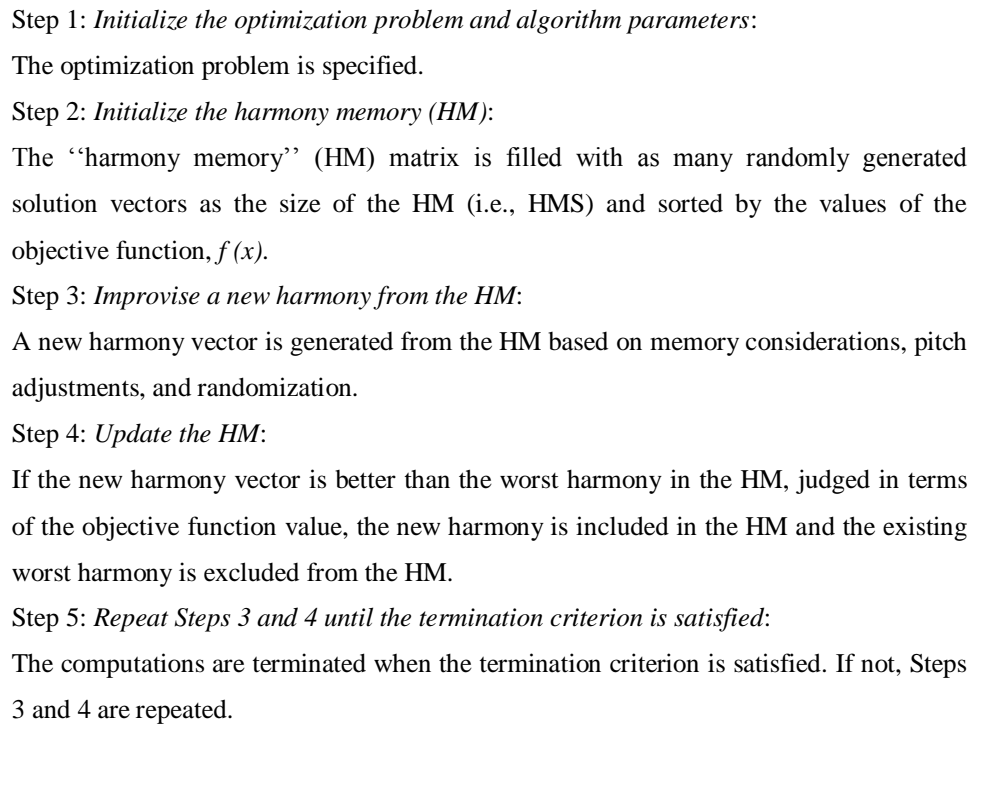


Figure 1.9 Harmony search optimization procedure

In this study, optimum topology of a single layer lamella domes is determined by using harmony search algorithm. This technique is discussed in detail in Chapter 4.

1.5 Literature Survey on the Optimum Design of Dome Structures

The studies and the algorithms developed in recent years for optimum design of dome structures can be reviewed in a historical order as follows;

An optimality criteria algorithm has been developed by Saka [18] for the optimum design of pin-jointed steel structures under multiple loading cases while considering displacements, buckling and minimum size constraints. In this study Saka designed a 112-bar pin-jointed steel dome based on minimum

weight as an example according to AISC design requirements. Hollow pipe sections were used as dome members and system was subjected to equipment loading. Optimum design was obtained after 12 iterations having the minimum volume of 44.47 mm³. In the design problem both buckling and displacement constraints were equally dominant. It is shown in this example that by means of optimality criteria method an optimum design algorithm can be developed for domes that can be effectively used in the design of large structures, which is of importance in practice.

The space trusses, including the geometrical nonlinearity due to large displacements, have been optimally designed based on the coupling the optimality criteria approach with tangent stiffness method by Saka and Ulker [19]. The nonlinear behavior of the space truss required for steps of optimality criteria method which was obtained by using iterative linear analysis. In each iteration the geometric stiffness matrix is constructed for the deformed structure and compensating load vector is applied to the system in order to adjust the joint displacements. During nonlinear analysis, tension members are loaded up to yield stress and compression members are stressed until their critical limits. The overall loss of elastic stability is checked throughout the steps of algorithm. The member forces resulted at the end of nonlinear analysis are used to obtain the new values of design variables for the next cycle. As a design example, 120-members and 37 joints steel dome truss was taken. The truss dome was subjected to a vertical loading at different joints acting in the negative direction of z-axis. The minimum weight was found to be 7587 kg considering nonlinear response of structure and by taking into account the linear behavior, optimum weight of the same structure was found to be 8511 kg. It is shown by this study that optimality criteria method can easily be used for nonlinear structures.

Huyber [20] implemented a study to express the effect of design shape in material properties, such as weight, cost, strength, thermal insulation, energy

requirement, for the optimization of dome structures when geometry was taken as a design variable. The surface of dome was subdivided into three triangular platonic solids, which are tetrahedron, octahedron, or icosohedron. These three basic patterns were compared and evaluated two different methods. The distribution of nodal points were considered as equal as possible on the surface as a start point of view to his study. The data obtained from developed algorithm give the opportunity to express the designed shape in material properties.

Saka and Kameshki [21] dealt with optimum design of a 18-member framed dome, a 96-member lamella dome, and a 110-member network dome to show the importance of nonlinearity due to the effect of axial forces in members on the optimization of three-dimensional rigidly jointed elastic framed domes. They used the optimality criteria approach together with the stiffness method which considers geometric nonlinearity. The algorithm developed considers displacement restrictions and combined stress constraints not to be more than yield stress. The stability functions for three-dimensional beam-columns are used to obtain the nonlinear response of the frame. These functions are derived by considering the effect of axial force on flexural stiffness and effect of flexure on axial stiffness. The algorithm begins with the optimum design at the selected load factor and carries out elastic instability analysis until the ultimate load factor is reached. During these iterations, overall stability of frame is checked. If the nonlinear response is obtained without loss of stability, the algorithm then proceeds to the next design cycle. This study shows that in framed dome without diagonal members, the effect of nonlinearity is important. Its consideration certainly leads to an economical structure.

Erbatur et. al. [22] investigated a 112-bar steel dome for verifying the correctness and efficiency of GAOS (genetic algorithm based structural optimization) program for optimum design of space steel structures. They collected the dome members in seven distinct groups, whereas with only two

groups were considered in the study carried out by Saka [18] for the same example before. Furthermore, in the place of AISC specifications, the allowable compressive stress for each member was computed according to the Turkish specifications. They applied the program on design examples, compared their results with formers' and showed the ability of genetic algorithms on structural optimization.

Lin and Albermani [23] focused on application of a knowledge-based system which is an integrated computer-aided environment used to design problems of lattice-domes. The knowledge- based system offers the possibility of gathering the various aspects of the design process into a unified whole.

Ülker and Hayalioglu [24] considered a 56-bar space dome truss as a design example to investigate the optimum design algorithm for the space trusses with the aid of spreadsheets considering displacements, stresses, and buckling constraints. Matrix displacement method is used for the analysis of design examples. The optimum designs obtained using the spreadsheets are compared with those employing a classical optimization method. The developed algorithm gives better results in comparison with those of the previous ones. The values of joint displacements obtained are much smaller than their upper bounds. As a result, it is deduced that the tensile and buckling stress constraints are dominant in the design. It is demonstrated that the spreadsheets algorithm can be effectively used in the optimum design of practical large plane and space trusses.

Missoum, Gürdal, and Gu [25] optimized a 30-bar space dome structure by using a displacement-based approach. Displacement-based approach uses iterative finite element analyses to determine the structural response as the sizing variables are varied by the optimizer, which makes it different from the traditional optimization approach. This method searches for an optimal solution by using the displacement degrees of freedom as design variables. As a result

of this study, they found lower weights than Khot and Kaman [26], who had studied the same example before.

Yuan, and Dong [27] studied optimization of cable domes by using nonlinear analysis. The nonlinear equilibrium equation of cable domes was developed and solved by Newton–Raphson method. They introduced the prestress which was very important factor for the design of a cable dome because it has no initial rigidity before the prestress. This study, also, showed that the impact of the level of prestress does not only effect the geometric configuration, but it also determines the load carrying capacity of cable domes.

A 616-member mallow dome is studied by Rajasekaran, Mohan, and Khamis [28] as a design example to illustrate the computational advantage of evolution strategies with functional neural networks for the optimization of space trusses. This dome truss was formed using the Formex algebra of the Formian software. The evolution strategies has been applied to find the optimal design of this kind of space trusses considering the areas of the members of the space structures as discrete variables. The objective function was obtained for first few generations by using a structural analysis package such as Feast, and for other generations by functional neural networks. They presented that this study was suitable for solving large scale space structure optimizations which have 700 degrees of freedom.

A study on a hemispherical space dome truss with 52-bar was taken by Lingyun, Mei, Guangming, and Gang [29] as a design example to show the validity, availability, and reliability of nice hybrid genetic algorithm to achieve size and shape truss optimization with frequency constraints. This example was a highly nonlinear dynamic optimization problem with frequency–prohibited band constraints. Lin had reported the optimal results by the optimal criteria for the same example dealt before. The optimal weight of this structure found from

nice hybrid genetic algorithm was much lesser than Lin's results by nearly %20.

Lamella-suspen dome systems were studied by Kitipornchai, Kang, Lam, and Albermani [30] with respect to a detailed parametric analysis. The results of this study demonstrate that the buckling is the most important problem for dome structures. They investigated the influence of geometric imperfection, asymmetric loading, rise-to-span ratio, and connection rigidity on buckling capacity. In the design examples cable prestress force method is used. As a result of this study it was shown that the bottom tensegrity system helps the dome structure to increase the buckling capacity and stiffness, and decrease the member stiffness. They also showed the geometric imperfection has very important effect on buckling capacity of suspen-dome system. They implemented extensive nonlinear buckling analysis to show the reduction of buckling capacity of a suspen-dome system up to 50%.

Togan, and Daloglu [31] proposed an adaptive genetic algorithm which is used to design 112-bar steel dome truss of Saka [18] and Erbatur [22]. They proved that the automatic grouping of members, penalty function and static or adaptive approach has important effect for solving the system. They compared their results with previous examples and showed that their algorithm finds lighter domes. They demonstrated that when they use proper grouping and a penalty function in the adaptive genetic algorithm, the design algorithm becomes quite effective.

López, Puente, and Serna [32] examined the influence of dome geometry, slenderness of members, joint rigidity, and loading of single-layer latticed domes with semi-rigid joints. They ascertained that the angle between members located along the same meridian line has effect on load carrying capacity of the dome.

Kameshki, and Saka [33] studied on a genetic algorithm for determining the optimum height, and the optimum steel section designations for the members of a braced dome. They considered the geometrical nonlinearity in their analysis to obtain realistic response of flexible dome under the external loads. They checked loss of stability during the nonlinear analysis due to its high importance. They optimally designed braced domes by using genetic algorithm and showed that the consideration of nonlinear behavior yields realistic results and leads to a lighter structure.

Saka [34] presented a comprehensive coupled genetic algorithm for calculation of the optimum number of rings, the optimum height of crown, and the tubular cross-sectional designations for the single layer latticed dome members under given external loading. The topological design of these structures present difficulty due to the fact that the number of joints and members as well as the height of the dome keeps on changing during the design process. The most important characteristic of this study is that currently no study was available covering the topological design of dome structures that give the optimum number of rings, the optimum height of crown and the tubular cross-sectional designations for the dome members under a given general external loading. It is shown in the design example considered that the optimum number of joints, members and the optimum height of a geodesic dome under a given external loading can be determined without designers' interference.

1.6 The Scope of This Study

The main goal of this study is to develop an algorithm for the optimum topology design of single layer lamella domes based on harmony search algorithm. In this thesis, Chapters are arranged as in the following; In Chapter 1, a cursory definition is given about domes and types of braced domes. Furthermore, engineering design optimization, structural optimization and the methods of structural optimization are discussed briefly. Besides these, a

literature survey on the optimum design of dome structures is included in a historical order. In Chapter 2, the elastic-critical load analysis of braced domes is discussed. General information about elastic critical load analysis, calculation of elastic critical load factor, stiffness matrix of a space member, nonlinear stiffness matrix with stability functions and nonlinear elastic critical load analysis are also described in this chapter respectively. The morphology, and the mathematical modeling of the optimum topology design of a single layer lamella dome are explained in Chapter 3. Chapter 4 contains the general concept of harmony search optimization method in a detailed manner and includes information about the harmony search based optimum design of single layer lamella dome algorithm developed. The last two parts of this study are allocated for design examples and conclusions, respectively. In Chapter 5, as a numerical example, a single layer lamella dome subjected to different types of external loading is designed by the algorithm developed and the results obtained are shown. The last chapter, Chapter 6, contains the conclusions of the study.

CHAPTER 2

ELASTIC-CRITICAL LOAD ANALYSIS OF SPATIAL STRUCTURES

2.1 Definition of Elastic Critical Load Analysis

Elastic Critical Load Analysis computes the elastic critical load factor, λ_c , for a structure subjected to a particular set of applied loads. This load factor is the ratio by which the axial forces in the members of the structure must be increased to cause the structure to become unstable due to the flexural buckling of one or more members (lateral torsional buckling of individual members is not taken into account). The elastic critical load of the structure is a function of the elastic properties of the structure and the pattern of loading.

Once the elastic critical load is known, member effective lengths can be calculated. The effective length of a member is defined as the length of an ideal pin-ended strut having the same elastic critical load as the load existing in the member when the structure is at its critical load. The effective length may be expressed as a factor multiplying the actual member length.

The effective length factor is calculated separately for each of the member principal axes for each load case. A load factor of less than 1.0 for any load case indicates that the structure is unstable under the applied loading.

The elastic critical load for any load case is determined by computing the axial forces in the members of the structure and then increasing them in proportion

until the structure becomes unstable. At this point the factor by which the axial forces have been increased is the elastic critical load factor for the structure under the current loading. The elastic critical load factor is also known as the buckling load factor.

2.2 Calculation of Elastic Critical Load Factor

The elastic behavior of a structure is governed by the equation:

$$\mathbf{P} = \mathbf{K}_s \Delta \quad (2.1)$$

or more precisely:

$$\lambda \mathbf{P} = \mathbf{K}_s(\lambda \mathbf{P}) \Delta \quad (2.2)$$

The use of $\mathbf{K}_s(\lambda \mathbf{P})$ implies that \mathbf{K}_s is a function of the applied load $\lambda \mathbf{P}$. This equation is nonlinear.

where;

- \mathbf{P} = external loads applied at the joints of the structure,
- Δ = joint displacements of the structure,
- \mathbf{K}_s = stiffness matrix of the structure,
- λ = the load factor.

To determine the value of the critical load factor, λ_c , the problem is linearized by carrying out a double iterative process. The value of λ is increased in a step-by-step manner, and at each load level the singularity of $\mathbf{K}_s(\lambda \mathbf{P})$ is checked. At each load level, also, an inner iteration is performed before the singularity check to find the correct values of the member axial forces shown

in equation (2.2) is solved repeatedly until a consistent set of deflections is obtained. The number of iterations required here depends on how the structure is near to instability, and how good a guess of axial force can be made initially [35].

2.3 Stiffness Matrix of a Space Member

$$\mathbf{p} = \mathbf{k}\mathbf{d} \quad (2.3)$$

This is the member stiffness equation in which \mathbf{p} and \mathbf{d} are 12-term vectors of member force and displacement respectively, and \mathbf{k} is a 12x12 member stiffness matrix for most general case of a prismatic member in space (shear deformation is neglected), and with the implicit condition that the deformations are so small as to leave the basic geometry unchanged.

If a member in space is taken into account, there is the possibility of three linear displacements and three rotations at each of the member as shown in Figure 2.1. The letter d_{x1} denotes linear displacements direction, and θ_{x1} denotes rotations. The first suffix denotes the displacement direction, or the axis about which a rotation takes place, while the second suffix denotes the member end concerned. There are thus 12 possible displacement components for the member, or 12 degrees of freedom.

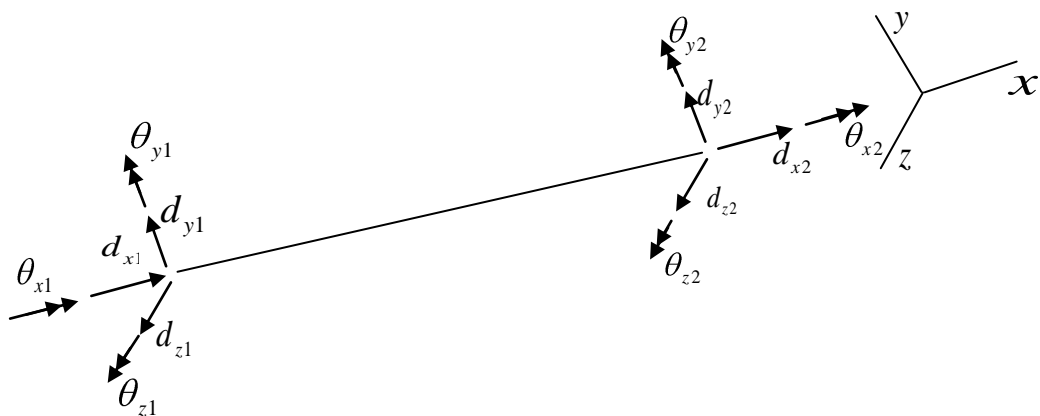


Figure 2.1 A Typical Space Member with Displacements and Rotations.

Associated with each displacement, there is a corresponding force or moment, and these are illustrated in Figure 2.2. The letter p denotes the direct forces and m denotes moments. p_x is an axial thrust, p_y and p_z are shears, m_x is a torsional moment, and m_y and m_z are bending moments.

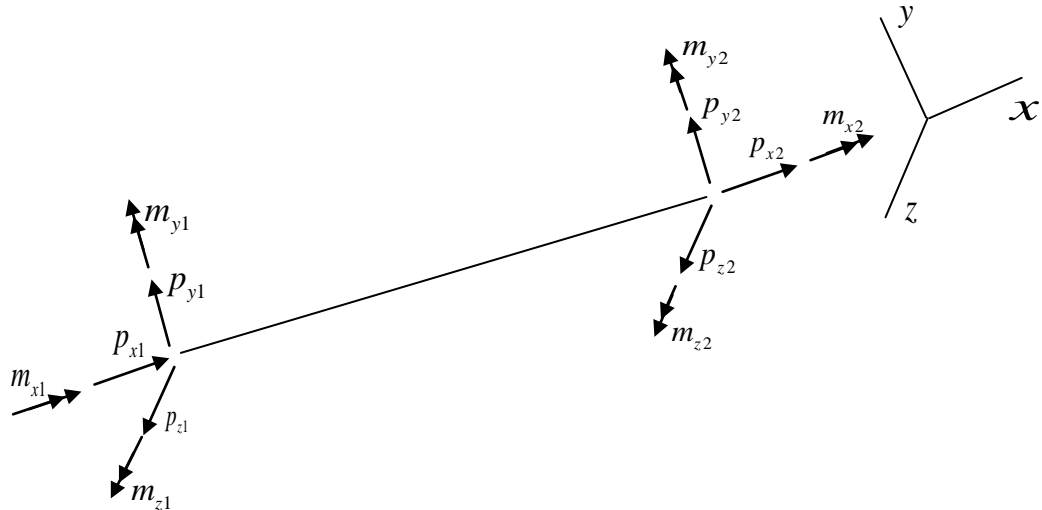


Figure 2.2 A Typical Space Member with Forces and Moments.

The physical properties of the member are designated in the conventional manner as E , G , L , and A , which denote Young's modulus, shear modulus, length, and cross-sectional area respectively. The principle second moments of area for bending are I_y and I_z , the subscripts indicating the axes about which the second moments are taken. The polar second moment of area, which should logically be denoted by I_x , is denoted by J which is the conventional symbol in torsion studies.

To allow Young's modulus E to be taken as a common factor, the shear modulus G has been replaced by $E/2(1+\nu)$, where ν is Poisson's ratio.

It is important to note that the member stiffness matrix \mathbf{k} is symmetrical about its main diagonal [35].

$$\begin{bmatrix} p_{x1} \\ p_{y1} \\ p_{z1} \\ m_{x1} \\ m_{y1} \\ m_{z1} \\ p_{x2} \\ p_{y2} \\ p_{z2} \\ m_{x2} \\ m_{y2} \\ m_{z2} \end{bmatrix} = \begin{bmatrix} \frac{EA}{L} & 0 & 0 & 0 & 0 & 0 & -\frac{EA}{L} & 0 & 0 & 0 & 0 & 0 \\ 0 & \frac{12EI_z}{L^3} & 0 & 0 & 0 & \frac{6EI_z}{L^2} & 0 & -\frac{12EI_z}{L^3} & 0 & 0 & 0 & \frac{6EI_z}{L^2} \\ 0 & 0 & \frac{12EI_y}{L^3} & 0 & -\frac{6EI_y}{L^2} & 0 & 0 & 0 & -\frac{12EI_y}{L^3} & 0 & -\frac{6EI_y}{L^2} & 0 \\ 0 & 0 & 0 & \frac{J}{2L(1+\nu)} & 0 & 0 & 0 & 0 & 0 & -\frac{J}{2L(1+\nu)} & 0 & 0 \\ 0 & 0 & -\frac{6EI_y}{L^2} & 0 & \frac{4EI_y}{L} & 0 & 0 & 0 & \frac{6EI_y}{L^2} & 0 & \frac{2EI_y}{L} & 0 \\ 0 & \frac{6EI_z}{L^2} & 0 & 0 & 0 & \frac{4EI_z}{L} & 0 & -\frac{6EI_z}{L^2} & 0 & 0 & 0 & \frac{2EI_z}{L} \\ -\frac{EA}{L} & 0 & 0 & 0 & 0 & 0 & \frac{EA}{L} & 0 & 0 & 0 & 0 & 0 \\ 0 & -\frac{12EI_z}{L^3} & 0 & 0 & 0 & -\frac{6EI_z}{L^2} & 0 & \frac{12EI_z}{L^3} & 0 & 0 & 0 & -\frac{6EI_z}{L^2} \\ 0 & 0 & -\frac{12EI_y}{L^3} & 0 & \frac{6EI_y}{L^2} & 0 & 0 & 0 & \frac{12EI_y}{L^3} & 0 & \frac{6EI_y}{L^2} & 0 \\ 0 & 0 & 0 & -\frac{J}{2L(1+\nu)} & 0 & 0 & 0 & 0 & 0 & \frac{J}{2L(1+\nu)} & 0 & 0 \\ 0 & 0 & -\frac{6EI_y}{L^2} & 0 & \frac{2EI_y}{L} & 0 & 0 & 0 & \frac{6EI_y}{L^2} & 0 & \frac{4EI_y}{L} & 0 \\ 0 & \frac{6EI_z}{L^2} & 0 & 0 & 0 & \frac{2EI_z}{L} & 0 & -\frac{6EI_z}{L^2} & 0 & 0 & 0 & \frac{4EI_z}{L} \end{bmatrix} \begin{bmatrix} d_{x1} \\ d_{y1} \\ d_{z1} \\ \theta_{x1} \\ \theta_{y1} \\ \theta_{z1} \\ d_{x2} \\ d_{y2} \\ d_{z2} \\ \theta_{x2} \\ \theta_{y2} \\ \theta_{z2} \end{bmatrix}$$

Figure 2.3 Stiffness matrix of a space member in local coordinate system.

Many structural members require less than the full matrix of 12 degrees of freedom to express their deformations. Since a member in a space truss has pin end connections, it cannot transmit any moment through its hinged ends. Consequently, its deformation depends only on the linear displacements at each end, which yields only three degrees of freedom at any joint. The stiffness matrices in such cases may be obtained by selecting relevant terms from the full matrix shown in Figure 2.3.

2.4 Derivation of a Nonlinear Stiffness Matrix Using Stability Functions

The axial forces in a member have a significant effect on its flexural bending that cause nonlinearity in the behavior of structures. Therefore, it is of importance to study this effect in the behavior of dome structures.

Structures which are subjected to both axial forces and bending moments are called beam-column. Members carrying both axial force and bending moments are exposed to an interaction between these effects. The lateral deflection of a member causes additional bending moment when an axial force is applied. This changes the flexural stiffness of the member. Similarly, the presence of bending moments affects the axial stiffness of the member due to shortening of the member caused by the bending deformations. If the deformations are small, the interaction between bending and axial forces can be ignored. In such a case, the force-deformation relationship for a beam-column is same as equation (2.3). However, if the deformations are large, the stiffness matrix \mathbf{k} is affected by the interaction between bending and axial forces, and it is not linear anymore [36]. The nonlinear stiffness matrix can be derived by using stability functions.

2.4.1 Stability Functions

The stability functions are the modification factors from s_1 to s_9 . These functions can be defined with respect to member length, cross-sectional properties, axial force, and the end moments. The effect of axial force on torsional stiffness and the effect of torsional moment on axial stiffness are neglected [36].

where;

s_1 : stability function for the effect of flexure on axial stiffness,

s_2 : stability function for the effect of axial force on flexural stiffness against rotation of near end about z-axis,

s_3 : stability function for the effect of axial force on flexural stiffness against rotation of far end about z-axis,

s_4 : stability function for the effect of axial force on flexural stiffness against rotation of near end about y-axis,

s_5 : stability function for the effect of axial force on flexural stiffness against rotation of far end about y-axis,

s_6 : stability function for the effect of axial force on flexural stiffness (about z-axis) against translation in y-direction,

s_7 : stability function for the effect of axial force on shear stiffness in y-direction against translation in y-direction,

s_8 : stability function for the effect of axial force on flexural stiffness (about y-axis) against translation in z-direction,

s_9 : stability function for the effect of axial force on shear stiffness in z-direction against translation in z-direction.

2.4.1.1 Effect of Flexure on Axial Stiffness

The axial stiffness of the beam in the absence of end moments is given by EA/L , and the axial deformation due to axial loading P is given by PL/EA . However, the end moments produce an additional axial deformation in the beam. In order to include the effect of flexure on axial deformation, the axial stiffness of the beam-column must be modified. For this purpose, the modified axial stiffness can be illustrated as $s_1(EA/L)$. An expression for s_1 is derived as follows [36].

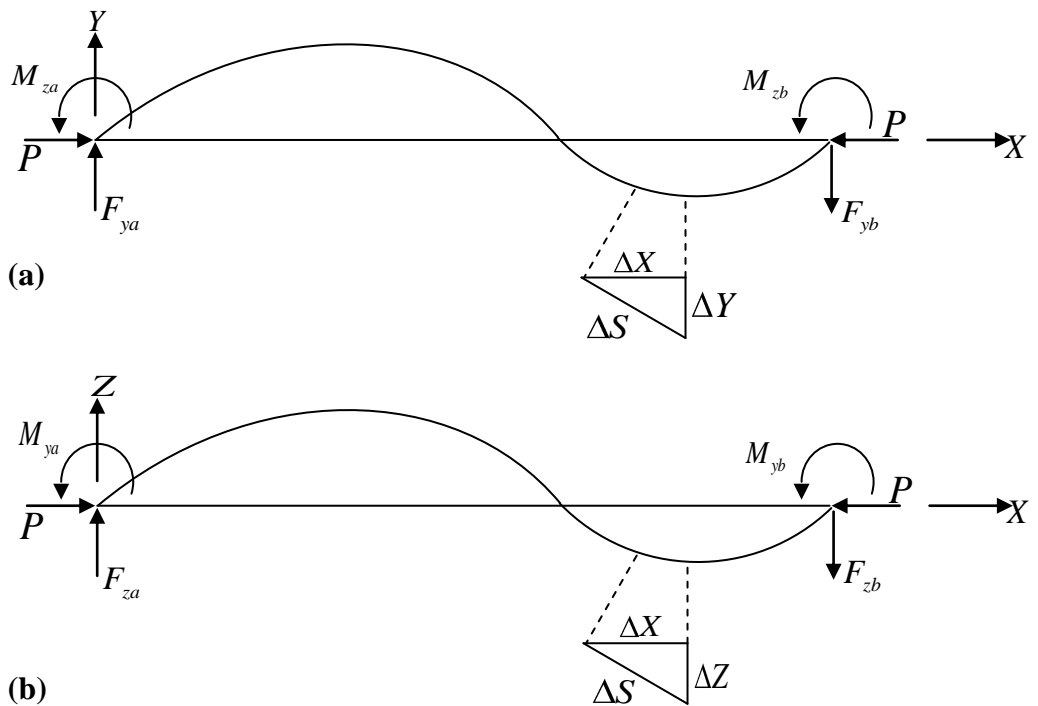


Figure 2.4 Effect of Flexure on Axial Stiffness: (a) Bending in X-Y plane; (b) Bending in X-Z plane

From Figure 2.4 (a) and (b);

$$ds^2 = dx^2 + dy^2 + dz^2 \quad (2.4)$$

by rearranging this equation,

$$\frac{ds^2}{dx^2} = 1 + \frac{dy^2}{dx^2} + \frac{dz^2}{dx^2} \quad (2.5)$$

Shortening due to bending can approximately be defined as,

$$d\delta_b = ds - dx \quad (2.6)$$

dividing equation (2.6) by dx ,

$$\frac{d\delta_b}{dx} = \frac{ds}{dx} - 1 \quad (2.7)$$

Neglecting higher order terms,

$$\frac{d\delta_b}{dx} = \frac{1}{2} \left[\left(\frac{dy}{dx} \right)^2 + \left(\frac{dz}{dx} \right)^2 \right] \quad (2.8)$$

Therefore, the shortening of the beam-column due to bending is,

$$\delta_b = \int_0^L \frac{d\delta_b}{dx} dx \quad (2.9)$$

$$\delta_b = \frac{1}{2} \int_0^L \left[\left(\frac{dy}{dx} \right)^2 + \left(\frac{dz}{dx} \right)^2 \right] dx \quad (2.10)$$

Total shortening of the beam-column is expressed,

δ_t = shortening due to axial load (δ_a) + shortening due to bending (δ_b)

$$\delta_t = \frac{PL}{EA} + \frac{1}{2} \int_0^L \left[\left(\frac{dy}{dx} \right)^2 + \left(\frac{dz}{dx} \right)^2 \right] dx \quad (2.11)$$

$$\delta_t = \frac{PL}{EA} + \left\{ 1 + \frac{EA}{2PL} \int_0^L \left[\left(\frac{dy}{dx} \right)^2 + \left(\frac{dz}{dx} \right)^2 \right] dx \right\} \quad (2.12)$$

$$\delta_t = \frac{P}{s_1 \left(\frac{EA}{L} \right)} \quad (2.13)$$

$$\text{and } s_1 = \frac{1}{1 + \frac{EA}{2PL} \int_0^L \left[\left(\frac{dy}{dx} \right)^2 + \left(\frac{dz}{dx} \right)^2 \right] dx} \quad (2.14)$$

The curvature $\left(\frac{d^2y}{dx^2} \right)$ can be defined from Figure (2.4) (a),

$$\left(\frac{d^2y}{dx^2} \right) = \frac{1}{EI_z} \left[-M_{za} + \frac{x}{L} (M_{za} + M_{zb}) - Py \right] \quad (2.15)$$

$$\text{Let } \alpha^2 = \frac{P}{EI_z} \quad (2.16)$$

Substituting equation (2.16) in equation (2.15) and rearranging the terms,

$$\left(\frac{d^2y}{dx^2}\right) + \alpha^2 y = \frac{\alpha^2}{PL} M_{za} + M_{zb} x - \frac{\alpha^2}{P} M_{za} \quad (2.17)$$

The solution for equation (2.17) is given by the summation of complementary function and particular integral;

$$y = A \sin \alpha x + B \cos \alpha x + \left\{ \frac{x}{PL} (M_{za} + M_{zb}) - \frac{M_{za}}{P} \right\} \quad (2.18)$$

Substituting the boundary conditions $y=0$ at $x=0$ and $x=L$,

$$\left. \begin{aligned} A &= -\frac{1}{P} \operatorname{cosec} \alpha L \left(M_{za} \cos \alpha L + M_{zb} \right) \\ \text{and} \\ B &= \frac{M_{za}}{P} \end{aligned} \right\} \quad (2.19)$$

The slope of beam in the X-Y plane is given by,

$$\frac{dy}{dx} = A \alpha \cos \alpha x - B \alpha \sin \alpha x + \frac{1}{PL} M_{za} + M_{zb} \quad (2.20)$$

Similarly, the equation of the beam-column for bending in the X-Z plane is

$$z = C \sin \beta x + D \cos \beta x + \left\{ \frac{x}{PL} M_{ya} + M_{yb} - \frac{M_{ya}}{P} \right\} \quad (2.21)$$

$$\text{where } \beta^2 = \frac{P}{EI_y} \quad (2.22)$$

Substituting the boundary conditions $z=0$ at $x=0$ and $x=L$,

$$\left. \begin{aligned}
C &= -\frac{1}{P} \operatorname{cosec} \beta L \left[M_{ya} \cos \beta L + M_{yb} \right] \\
\text{and} \\
D &= \frac{M_{ya}}{P}
\end{aligned} \right\} \quad (2.23)$$

The slope of the beam in the X-Z plane is given by,

$$\frac{dz}{dx} = C \beta \cos \beta x - D \beta \sin \beta x + \frac{1}{PL} M_{ya} + M_{yb} \quad (2.24)$$

Now the integrals in equation (2.14) can be evaluated. The final result of the integration is;

$$\begin{aligned}
\int_0^L \left(\frac{dy}{dx} \right)^2 dx &= \frac{1}{2P^2L} \left[\alpha L M_{za}^2 + M_{zb}^2 \cot \alpha L + \alpha L \operatorname{cosec}^2 \alpha L \right. \\
&\quad \left. - 2 M_{za} + M_{zb}^2 + 2\alpha L M_{za} M_{zb} \operatorname{cosec} \alpha L \quad 1 + \alpha L \cot \alpha L \right] \quad (2.25)
\end{aligned}$$

$$\begin{aligned}
\text{where; } H_z &= \left[\alpha L M_{za}^2 + M_{zb}^2 \cot \alpha L + \alpha L \operatorname{cosec}^2 \alpha L \right. \\
&\quad \left. - 2 M_{za} + M_{zb}^2 + 2\alpha L M_{za} M_{zb} \operatorname{cosec} \alpha L \quad 1 + \alpha L \cot \alpha L \right] \\
&= \frac{1}{2P^2L} H_z \quad (2.26)
\end{aligned}$$

and

$$\begin{aligned}
\int_0^L \left(\frac{dz}{dx} \right)^2 dx &= \frac{1}{2P^2L} \left[\beta L M_{ya}^2 + M_{yb}^2 \cot \beta L + \beta L \operatorname{cosec}^2 \beta L \right. \\
&\quad \left. - 2 M_{ya} + M_{yb}^2 + 2\beta L M_{ya} M_{yb} \operatorname{cosec} \beta L \quad 1 + \beta L \cot \beta L \right] \quad (2.27)
\end{aligned}$$

$$\begin{aligned}
\text{where; } H_y &= [\beta L M_{ya}^2 + M_{yb}^2 \cot \beta L + \beta L \operatorname{cosec}^2 \beta L \\
&\quad - 2 M_{ya} + M_{yb}^2 + 2\beta L M_{ya} M_{yb} \operatorname{cosec} \beta L \quad 1 + \beta L \cot \beta L] \\
&= \frac{1}{2P^2 L} H_y \tag{2.28}
\end{aligned}$$

Therefore, equation (2.14) becomes,

$$s_1 = \frac{1}{1 + \frac{EA}{4P^3 L^2 [H_y + H_z]}} \tag{2.29}$$

Note that; when end moments are absent, s_1 becomes unity.

A similar approach can be used to derive an expression for s_1 for a beam-column with axial tensile force P . The final expression is as follows:

$$s_1 = \frac{1}{1 + \frac{EA}{4P^3 L^2 [H_y' + H_z']}} \tag{2.30}$$

$$\begin{aligned}
\text{where; } H_y' &= [\beta L M_{ya}^2 + M_{yb}^2 \coth \beta L + \beta L \operatorname{cosech}^2 \beta L] \\
&\quad - 2 M_{ya} + M_{yb}^2 + 2\beta L M_{ya} M_{yb} \operatorname{cosech} \beta L \quad 1 + \beta L \coth \beta L \tag{2.31}
\end{aligned}$$

and

$$\begin{aligned}
H_z' &= [\alpha L M_{za}^2 + M_{zb}^2 \coth \alpha L + \alpha L \operatorname{cosech}^2 \alpha L] \\
&\quad - 2 M_{za} + M_{zb}^2 + 2\alpha L M_{za} M_{zb} \operatorname{cosech} \alpha L \quad 1 + \alpha L \coth \alpha L \tag{2.32}
\end{aligned}$$

2.4.1.2 Effect of Axial Force on Flexural Stiffness

2.4.1.2.1 Bending in X-Y Plane

From Figure 2.4 (a), the differential equation of the beam-column bending in the X-Y plane is given by Equation (2.17) for which the solution is given by equation (2.18). The constants A and B are obtained from Equation (2.19). The end slopes of the beam-column are obtained by substituting $x=0$ and $x=L$ in equation (2.20);

$$\left(\frac{dy}{dx}\right)_{x=0} = \theta_{za} = A\alpha + \frac{1}{PL} M_{za} + M_{zb} \quad (2.33)$$

$$\left(\frac{dy}{dx}\right)_{x=L} = \theta_{zb} = A\alpha \cos \alpha L - B\alpha \sin \alpha L + \frac{1}{PL} [M_{ya} + M_{yb}] \quad (2.34)$$

Equations (2.33) and (2.34) can be rearranged and rewritten in matrix form as;

$$\begin{Bmatrix} M_{za} \\ M_{zb} \end{Bmatrix} = \begin{vmatrix} s_2 \left(\frac{4EI_z}{L} \right) & s_3 \left(\frac{2EI_z}{L} \right) \\ s_3 \left(\frac{2EI_z}{L} \right) & s_2 \left(\frac{4EI_z}{L} \right) \end{vmatrix} \begin{Bmatrix} \theta_{za} \\ \theta_{zb} \end{Bmatrix} \quad (2.35)$$

when P is compressive, the s_2 and s_3 functions take the following form;

$$s_2 = \frac{1}{4} \alpha L \frac{\sin \alpha L - \alpha L \cos \alpha L}{2 - 2 \cos \alpha L - \alpha L \sin \alpha L} \quad (2.36)$$

$$s_3 = \frac{1}{2} \alpha L \frac{\alpha L - \sin \alpha L}{2 - 2 \cos \alpha L - \alpha L \sin \alpha L} \quad (2.37)$$

For members subject to axial tensile force P and bending in the X - Y plane, P is replaced by $-P$ in equation (2.15). Solving the resulting differential equation, equation (2.35) can again be obtained as;

$$s_2 = \frac{1}{4} \alpha L \frac{\alpha L \cosh \alpha L - \sinh \alpha L}{2 - 2 \cosh \alpha L + \alpha L \sinh \alpha L} \quad (2.38)$$

$$s_3 = \frac{1}{2} \alpha L \frac{\sinh \alpha L - \alpha L}{2 - 2 \cosh \alpha L + \alpha L \sinh \alpha L} \quad (2.39)$$

2.4.1.2.2 Bending in X - Z Plane

From Figure 2.4 (b), and following the same procedure previously mentioned, the stability functions for bending in X - Z plane can be derived. The relationship between end moments and end slopes is given by;

$$\begin{vmatrix} M_{ya} \\ M_{yb} \end{vmatrix} = \begin{vmatrix} s_4 \left(\frac{4EI_y}{L} \right) & s_5 \left(\frac{2EI_y}{L} \right) \\ s_5 \left(\frac{2EI_y}{L} \right) & s_4 \left(\frac{4EI_y}{L} \right) \end{vmatrix} \begin{Bmatrix} \theta_{ya} \\ \theta_{yb} \end{Bmatrix} \quad (2.40)$$

where;

$$s_4 = \frac{1}{4} \beta L \frac{\sin \beta L - \beta L \cos \beta L}{2 - 2 \cos \beta L - \beta L \sin \beta L} \quad \text{for compressive } P \quad (2.41)$$

$$s_4 = \frac{1}{4} \beta L \frac{\beta L \cosh \beta L - \sinh \beta L}{2 - 2 \cosh \beta L + \beta L \sinh \beta L} \quad \text{for tensile } P \quad (2.42)$$

and

$$s_5 = \frac{1}{2} \beta L \frac{\beta L - \sin \beta L}{2 - 2 \cos \beta L - \beta L \sin \beta L} \text{ for compressive } P \quad (2.43)$$

$$s_5 = \frac{1}{2} \beta L \frac{\sinh \beta L - \beta L}{2 - 2 \cosh \beta L + \alpha L \sinh \beta L} \text{ for tensile } P \quad (2.44)$$

2.4.1.3 Effect of Axial Force on Stiffness Against Translation

If both of the ends of a beam-column are restrained against rotation, but one end is translated through a distance Δ relative to the other, the flexural and shear stiffnesses of the beam against this translation are affected by the axial force P .

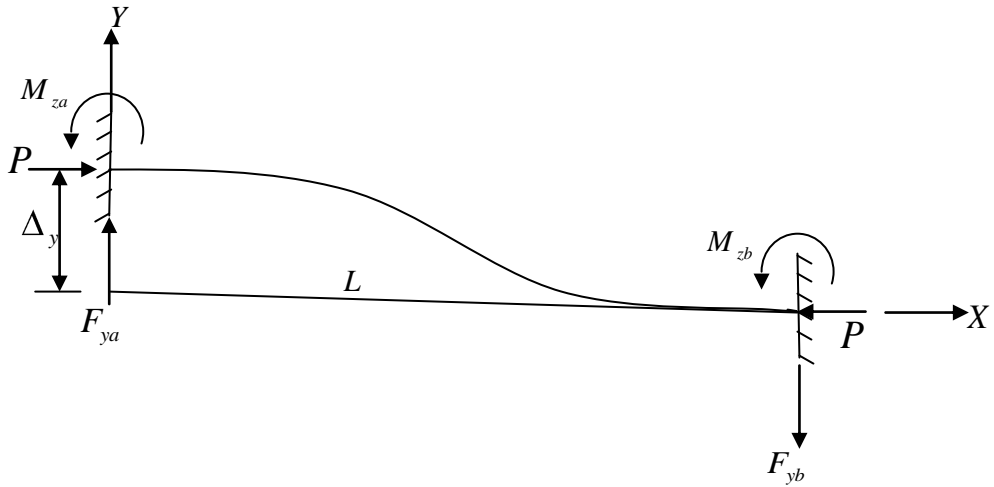


Figure 2.5 Effect of Axial Force on Stiffness Against Translation

2.4.1.3.1 Translation in X-Y Plane

From Figure 2.5, and using the slope-deflection equation;

$$M_{za} = s_2 \left(\frac{4EI_z}{L} \right) \frac{\Delta_y}{L} + s_3 \left(\frac{2EI_z}{L} \right) \frac{\Delta_y}{L} \quad (2.45)$$

$$= \left(\frac{6EI_z}{L^2} \right) \Delta_y \left\{ \frac{2}{3} s_2 + \frac{1}{3} s_3 \right\} \quad (2.46)$$

$$= s_6 \left(\frac{6EI_z}{L^2} \right) \Delta_y \quad (2.47)$$

where;

$$s_6 = \frac{2}{3} s_2 + \frac{1}{3} s_3 \quad (2.48)$$

Substituting the values of s_2 and s_3 from equations (2.36) and (2.37) when the axial force is compressive, and from equations (2.38) and (2.39) when the axial force is tensile, the expressions for s_6 can be obtained as;

When P is compressive;

$$s_6 = \frac{1}{6} \frac{\alpha^2 L^2 (1 - \cos \alpha L)}{(2 - 2 \cos \alpha L - \alpha L \sin \alpha L)} \quad (2.49)$$

When P is tensile;

$$s_6 = \frac{1}{6} \frac{\alpha^2 L^2 (\cosh \alpha L - 1)}{(2 - 2 \cosh \alpha L - \alpha L \sinh \alpha L)} \quad (2.50)$$

Once again from Figure 2.5,

$$F_{y\alpha} = \frac{\sum M}{L} \quad (2.51)$$

where;

$$\sum M = M_{za} + M_{zb} - P\Delta_y \quad (2.52)$$

and

$$M_{za} = s_2 \left(\frac{4EI_z}{L} \right) \frac{\Delta_y}{L} + s_3 \left(\frac{2EI_z}{L} \right) \frac{\Delta_y}{L} \quad (2.53)$$

$$M_{zb} = s_3 \left(\frac{2EI_z}{L} \right) \frac{\Delta_y}{L} + s_2 \left(\frac{4EI_z}{L} \right) \frac{\Delta_y}{L} \quad (2.54)$$

Thus,

$$F_{ya} = \left[s_2 \left(\frac{8EI_z}{L^3} \right) + s_3 \left(\frac{4EI_z}{L^3} \right) - \frac{P}{L} \right] \Delta_y \quad (2.55)$$

If $\alpha^2 = \frac{P}{EI_z}$ is taken;

$$F_{ya} = \frac{12EI_z}{L^3} \left\{ \frac{2}{3}s_2 + \frac{1}{3}s_3 - \frac{\alpha^2 L^2}{12} \right\} = s_7 \left(\frac{12EI_z}{L^3} \right) \quad (2.56)$$

where;

$$s_7 = \frac{2}{3}s_2 + \frac{1}{3}s_3 - \frac{\alpha^2 L^2}{12} \quad (2.57)$$

Substituting for s_2 and s_3 from equations (2.36) and (2.37) when axial force is compressive;

$$s_7 = \frac{1}{6} \frac{\alpha^2 L^2 (1 - \cos \alpha L)}{2 - 2 \cos \alpha L - \alpha L \sin \alpha L} - \frac{\alpha^2 L^2}{12} \quad (2.58)$$

When the axial force P is tensile, P is replaced by $-P$ in equation (2.52) and values of s_2 and s_3 are obtained from equations (2.38) and (2.39);

$$s_7 = \frac{1}{6} \frac{\alpha^2 L^2 (\cosh \alpha L - 1)}{2 - 2 \cosh \alpha L + \alpha L \sinh \alpha L} + \frac{\alpha^2 L^2}{12} \quad (2.59)$$

2.4.1.3.2 Translation in X-Z Plane

Proceeding as in the previous section, s_8 can be given;

$$s_8 = \frac{2}{3} s_4 + \frac{1}{3} s_5 \quad (2.60)$$

Substituting the values of s_4 and s_5 from equations (2.41) and (2.43) when the axial force is compressive, and from equations (2.42) and (2.44) when the axial force is tensile, the expressions for s_8 is shown as;

$$s_8 = \frac{1}{6} \frac{\beta^2 L^2 (1 - \cos \beta L)}{2 - 2 \cos \beta L - \beta L \sin \beta L} \quad (2.61)$$

When P is tensile;

$$s_8 = \frac{1}{6} \frac{\beta^2 L^2 (\cosh \beta L - 1)}{2 - 2 \cosh \beta L + \beta L \sinh \beta L} \quad (2.62)$$

Proceeding as in the previous section, s_9 can be derived;

$$s_9 = \frac{2}{3}s_4 + \frac{1}{3}s_5 - \frac{\beta^2 L^2}{12} \quad \text{when the axial force } P \text{ is compressive} \quad (2.63)$$

$$s_9 = \frac{2}{3}s_4 + \frac{1}{3}s_5 + \frac{\beta^2 L^2}{12} \quad \text{when the axial force } P \text{ is tensile} \quad (2.64)$$

Substituting the values of s_4 and s_5 from equations (2.41) and (2.43) when the axial force is compressive, and from equations (2.42) and (2.44) when the axial force is tensile, the expressions for s_9 is shown as;

When P is compressive;

$$s_9 = \frac{1}{6} \frac{\beta^2 L^2 (1 - \cos \beta L)}{2 - 2 \cos \beta L - \beta L \sin \beta L} - \frac{\beta^2 L^2}{12} \quad (2.65)$$

When P is tensile;

$$s_9 = \frac{1}{6} \frac{\beta^2 L^2 (\cosh \beta L - 1)}{2 - 2 \cosh \beta L + \beta L \sinh \beta L} + \frac{\beta^2 L^2}{12} \quad (2.66)$$

The nonlinear stiffness matrix using the stability functions s_1 through s_9 is shown below in Figure 2.6.

$$\begin{bmatrix} p_{x1} \\ p_{y1} \\ p_{z1} \\ m_{x1} \\ m_{y1} \\ m_{z1} \\ p_{x2} \\ p_{y2} \\ p_{z2} \\ m_{x2} \\ m_{y2} \\ m_{z2} \end{bmatrix} = \begin{bmatrix} s_1 \frac{EA}{L} & 0 & 0 & 0 & 0 & 0 & s_1 \frac{-EA}{L} & 0 & 0 & 0 & 0 & 0 \\ 0 & s_7 \frac{12EI_z}{L^3} & 0 & 0 & 0 & s_6 \frac{6EI_z}{L^2} & 0 & s_7 \frac{-12EI_z}{L^3} & 0 & 0 & 0 & s_6 \frac{6EI_z}{L^2} \\ 0 & 0 & s_9 \frac{12EI_y}{L^3} & 0 & s_8 \frac{-6EI_y}{L^2} & 0 & 0 & 0 & s_9 \frac{-12EI_y}{L^3} & 0 & s_8 \frac{-6EI_y}{L^2} & 0 \\ 0 & 0 & 0 & \frac{GJ}{L} & 0 & 0 & 0 & 0 & 0 & -\frac{GJ}{L} & 0 & 0 \\ 0 & 0 & s_8 \frac{-6EI_y}{L^2} & 0 & s_4 \frac{4EI_y}{L} & 0 & 0 & 0 & s_8 \frac{6EI_y}{L^2} & 0 & s_5 \frac{2EI_y}{L} & 0 \\ 0 & s_6 \frac{6EI_z}{L^2} & 0 & 0 & 0 & s_2 \frac{4EI_z}{L} & 0 & s_6 \frac{-6EI_z}{L^2} & 0 & 0 & 0 & s_3 \frac{2EI_z}{L} \\ s_1 \frac{-EA}{L} & 0 & 0 & 0 & 0 & 0 & s_1 \frac{EA}{L} & 0 & 0 & 0 & 0 & 0 \\ 0 & s_7 \frac{-12EI_z}{L^3} & 0 & 0 & 0 & s_6 \frac{-6EI_z}{L^2} & 0 & s_7 \frac{12EI_z}{L^3} & 0 & 0 & 0 & s_6 \frac{-6EI_z}{L^2} \\ 0 & 0 & s_9 \frac{-12EI_y}{L^3} & 0 & s_8 \frac{6EI_y}{L^2} & 0 & 0 & 0 & s_9 \frac{12EI_y}{L^3} & 0 & s_8 \frac{6EI_y}{L^2} & 0 \\ 0 & 0 & 0 & -\frac{GJ}{L} & 0 & 0 & 0 & 0 & 0 & \frac{GJ}{L} & 0 & 0 \\ 0 & 0 & s_8 \frac{-6EI_y}{L^2} & 0 & s_5 \frac{2EI_y}{L} & 0 & 0 & 0 & s_8 \frac{6EI_y}{L^2} & 0 & s_4 \frac{4EI_y}{L} & 0 \\ 0 & s_6 \frac{6EI_z}{L^2} & 0 & 0 & 0 & s_3 \frac{2EI_z}{L} & 0 & s_6 \frac{-6EI_z}{L^2} & 0 & 0 & 0 & s_2 \frac{4EI_z}{L} \end{bmatrix} \begin{bmatrix} d_{x1} \\ d_{y1} \\ d_{z1} \\ \theta_{x1} \\ \theta_{y1} \\ \theta_{z1} \\ d_{x2} \\ d_{y2} \\ d_{z2} \\ \theta_{x2} \\ \theta_{y2} \\ \theta_{z2} \end{bmatrix}$$

Figure 2.6 Nonlinear stiffness matrix for three-dimensional beam-column element in local coordinate system.

2.5 Geometric Nonlinearity

A variety of classifications may be used to describe the deformational response of structures; for example, small or large, elastic or inelastic, etc. In general, deformations of structures under the external loads are small, and hence the application of the equilibrium equations on the undeformed shape of the structure does not introduce large errors. However, when structure consists of slender members, the deformations become large and small deflection theory is no longer valid. The equilibrium equations are required to be written in such structures on the deformed shape of its elements. In other words, the deflected shape of the structure should be taken into account. When this is considered in the displacement computations, the relationship between the external loads and displacements become nonlinear.

Geometric nonlinearity is required to be considered in the analysis of a structure, if its deflections are large compared with its initial dimensions. In structures with large displacements, although the material behaves linear elastic, the response of the structure becomes nonlinear [19]. Under certain types of loading, namely, even when small deformations are presumed, nonlinear behavior can be predicted. Changes in stiffness and loads occur as the structure deforms. When geometric nonlinearity occurs in a structure, the effect of axial forces to member stiffness must be taken into account.

2.5.1 Construction of Overall Stiffness Matrix

After setting up the nonlinear member stiffness matrix in local coordinate system displacement transformation matrix is conducted.

The equation (2.3) can be rewritten for a 3D truss member in local coordinates;

$$p=kd \tag{2.67}$$

Now, the stiffness matrix in terms of local coordinates (\mathbf{k}) must be converted to stiffness matrix in terms of global coordinates (\mathbf{K}). The transformation equation of stiffness matrix from local to global coordinates is given below;

$$\mathbf{K} = \mathbf{T}^T \mathbf{k} \mathbf{T} \quad (2.68)$$

where;

\mathbf{K} = global stiffness matrix,

\mathbf{k} = local stiffness matrix,

\mathbf{T} = transformation matrix (from local to global coordinates).

Although in theory the direction cosine matrices for each member of a structure may be set up from the orientation of the members in terms of the structure axes, in practice this can cause some difficulty. It is convenient, therefore, to restate a rotation matrix \mathbf{R}_0 in terms of the projections of the members on the structure axes. This can most easily be done by imagining the members as initially lying in the x' -direction with their y - and z -axes coinciding with y' and z' , and then moving by a series of three rotations to their final positions. The rotations are *i*) a rotation α about y -axis; *ii*) a rotation β about the z -axis; and *iii*) a rotation γ about the x -axis. (Although there is a number of ways in which a member might be moved from its initial to its final position, it is essential to this derivation that the order indicated is preserved.)

Rotation α about y -axis : Figure 2.7 shows the rotation α of the member OA to OA'. It is a rotation in the xy plane. The rotation matrix \mathbf{R}_α ;

$$\mathbf{R}_\alpha = \begin{bmatrix} \cos \alpha & 0 & \sin \alpha \\ 0 & 1 & 0 \\ \sin \alpha & 0 & \cos \alpha \end{bmatrix} \quad (2.69)$$

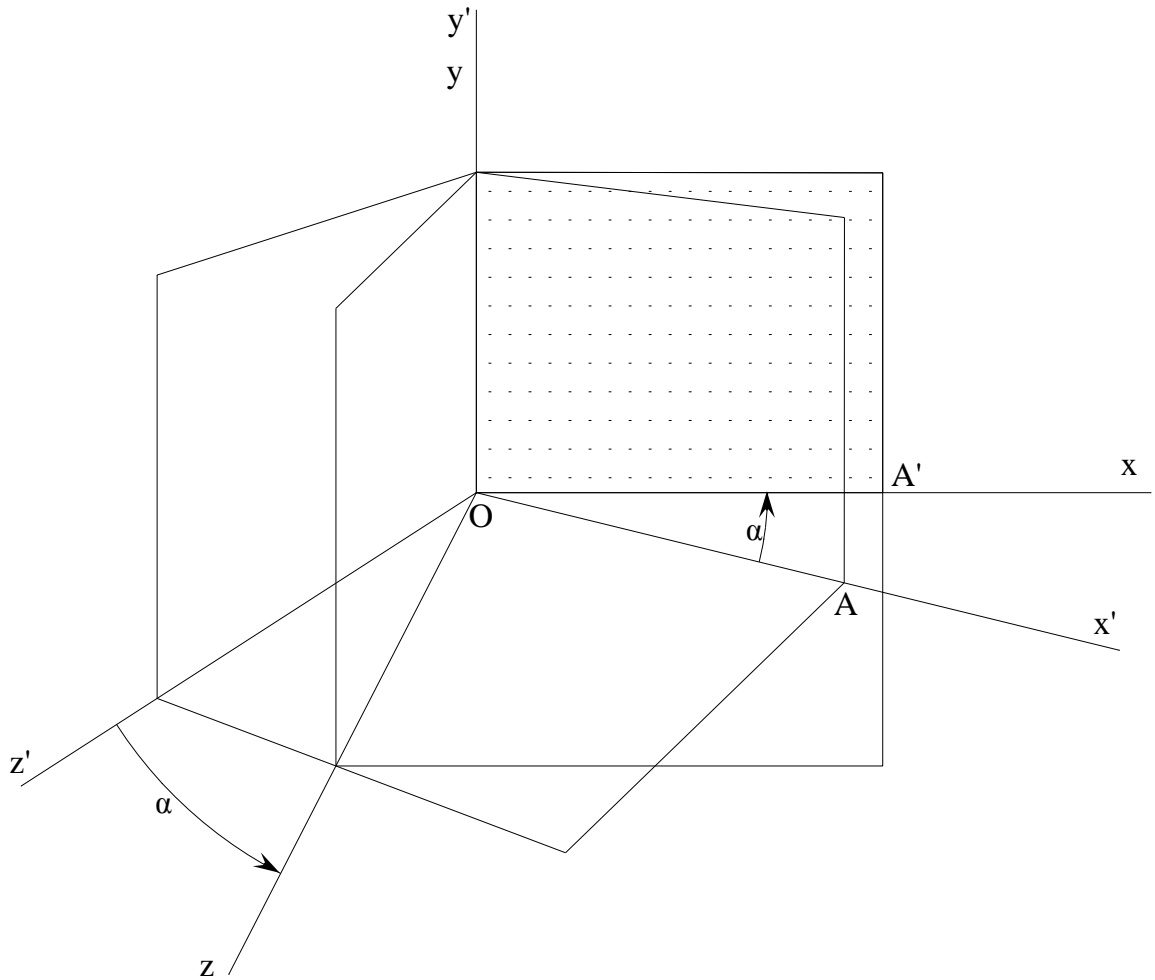


Figure 2.7 Rotation α about y-axis

At this stage;
$$\begin{bmatrix} x \\ y \\ z \end{bmatrix} = R_{\alpha} \begin{bmatrix} x' \\ y' \\ z' \end{bmatrix} \quad (2.70)$$

Rotation β about z-axis; Figure 2.8 shows the rotation β of the member from position OA' to OA'' . It is rotation in the xy plane. The rotation matrix \mathbf{R}_{β} ;

$$\mathbf{R}_{\beta} = \begin{bmatrix} \cos \beta & \sin \beta & 0 \\ -\sin \beta & \cos \beta & 0 \\ 0 & 0 & 1 \end{bmatrix} \quad (2.71)$$

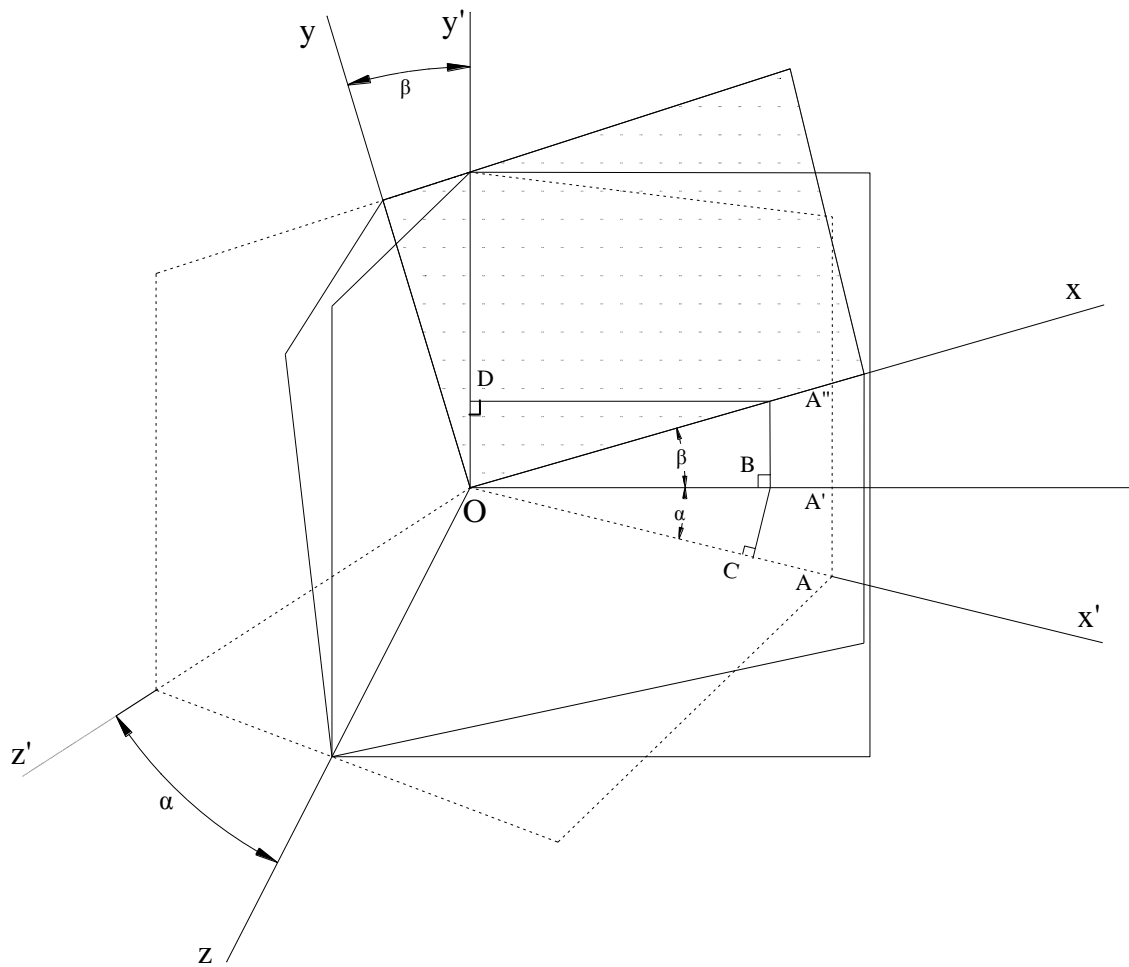


Figure 2.8 Rotation β about z-axis

The effect of this second rotation is obtained by premultiplying the result of Equation (2.70) by R_β .

$$\text{At this stage ; } \begin{bmatrix} x \\ y \\ z \end{bmatrix} = R_\beta R_\alpha \begin{bmatrix} x' \\ y' \\ z' \end{bmatrix} \quad (2.72)$$

Rotation γ about x-axis; Rotations α and β bring the member to its final position, but its z-axis need not to be in the $x'z'$ plane. If, for instance, the $x'y'$ plane is a vertical plane, and the member is an I section with its web vertical

when first placed along the x' -axis, then the web is still in a vertical plane after rotations α and β . If the web is inclined to the vertical in the final position, then a further rotation γ is required as shown in Figure 2.9.

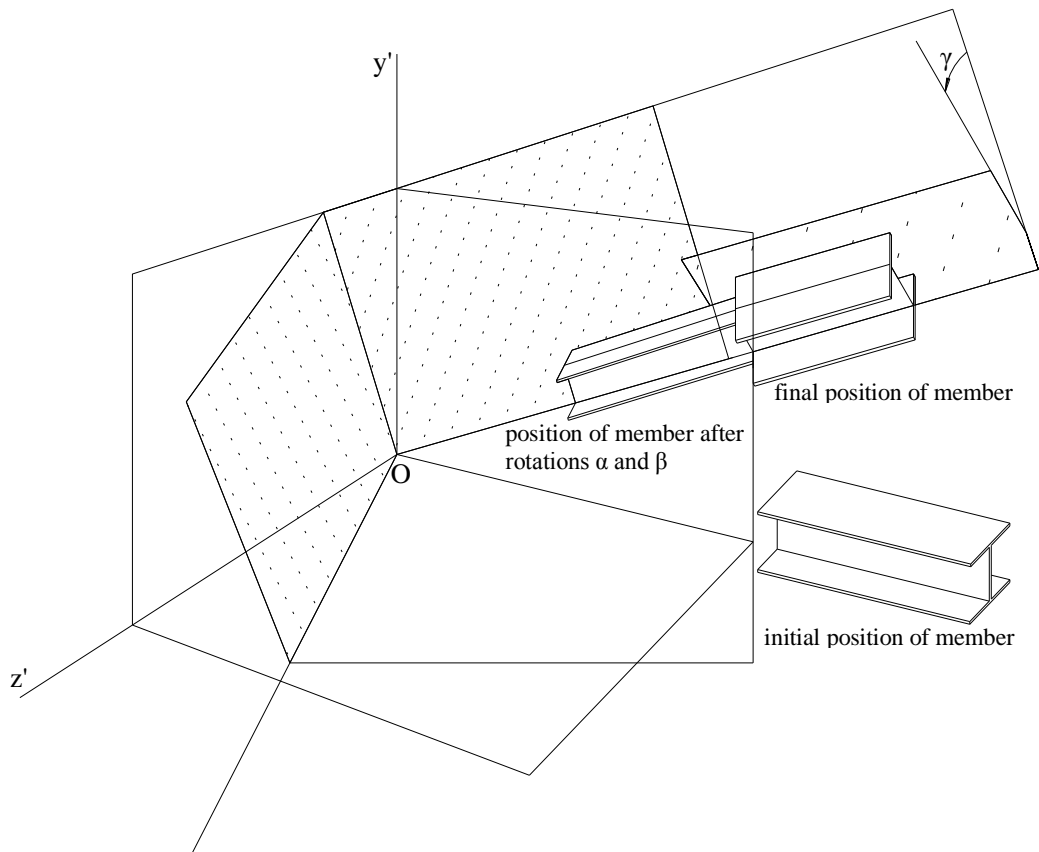


Figure 2.9 Final rotation γ of the member about yz plane

The rotation matrix \mathbf{R}_γ ;

$$\mathbf{R}_\gamma = \begin{bmatrix} 1 & 0 & 0 \\ 0 & \cos \gamma & \sin \gamma \\ 0 & -\sin \gamma & \cos \gamma \end{bmatrix} \quad (2.73)$$

The effect of this final rotation is obtained by premultiplying the result of Equation (2.72) by \mathbf{R}_γ . The final state is

$$\begin{bmatrix} x \\ y \\ z \end{bmatrix} = \mathbf{R}_\gamma \mathbf{R}_\beta \mathbf{R}_\alpha \begin{bmatrix} x' \\ y' \\ z' \end{bmatrix} \quad (2.74)$$

Then; $\mathbf{R}_0 = \mathbf{R}_\gamma \mathbf{R}_\beta \mathbf{R}_\alpha$

If the member OA is of length L , and its projections in its final position OA'' on the x' -, y' -, and z' -axes are L_x , L_y , and L_z respectively, then it can be seen from Figure 2.8 that;

$$OC = L_x, \quad OD = L_y = BA'', \quad BC = -L_z, \quad OB = \sqrt{(L^2 - L_y^2)} = \sqrt{(L_x^2 + L_z^2)}$$

Hence;

$$\cos \alpha = OC / OB = L_x / \sqrt{(L_x^2 + L_z^2)}$$

$$\sin \alpha = -L_z / \sqrt{(L_x^2 + L_z^2)}$$

$$\cos \beta = \sqrt{(L_x^2 + L_z^2)} / L$$

$$\sin \beta = L_y / L$$

$$\mathbf{R}_0 = \mathbf{R}_\gamma \mathbf{R}_\beta \mathbf{R}_\alpha = \begin{bmatrix} L_x / L & L_y / L & L_z / L \\ \frac{(-L_x L_y \cos \gamma - L L_z \sin \gamma)}{L \sqrt{(L_x^2 + L_z^2)}} & \frac{\sqrt{(L_x^2 + L_z^2)} \cos \gamma}{L} & \frac{(-L_y L_z \cos \gamma + L L_x \sin \gamma)}{L \sqrt{(L_x^2 + L_z^2)}} \\ \frac{(-L_x L_y \sin \gamma - L L_z \cos \gamma)}{L \sqrt{(L_x^2 + L_z^2)}} & -\frac{\sqrt{(L_x^2 + L_z^2)} \sin \gamma}{L} & \frac{(-L_y L_z \sin \gamma + L L_x \cos \gamma)}{L \sqrt{(L_x^2 + L_z^2)}} \end{bmatrix} \quad (2.75)$$

Equation (2.75) gives the most general form of the rotation matrix.

So, that is to say, direct forces in structure axes are affected only by the direct forces in member axes, and moments in structure axes are affected only by the direct forces in member axes. The form of transformation matrix (\mathbf{T}) is;

$$T = \begin{bmatrix} R_0 & 0 & 0 & 0 \\ 0 & R_0 & 0 & 0 \\ 0 & 0 & R_0 & 0 \\ 0 & 0 & 0 & R_0 \end{bmatrix}_{(12 \times 12)} \quad (2.76)$$

After developing the stiffness matrices for each member of the entire structure in terms of local coordinates, these matrices can be assembled to form the global stiffness matrix for the entire structure. Total stiffness at a coordinate is the sum of the stiffnesses contributed to that coordinate by each element attached to that coordinate.

The nonlinear response of a structure is obtained through successive linear elastic analysis as shown in Figure 2.10. Initially the axial forces are presumed to be zero. With zero values of axial forces, stability functions become equal to 1. Linear elastic analysis of the structure is carried out and axial forces in members are determined. With these values of axial forces the stability functions are calculated and structural analysis is repeated. This process are continued until the convergence is obtained in the axial force values of members.

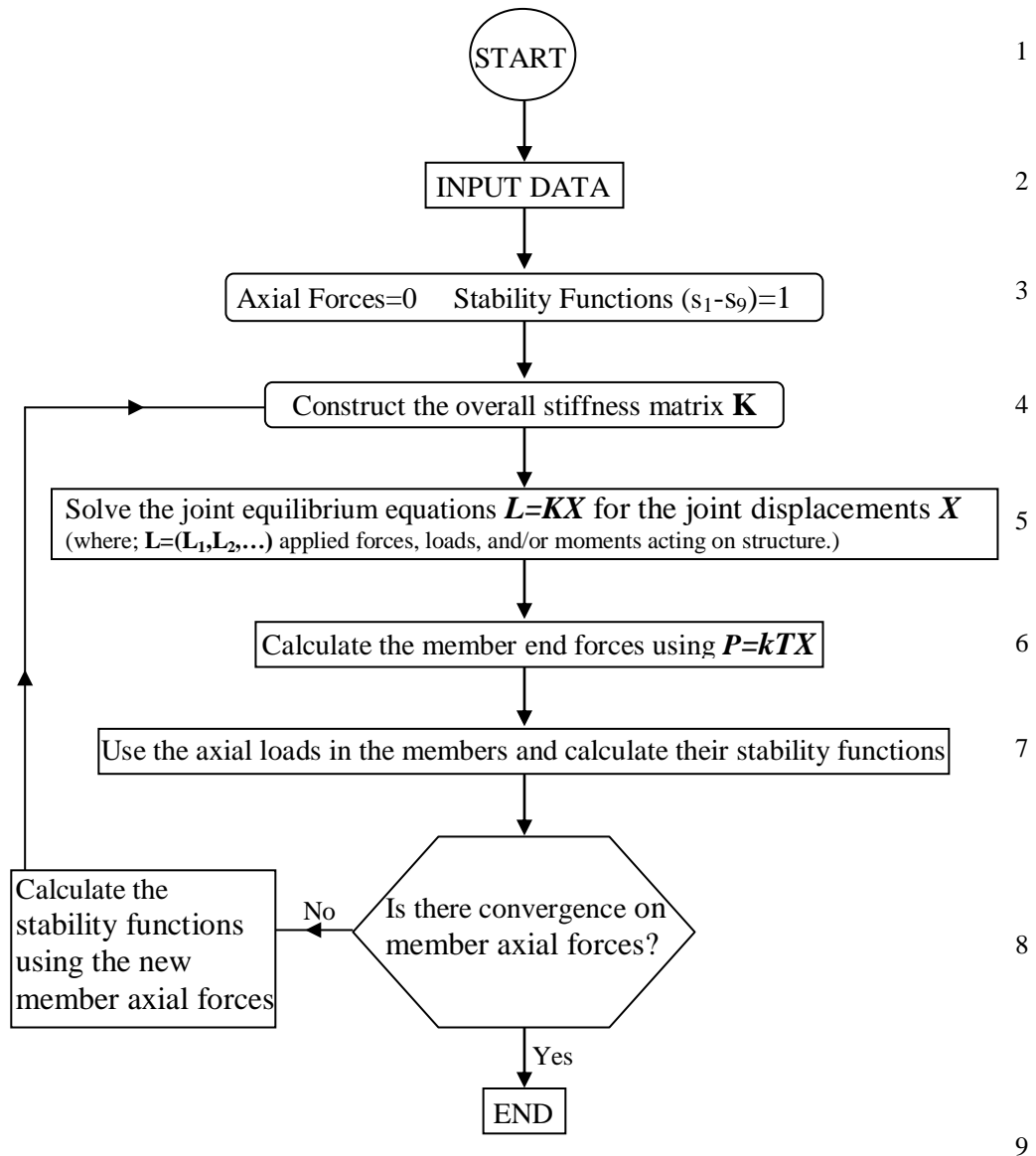


Figure 2.10 Nonlinear response of a structure obtained through successive elastic linear analysis.

From Figure 2.10, an accurate set of joint displacements and member forces become available for each load factor and nonlinear load-displacement diagram of the structure can be plotted as shown in Figure 2.12 below.

Table 1 Y-displacement values of the joint 1 of the dome under different external loads.

Loads (P) (kN)	Number of Nonlinear Iterations	Y-displacements of the joint 1 of the dome (mm)	
		From Nonlinear Analysis	From Linear Analysis
100	3	4.482	4.454
200	3	9.023	8.908
400	3	18.300	17.820
600	4	27.860	26.720
800	4	37.770	35.630
1000	4	48.140	44.540
1200	5	59.380	53.450

In order to show the difference between the displacement values obtained through linear and nonlinear analysis, the dome structure shown in Figure 2.11 is considered.

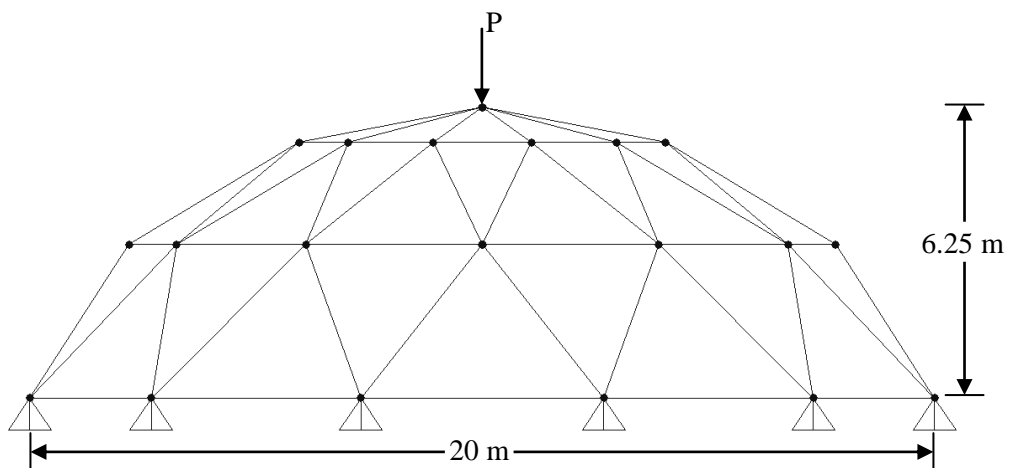


Figure 2.11 A single layer lamella dome with 3 rings subjected to different concentrated loads on its crown.

The dome is subjected to a concentrated load in Y-direction at its crown. Y-displacements of the crown which is the first joint of the dome are calculated by using linear and nonlinear analysis under different load levels. These are shown in Table 1. The results obtained are plotted in Figure 2.12. The effect of the geometrical nonlinearity on the values of Y-displacement of joint 1 is clearly seen in this figure. At the load of 1200 kN, the nonlinear displacement is 11.1% more than the linear displacement. It is clear that when the load is increased, the axial forces increase in the members and their effect on the flexural bending of the member become more emphasized. As a result nonlinear displacement becomes larger.

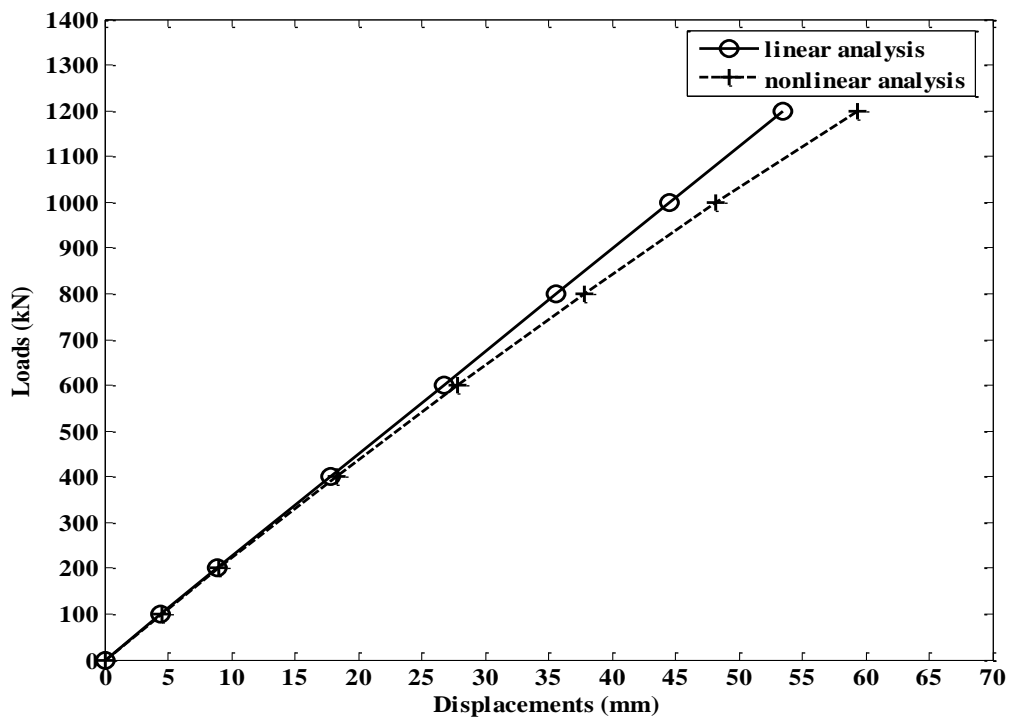


Figure 2.12 Linear and nonlinear Y-displacements of joint 1 of the lamella dome.

Figure 2.12 clearly reveals the fact that when the vertical loads become larger in dome structures, the displacements become larger and inclusion of geometric nonlinearity in the analysis of such structures becomes a necessity.

2.6 Elastic Critical Load Analysis

Elastic critical load analysis determines the load factor such that when the loads are increased by this factor a structure loses its stability. The elastic critical load analysis of structures involves iterative nonlinear analysis with load increments. The flowchart shown in Figure 2.13 displays the steps of the algorithm [35].

The stiffness matrix of a stable structure has the property of positive-definiteness, and a test for this property is performed at each load level. At the critical load the determinant of the stiffness matrix becomes zero which means the stiffness matrix becomes singular. It is not easy to determine exactly at what value of the load factor the determinant becomes zero. In practice when the sign of the determinant of the stiffness matrix changes from positive to negative, it is understood that the structure becomes unstable. The steps of the algorithm are explained below;

1) The preparatory data should include the type of structure, such as space frame, grillage, dome, etc., the number of the members, number of joints, number of load cases and common material properties, such as Young's modulus, shear modulus. The coordinates of each joint in the structure axes are listed against the joint number. The members of structure with same sectional properties are shown with the same group numbers. The support kind of the members are given. The load case should be revealed in preliminary data. In addition to this basic information, the preliminary data must include an initial value for the load factor (LF), and the increment applied to load factor (INC).

2) N denotes the number of loading cycles and DET1, DET2, and DET3 are the values of the determinant of the stiffness matrix. The axial forces in members of the structure are not always known before the analysis begins, and this chart assumes them all zero initially.

3) To prevent convergence due to ill-conditioning, the number of load cycles can be limited by inserting a check on N.

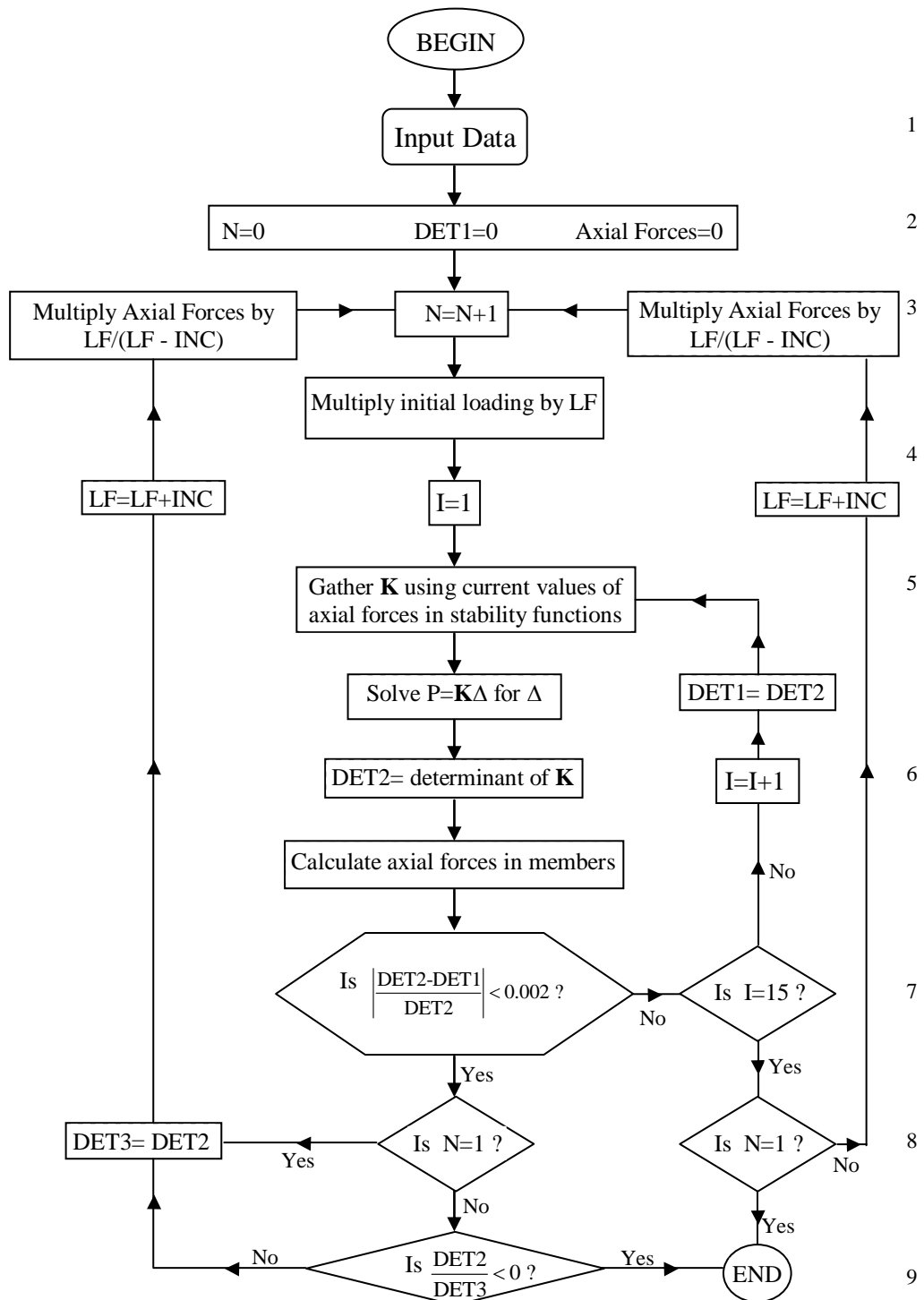


Figure 2.13 Flowchart for the determination of nonlinear elastic critical load

4) A number of solutions which is counted by I are performed because initially the axial forces at each load level are only known approximately.

5) The structure stiffness matrix \mathbf{K} is set up by using stability functions as shown in Figure 2.6.

6) When the terms of the stiffness matrix converge to a steady state at consecutive cycles, the recurrent performed analysis at each load level should be canceled. The determinant of the stiffness matrix DET2 is used as a suitable control parameter as its value depends upon the stiffness matrix terms.

7) Once the proportional alteration in the determinant is less than %0.2, the recurrent analysis is called off. This restriction value is completely random, but it is reasonable in practice. The final determinant value is taken as the stiffness matrix determinant stored in DET3 and this value is used for checking the positive-definiteness.

8) When the loading approaches to the critical level, the stiffness matrix becomes increasingly ill-conditioned and the determinant values become very large. In such a case it is meaningless to keep repeated analysis going and it should be terminated when $I=15$. If this termination occurs at first load level ($N=1$), it means the loading is very near to critical level at the beginning. In this case the analysis must be terminated and has to be renewed with a smaller set of loads. In other respects, the load factor can be increased so that the axial forces increase by the same ratio for examining further load levels.

9) As soon as the load level holds the satisfactory convergence, the value of the determinant obtained is compared with that from the previous cycle. If no sign change is observed then the load factor and axial forces are increased by one step and a new load level is studied. If a sign change comes out (changing from positive to negative), then the process is terminated.

As an example, if the dome in Figure 2.11 is considered once again under different external loading, the determinant values of the stiffness matrix of the dome for the last nonlinear analysis cycle which is the optimum design stored as DET3 is shown in Table 2. It is obvious that dome can resist up to 1200 kN external concentrated loading at its crown. If the loading exceeds this value, the stiffness matrix of the dome changes its sign from positive to negative. This means after critical loading value (1200 kN) the dome lost its stability and fail.

Table 2 Determinant values of the stiffness matrix of the dome.

<i>Loads (P)</i> <i>(kN)</i>	<i>Number of</i> <i>nonlinear iterations</i>	<i>DET3</i> <i>(stiffness matrix determinant)</i>
100	3	0.397E+231
200	3	0.975E+230
400	3	0.350E+229
600	4	0.538E+227
800	4	0.263E+225
1000	4	0.234E+222
1200	5	0.100E+218
1400	3	-0.999E+194

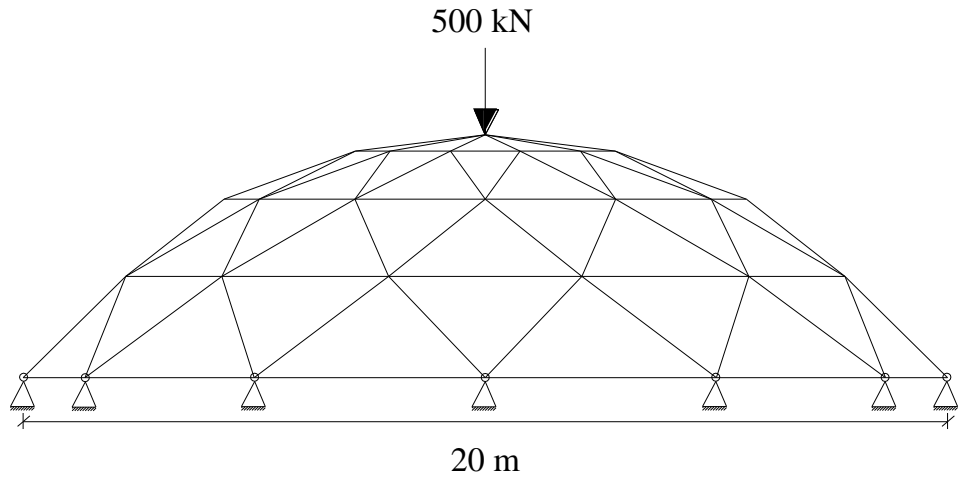
CHAPTER 3

OPTIMUM DESIGN OF LAMELLA DOMES

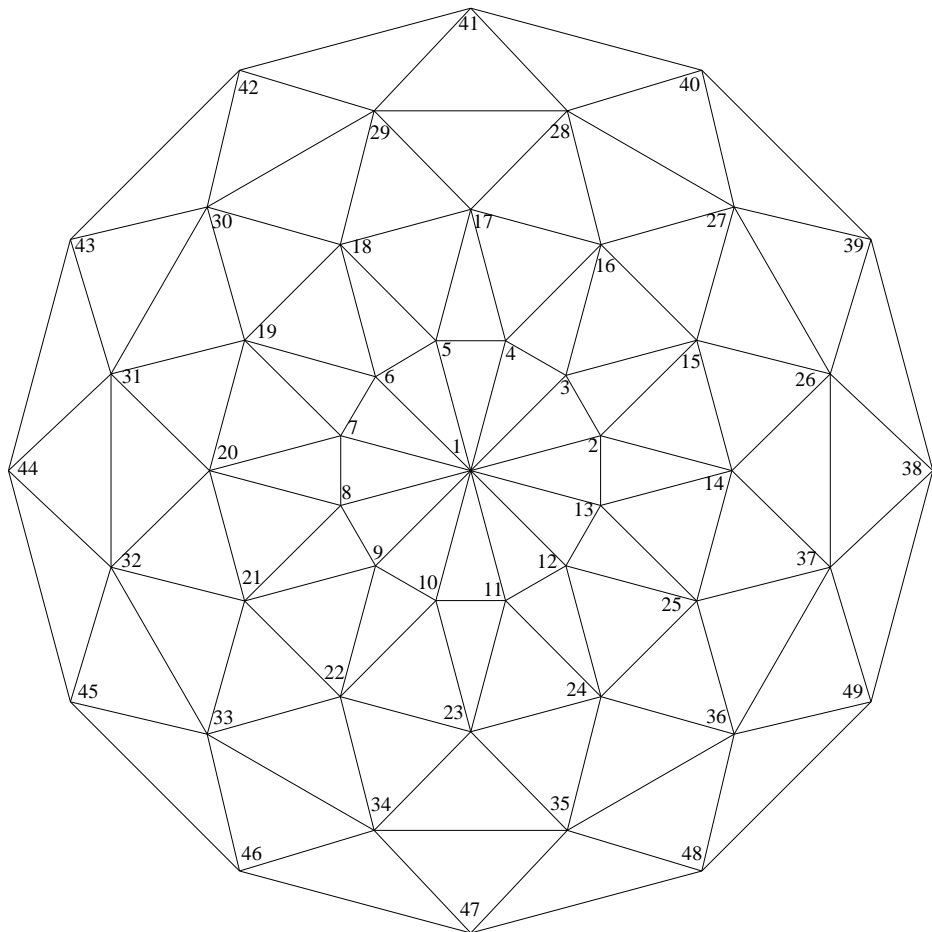
3.1 Morphology of Lamella Domes

The morphology of the single layer lamella dome has a simple geometric form. If the total number of rings and the height of the crown of the dome are known, then it is very simple to get the whole topological information about the dome. Utilizing the geometrical features of the lamella dome, the total number of members and joints, and the member incidences can be established by the knowledge about the total number of rings. One additional step to this, using the geometric configuration and the height of crown of the dome, the exact coordinates of all joint nodes can also be determined. Lamella domes with varying crown heights and rings number, therefore, have dissimilar topology from each other [33-34-37].

The form of commonly used single layer lamella dome is shown in Figure 3.1. If the diameter of the dome D , the total number of rings n_r , and the height of the crown h are known, then all of the structural data about geometry of the dome can be computed automatically. The distance between the rings in the dome on the meridian line has to be equal. It can be easily seen from Figure 3.2 (b) that all the joints are located with equal distance from each other on the same ring. The top joint at the crown is numbered as the first joint (joint number 1). Every ring has 12 joints on itself. The first joint on the first ring according to the positive z direction making an angle of $360^\circ / 24 = 15^\circ$ with the radius drawn on the x axis is numbered as joint 2 and all of the first joints of the other rings are placed as;

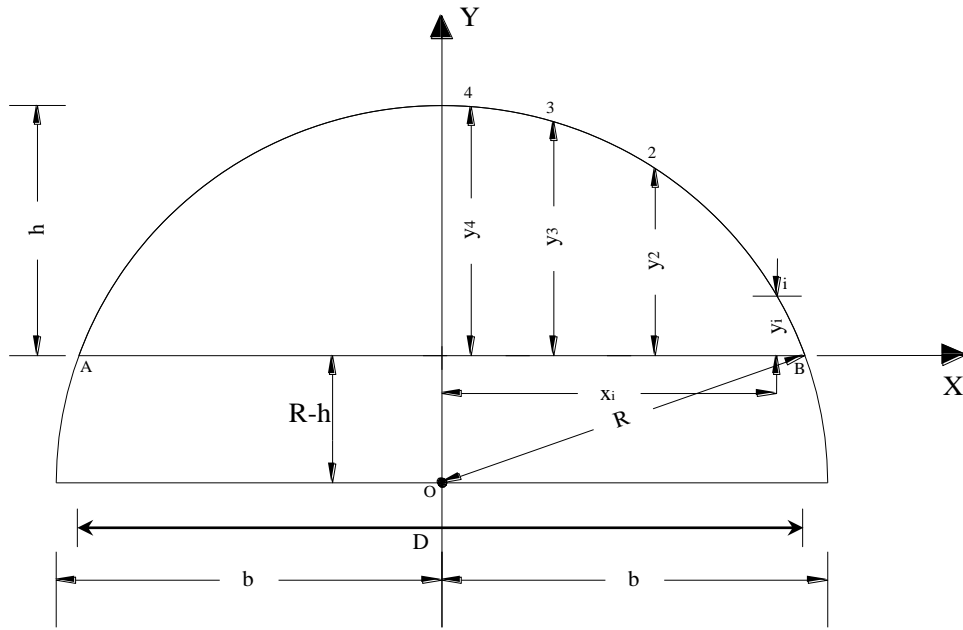


(a) Elevation

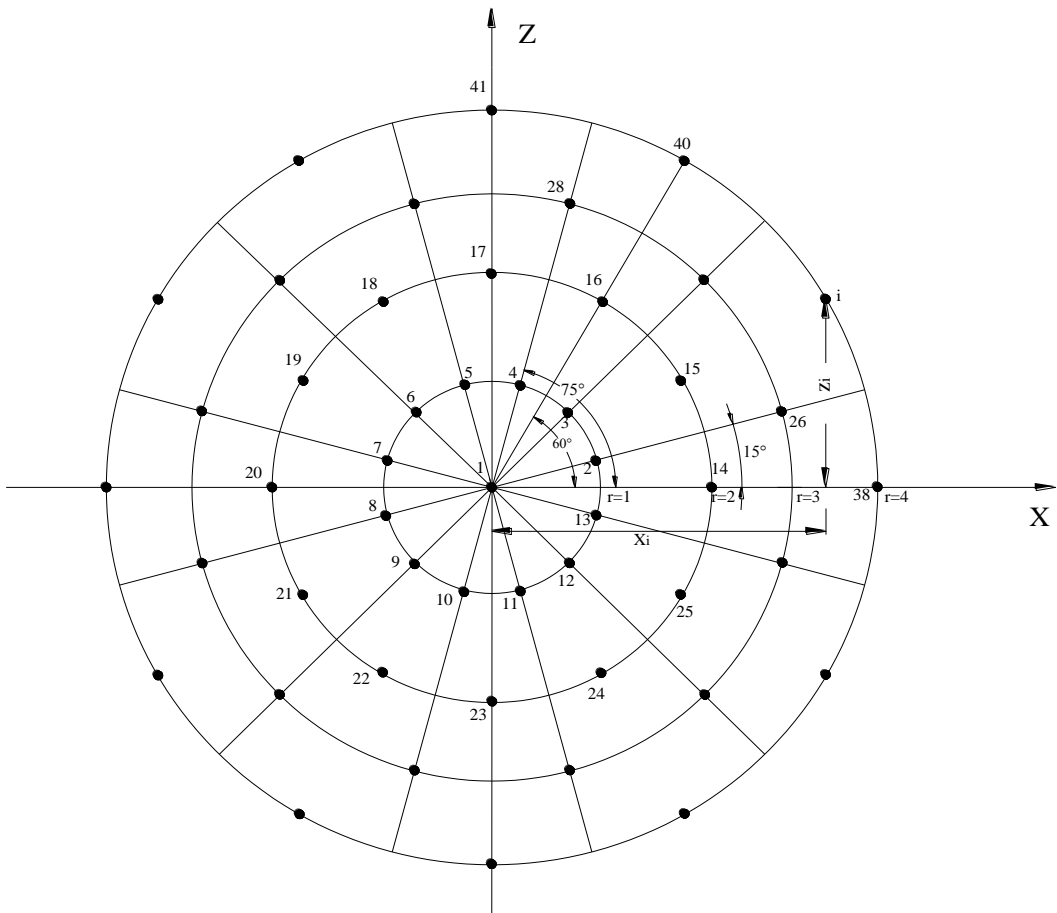


(b) Plan

Figure 3.1 Lamella Dome.



(a) Elevation



(b) Plan

Figure 3.2 Automated computation of joint coordinates in a lamella dome.

$$[J_{r1} + (r-1)*12] \quad (3.1)$$

where r is the ring number and J_{r1} is the first joint number of the first ring namely 2.

It is worthwhile to mention that all of the first joints of the odd numbered rings (ring 1, ring 3, ring 5, etc.) are located on the x axis with same angle of 15° . Beside this, the first joints of the even numbered rings (ring 2, ring 4, etc.) are located on the intersection points of that rings and x-axis. For example the first joint number of the third ring is numbered as $2 + (3-1)*12 = 26$ and it makes 15° angle with x-axis. On the other hand, the first joint number of the fourth ring is numbered as $2 + (4-1)*12 = 38$ and this joint is located on the intersection point of fourth ring and x-axis. By the aid of this relation every joint on the rings is numbered in a regular sequence.

Member incidences are arranged in similar manner. First member is taken as the one which is on the x axis and connects joint 1 to joint 2. The other 11 members connect joint 1 to joints 3, 4, 5, 6, 7, 8, 9, 10, 11, 12, 13. This is followed by the members that connect joints on the ring as 2-3, 3-4, 4-5, 5-6, 6-7, 7-8, 8-9, 9-10, 10-11, 11-12, 12-13, 13-2. This process is repeated for each ring and member incidences for all the members in the dome are determined and stored in an array.

Computation of x, y, and z coordinates of a joint on the dome requires the angle between the line that connects the joint under consideration to joint 1 and the x-axis as shown in Figure 3.2 (a) and (b). This angle can be calculated for joint i shown in the same figure.

For the odd numbered rings;

$$\alpha_i = \frac{360}{24} + \frac{360*(i - j_{r,1})}{12} \quad (3.2)$$

For the even numbered rings;

$$\alpha_i = \frac{360*(i - j_{r,1})}{12} \quad (3.3)$$

where α_i is shown in Figure 3.2 (b), r is the ring number that joint i is placed on it and j is the first joint number on the ring number r which is on the x-axis. For example, the angle between the radius that connects joint 1 to joint 16 located on a even numbered ring (ring 2) and the x-axis;

$$\alpha_{16} = \frac{360*(16-14)}{12} = 60^\circ \quad (3.4)$$

On the other hand, the angle between the radius that connects joint 1 to joint 28 located on a odd numbered ring (ring 3) and x-axis;

$$\alpha_{28} = \frac{360}{24} + \frac{360*(28-26)}{12} = 75^\circ$$

The x_i and z_i coordinates of joint i can be calculated as;

$$\left. \begin{aligned} x_i &= ra \cos(\alpha_i) \\ z_i &= -ra \sin(\alpha_i) \end{aligned} \right\} \quad (3.5)$$

where r is the ring number that joint i is on it and a is the radius of ring r in x-z plane.

If the distance between rings are equal to a , then a becomes $D/(2n_r)$. The y_i coordinate of joint i ;

$$y_i = \sqrt{R^2 - x_i^2} - \sqrt{R - h} \quad (3.6)$$

where R is the radius of the semi-circle shown in Figure 3.2 (a) computed from $(D^2 + 4h^2) / (8h)$. By use of equations (3.5) and (3.6) for each joint, it is possible to obtain the coordinates of the joints in the dome automatically.

3.2 Optimum Topology Design of Lamella Domes

Topological design of a lamella dome with a given base diameter necessitates the finding out of the optimum number of rings and the height of the crown, and the steel sections designations for each member group in the dome selected from a standard steel sections table. These should be specified such that the strength and serviceability requirements are satisfied according to code of practice and the overall cost or only the material cost of the dome is minimum.

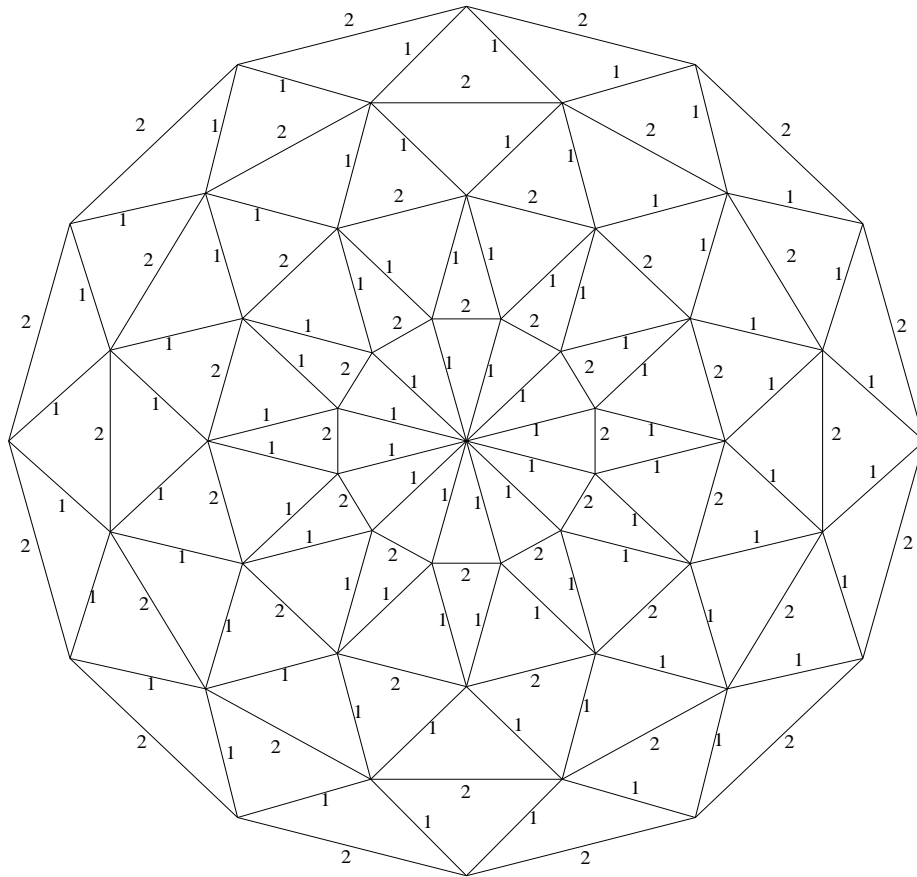


Figure 3.3 (a) Lamella Dome with Two Different Member Groups.

It is possible for the members of a dome to be made of the same section in practice. However in some cases they can be grouped together to achieve the minimum construction cost for the structure. The optimum topology design of single layer lamella domes differs in formulation depending on the way member grouping is decided in the dome [33-34]. If the members are chosen to belong to the same group, dome becomes simple to design and member grouping is independent of the number of rings. In another case, members located in a meridian line can be one group and members on the rings are another, total of two groups as shown in Figure 3.3 (a). In both cases number of groups in the dome is not function of the number of rings and automatic grouping of the members can be performed without the need of the total

number of rings in the dome. However, it is also possible that the members of the dome can be grouped such that the members between each ring are to be assigned one group and the members on each ring are another group as shown in Figure 3.3 (b) [34-37]. In this case, the members between the crown and the first ring are assigned as group 1, the members on the first ring are assigned as group 2, the members between rings 1 and 2 are assigned as group 3, and the group number of members on the ring 2 is assigned as group 4 and so on. Under this circumstance, grouping of the members depend upon the total number of rings which is one of the design variables of the problem. Hence the total number of groups in the dome becomes twice the total number of rings in the design problem. For example, if a dome with three rings is considered, the total number of design variables becomes 7, six of which are the sectional designation to be selected for each group and the last one is the height of the dome. In the case of five rings in the dome the total number of design variables is 11, ten of which represents the sectional designations to be assigned for each group and the last one gives the height of the crown in the dome.

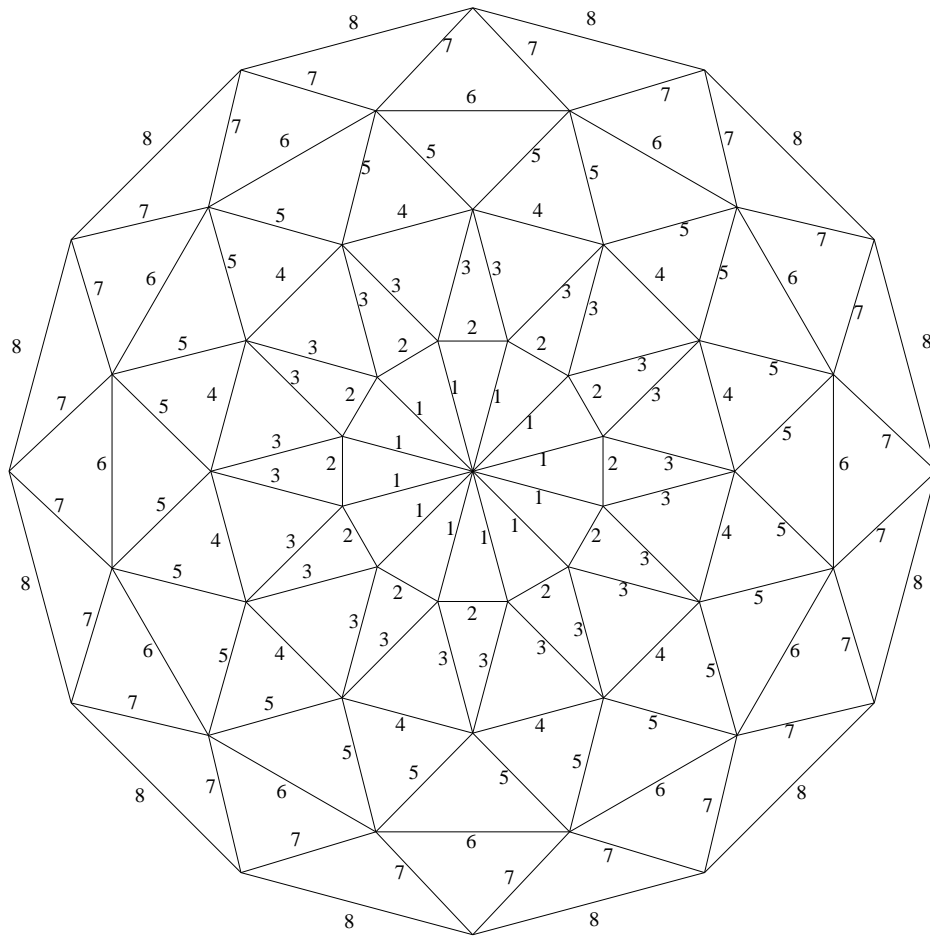


Figure 3.3 (b) Lamella Dome with Eight Different Member Groups.

3.3 Mathematical Model of Optimum Design Problem of Lamella Domes According to LRFD-AISC

In three dimensional modeling of lamella domes, joints are considered to be rigidly connected in order to represent real behavior of these domes. As a result of such modeling, all members of the lamella dome are exposed to both axial forces and bending moments. Consequently, axial stiffness of the members of lamella dome are influenced by the bending moments directly because of members' slenderness, which requires the consideration of the geometric nonlinearity in the analysis of these structures.

The design of lamella domes requires the selection of steel sections for its members from a standard steel pipe section tables such that the dome satisfies the serviceability and strength requirements specified by the code of practice while the economy is observed in the overall or material cost of the dome. When the design constraints are implemented from LRFD-AISC [38-39] in the formulation of the design problem the following mathematical programming problem is obtained.

$$\min W = \sum_{i=1}^{ng} m_i \sum_{j=1}^{s_i} l_j \quad (3.7)$$

Subject to;

$$\delta_k < \delta_{ku} \quad , \quad k = 1, 2, \dots, p \quad (3.8)$$

For $\frac{P_u}{\phi P_n} \geq 0.2$;

$$\frac{P_u}{\phi P_n} + \frac{8}{9} \left(\frac{M_{ux}}{\phi_b M_{nx}} + \frac{M_{uy}}{\phi_b M_{ny}} \right) \leq 1 \quad (3.9)$$

For $\frac{P_u}{\phi P_n} < 0.2$;

$$\frac{P_u}{2\phi P_n} + \left(\frac{M_{ux}}{\phi_b M_{nx}} + \frac{M_{uy}}{\phi_b M_{ny}} \right) \leq 1 \quad (3.10)$$

$$\phi_v V_{nr} \geq V_{ur} \quad , \quad r = 1, 2, \dots, nm \quad (3.11)$$

where m_i in equation (3.7) gives the unit weight of a lamella dome member belonging to group i selected from steel pipe section list of LRFD-AISC, s_i is the total number of members in group i , and ng is the total number of groups in the dome system. l_j is the length of member j . δ_k in equation (3.8) is the displacement of joint k and δ_{ku} is its upper bound. The joint displacements are computed by carrying out elastic-critical load analysis for lamella dome system.

Equations (3.9) and (3.10) represent the strength requirements for a member subjected to both bending and axial force according to LRFD. In these inequalities ϕ_b is the resistance factor for flexure given as 0.9, ϕ_c is the resistance factor for compression given as 0.85, M_{ux} is the required flexural strength relating to strong axis (x) bending, M_{uy} is the required flexural strength related with the weak axis (y) bending, M_{nx} and M_{ny} are the nominal flexural strength related with strong axis (x) bending and weak axis (y) bending respectively. P_u is the required compressive strength, and P_n is the nominal compressive strength which is computed from;

$$P_n = A_g F_{cr} \quad (3.12)$$

Subjected to;

For $\lambda_c \leq 1.5$

$$F_{cr} = (0.658^{\lambda_c^2}) F_y \quad (3.13)$$

For $\lambda_c > 1.5$

$$F_{cr} = \left[\frac{0.877}{\lambda_c^2} \right] F_y \quad (3.14)$$

where in equation (3.12) A_g is the gross area of a lamella dome member, and F_{cr} is found from equation (3.13) or (3.14) in which F_y is the specified yield stress taken as 250 MPa and λ_c is obtained from;

$$\lambda_c = \frac{Kl}{r\pi} \sqrt{\frac{F_y}{E}} \quad (3.15)$$

where K is the effective length factor taken as 1, l is the length of a dome member, r is governing radius of gyration about the axis of buckling, and E is the modulus of elasticity.

Equation (3.11) represents the shear strength requirement in load and resistance factor design according to LRFD. In this inequality ϕ_v represents the resistance factor for shear given as 0.9, V_{nr} is the nominal strength in shear and V_{ur} is the factored service load shear for member r .

The programming problem described with equations (3.7) to (3.11) is discrete programming problem due to the fact that pipe sections for the groups of the dome are to be selected from the available steel pipe section lists. Harmony search method is used to obtain the solution of this problem. It should be pointed out that the nominal flexural strength and the axial strength of the dome members are calculated by carrying out elastic critical load factor analysis of the dome as explained in Chapter 2.

CHAPTER 4

HARMONY SEARCH METHOD BASED OPTIMUM DESIGN ALGORITHM

4.1 General Concept of Harmony Search Algorithm

Numerical methods which have the shortcomings, such as using gradient information and motivated improving the solution in the neighborhood of a starting point, have compelled researchers to use meta-heuristic algorithms counterfeiting a natural phenomena such as genetic algorithms (GAs), tabu search (TS), simulated annealing (SA), evolutionary strategies (ES), etc.

Among these methods, a new meta-heuristic algorithm is called harmony search (HS) method is developed by Geem [16]. This numerical technique simulates the musical performance process that comes about once a musician is looking for a better state of harmony. Jazz improvisation seeks to find musically pleasing harmony similar to the optimum design process which seeks to find the optimum solution. The HS algorithm demands fewer mathematical requirements and does not need initial values for decision variables and the derivative information of the objective function and constraints when compared to mathematical programming methods mentioned above. Thereby, the harmony search method enables easy programming among the combinatorial optimization algorithms.

The harmony search method consists of five basic steps [40];

Step 1. Initialize the problem and algorithm parameters.

Step 2. Initialize the harmony memory.

Step 3. Improvise a new harmony.

Step 4. Update the harmony memory.

Step 5. Check the stopping criteria.

The detailed descriptions of these steps can be useful to comprehend the HS method clearly.

Step 1. Harmony search parameters are initialized.

A possible value range for each design variable of the optimum design problem is specified as:

$$\text{Minimize } f(\mathbf{x}), \mathbf{x} \in \mathbf{X} \quad (4.1)$$

$$\text{Subject to } g(\mathbf{x}) \geq 0 \text{ and } h(\mathbf{x}) = 0 \quad (4.2)$$

where; $f(\mathbf{x})$ is the objective function and $g(\mathbf{x})$ is the inequality constraint function; $h(\mathbf{x})$ is the equality constraint function. \mathbf{x} is the set of each decision variable, x_i , and \mathbf{X} is the set of the possible range of values for each decision variable, that is ${}_{L}x_i \leq X_i \leq {}_{U}x_i$, where ${}_{L}x_i$ and ${}_{U}x_i$ are the lower and upper bounds for each decision variable.

A pool is constructed by collecting these values together from which the algorithm selects values for the design variables. Furthermore the number of solution vectors in harmony memory (HMS) that is the size of the harmony memory matrix, harmony considering rate (HMCR), pitch adjusting rate (PAR) and the maximum number of searches are also specified in this step.

Step 2. Harmony memory matrix (HM) is initialized.

Harmony memory matrix is initialized. Each row of harmony memory matrix contains the values of design variables which are randomly selected feasible solutions from the design pool for that particular design variable. Hence, this matrix has n columns where n is the total number of design variables, and HMS rows are selected in the first step. HMS is similar to the total number of individuals in the population matrix of the genetic algorithm. The harmony memory matrix has the following form:

$$[H] = \begin{bmatrix} x_{1,1} & x_{2,1} & \dots & \dots & x_{n-1,1} & x_{n,1} \\ x_{1,2} & x_{2,2} & \dots & \dots & x_{n-1,2} & x_{n,2} \\ \dots & \dots & \dots & \dots & \dots & \dots \\ \dots & \dots & \dots & \dots & \dots & \dots \\ x_{1,hms-1} & x_{2,hms-1} & \dots & \dots & x_{n-1,hms-1} & x_{n,hms-1} \\ x_{1,hms} & x_{2,hms} & \dots & \dots & x_{n-1,hms} & x_{n,hms} \end{bmatrix} \quad (4.3)$$

$x_{i,j}$ is the value of the i^{th} design variable in the j^{th} randomly selected feasible solution. These candidate designs are sorted such that the objective function value corresponding to the first solution vector is the minimum. In other words, the feasible solutions in the harmony memory matrix are sorted in descending order according to their objective function values. It is worthwhile to mention that only the feasible designs which satisfy the constraints are inserted into harmony memory matrix. Those designs having a small infeasibility are also included in the harmony memory matrix with a penalty on their objective

function. A detailed flowchart for the improvisation of a new harmony memory matrix is given in Figure 4.1.

Step 3. New harmony memory matrix is improvised.

In generating a new harmony matrix the new value of the i^{th} design variable can be chosen from any discrete value within the range of i^{th} column of the harmony memory matrix with the probability of $HMCR$ which varies between 0 and 1. In other words, the new value of x_i can be one of the discrete values of the vector $\{x_{i,1}, x_{i,2}, \dots, x_{i,hms}\}^T$ with the probability of $HMCR$. The same is applied to all other design variables. In the random selection, the new value of the i^{th} design variable can also be chosen randomly from the entire pool with the probability of $1 - HMCR$. That is

$$x_i^{new} = \begin{cases} x_i \in \{x_{i,1}, x_{i,2}, \dots, x_{i,hms}\}^T & \text{with probability } HMCR \\ x_i \in \{x_1, x_2, \dots, x_{ns}\}^T & \text{with probability } (1 - HMCR) \end{cases} \quad (4.4)$$

where ns is the total number of values for the design variables in the pool. If the new value of the design variable is selected among those of harmony memory matrix, this value is then checked whether it should be pitch-adjusted. This operation uses pitch adjustment parameter PAR that sets the rate of adjustment for the pitch chosen from the harmony memory matrix as follows:

$$\text{Is } x_i^{new} \text{ to be pitch-adjusted? } \begin{cases} \text{Yes} & \text{with probability of } PAR \\ \text{No} & \text{with probability of } 1 - PAR \end{cases} \quad (4.5)$$

Supposing that the new pitch-adjustment decision for x_i^{new} came out to be yes from the test and if the value selected for x_i^{new} from the harmony memory is the k^{th} element in the general discrete set, then the neighboring value $k+1$ or

k-1 is taken for new x_i^{new} . This operation prevents stagnation and improves the harmony memory for diversity with a greater change of reaching the global optimum.

Constraint handling: Once the new harmony vector x_i^{new} is obtained using the above-mentioned rules, it is then checked whether it violates problem constraints. If the new harmony vector is severely infeasible, it is discarded. If it is slightly infeasible, there are two ways to follow. One is to include them in the harmony memory matrix by imposing a penalty on their objective function value. In this way the violated harmony vector which may be infeasible slightly in one or more constraints, is used as a base in the pitch adjustment operation to provide a new harmony vector that may be feasible. The other way is to use larger error values such as 0.08 initially for the acceptability of the new design vectors and reduce this value gradually during the design cycles and use finally an error value of 0.001 towards the end of the iterations. This adaptive error strategy is found quite effective in handling the design constraints in large design problems.

Step 4. Harmony Memory matrix is updated.

After selecting the new values for each design variable the objective function value is calculated for the new harmony vector. If this value is better than the worst harmony vector in the harmony matrix, it is then included in the matrix while the worst one is taken out of the matrix. The harmony memory matrix is then sorted in descending order by the objective function value.

Step 5. Steps 3 and 4 are repeated until the termination criterion which is the pre- selected maximum number of cycles is reached. This number is selected large enough such that within this number of design cycles no further improvement is observed in the objective function.

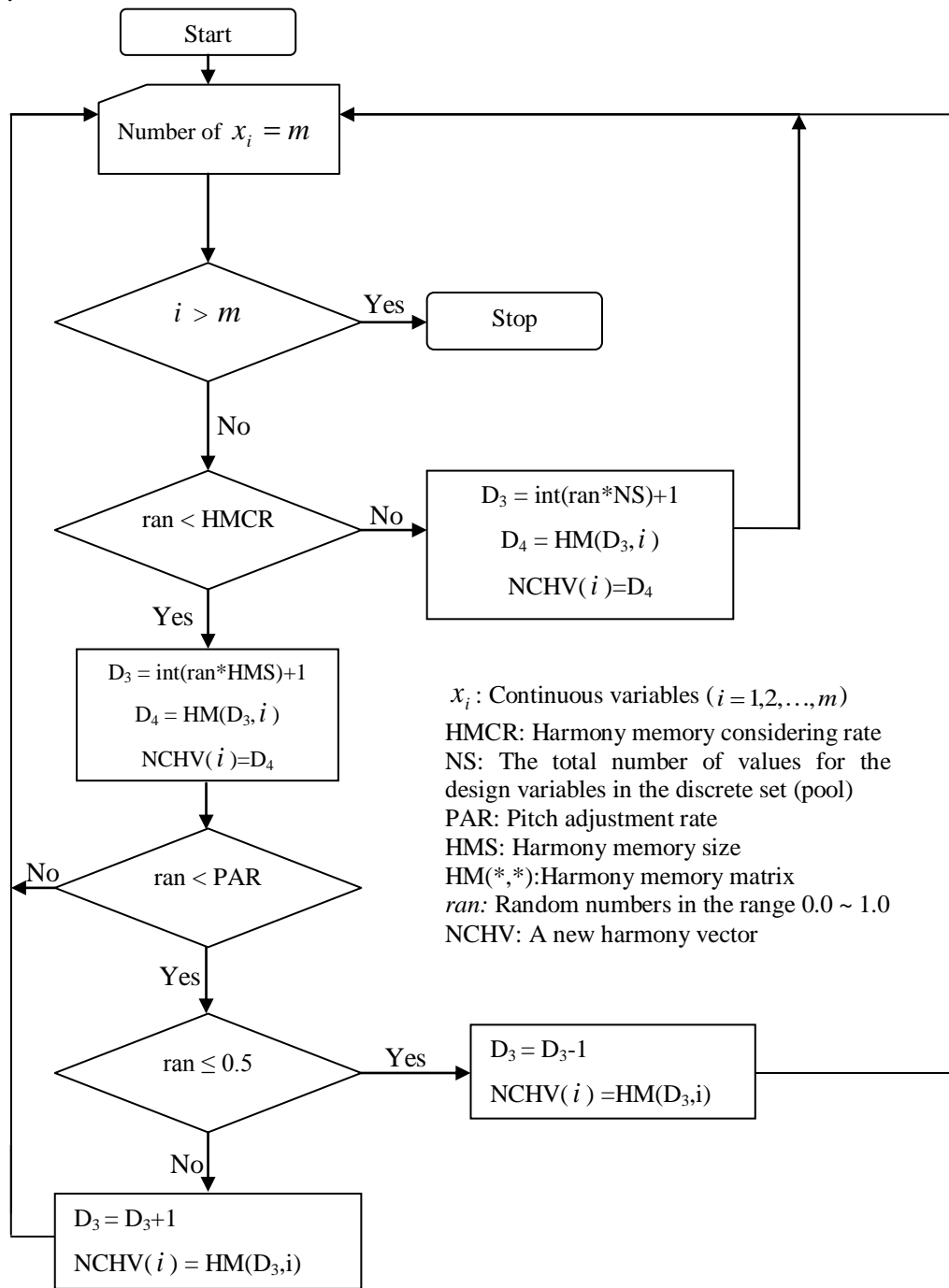


Figure 4.1 Improvisation of a new harmony memory vector.

4.2 A Harmony Search Algorithm Based Optimum Design Method For Single Layer Lamella Domes

Optimum topological design problem of single layer lamella domes under a given loading case, mathematical formulation of which is shown in Equations 3.7-3.11, is solved by using harmony search method. The steps of the design algorithm developed are given as follows;

1. Prepare the discrete sets. In this step, discrete design pools are prepared for the design variables since there are three different types of design variables, three different design pools are prepared; one for each. There are a set of steel sections selected from the available pipe section lists, a set of discrete height values and a set of total ring numbers. The steel pipe sections, height values, and number of rings are sorted in ascending order according to weight per meter, minimum height to maximum height, and minimum ring number to maximum ring number, respectively. The design pool for the total number of rings for the dome contains 4 values that are 3, 4, 5 and 6. For the height of the crown a list is prepared starting from 1 m to 8.75 m with the increment of 0.25 m, resulting 32 discrete values as shown in Table 4.1. The size design variables (members' ready sections) are selected from 37 steel pipe sections given in LRFD-AISC [38] as listed in Table 4.2. The sectional designations selected vary from PIPST13 to PIPDEST203 where abbreviations ST, EST, and DEST stands for standard weight, extra strong, and double-extra strong respectively.
2. Select the values of harmony parameters. The harmony memory size HMS, the harmony memory considering rate HMCR and the pitch adjustment rate PAR are selected. These parameters are decided after carrying out several trials.

3. Generate a harmony memory matrix. Select randomly total number of rings, crown height and sequence number of a steel pipe section from the discrete list for each group in the dome. The sequence numbers of steel pipe sections, height values, and total number of rings varying between 1 to total number of pipe sections, heights, and total number of ring are included in the design pool. These sequence numbers are treated as design variable. For example, if there are 37 steel pipe sections, 32 height values, and 4 ring numbers in the design pool and 6 member groups in the truss dome to be designed then the Harmony Search algorithm selects randomly integer numbers which vary from 1 to 37 for steel pipe sections, 1 to 32 for height values, and 1 to 4 for ring number for each member group. Once the selection is carried out for each member group, the cross sectional properties of each steel pipe section become available from the design pool. The structure is then analyzed under the external loads with these sections to find out whether its response is within the limitations imposed by the design code.

Table 4.1 Discrete Set of Height Values.

Sequence Number	Height (m)	Sequence Number	Height (m)
1	1.00	17	5.00
2	1.25	18	5.25
3	1.50	19	5.50
4	1.75	20	5.75
5	2.00	21	6.00
6	2.25	22	6.25
7	2.50	23	6.50
8	2.75	24	6.75
9	3.00	25	7.00
10	3.25	26	7.25
11	3.50	27	7.50
12	3.75	28	7.75
13	4.00	29	8.00
14	4.25	30	8.25
15	4.50	31	8.50
16	4.75	32	8.75

Table 4.2 Dimensions and Properties of Steel Pipe Sections.

1	2	3	4	5	6	7	8	9	10	11
1	PIPST13	21,3	2,77	160	0,00704	0,661	6,63	14,1	0,953	0,0125
2	PIPEST13	21,3	3,73	205	0,00827	0,777	6,35	16,5	1,16	0,0159
3	PIPST19	26,7	2,87	217	0,0156	1,17	8,48	31,2	1,65	0,0165
4	PIPEST19	26,7	3,91	282	0,0188	1,41	8,16	37,6	2,06	0,0215
5	PIPST25	33,4	3,38	320	0,0365	2,19	10,7	73	3,07	0,0245
6	PIPEST25	33,4	4,55	412	0,044	2,63	10,3	87,9	3,82	0,0317
7	PIPST32	42,2	3,56	431	0,0812	3,85	13,7	162	5,32	0,0332
8	PIPST38	48,3	3,68	518	0,13	5,38	15,8	260	7,38	0,0397
9	PIPEST32	42,2	4,85	569	0,101	4,79	13,3	202	6,8	0,0439
10	PIPEST38	48,3	5,08	692	0,164	6,79	15,4	327	9,56	0,0531
11	PIPST51	60,3	3,91	691	0,276	9,15	20	552	12,4	0,0534
12	PIPEST51	60,3	5,54	947	0,359	11,9	19,5	718	16,6	0,0734
13	PIPST64	73	5,16	1100	0,635	17,4	24	1270	23,8	0,0846
14	PIPST76	88,9	5,49	1440	1,26	28,3	29,6	2520	38,3	0,111
15	PIPEST64	73	7,01	1450	0,799	21,9	23,5	1600	30,6	0,112
16	PIPDEST51	60,3	11,1	1710	0,544	18	17,8	1090	27,3	0,132
17	PIPST89	102	5,74	1800	2,08	40,8	34	4160	55	0,133
18	PIPEST76	88,9	7,62	1940	1,62	36,4	28,9	3240	50,4	0,15
19	PIPST102	114	6,02	2040	2,98	52,3	38,2	5950	70,1	0,158
20	PIPEST89	102	8,08	2440	2,7	52,9	33,3	5400	73,1	0,183
21	PIPDEST64	73	14	2590	1,19	32,6	21,4	2390	49,6	0,2
22	PIPST127	141	6,55	2750	6,23	88,4	47,6	12500	118	0,214
23	PIPEST102	114	8,56	2790	3,91	68,6	37,4	7820	93,9	0,219
24	PIPDEST76	88,9	15,2	3530	2,5	56,2	26,6	4990	83,9	0,271
25	PIPST152	168	7,11	3540	11,5	137	57	23000	182	0,277
26	PIPEST127	141	9,53	3920	8,53	121	46,6	17100	165	0,304
27	PIPDEST102	114	17,1	5170	6,27	110	34,8	12500	161	0,402
28	PIPST203	219	8,18	5300	29,6	270	74,7	59100	356	0,417
29	PIPEST152	168	11	5430	16,8	200	55,6	33600	272	0,418
30	PIPDEST127	141	19,1	7280	13,9	197	43,7	27800	285	0,564
31	PIPST254	273	9,27	7460	65,1	477	93,4	130000	628	0,591
32	PIPEST203	219	12,7	8110	43,4	396	73,2	86800	534	0,634
33	PIPST305	324	9,53	9390	116	716	111	232000	940	0,724
34	PIPDEST152	168	21,9	10100	27,5	327	52,2	55000	473	0,777
35	PIPEST254	273	12,7	10200	87	637	92,4	174000	849	0,8
36	PIPEST305	324	12,7	12700	154	951	110	308000	1260	0,956
37	PIPDEST203	203	22,2	13600	66,9	611	70,1	134000	857	1,06

where; Column 1 of Table 4.2 shows the sequence number, Column 2 is the sectional designation of the pipe sections, Column 3 is the outside diameter (mm), Column 4 is the wall thickness (mm), Column 5 is the area (mm²), Column 6 is the moment of inertia/10⁶ (mm⁴), Column 7 is the elastic section modulus/10³ (mm³), Column 8 is the governing radius of gyration (mm), Column 9 is the torsional constant for a section/10³ (mm⁴), Column 10 is the plastic section modulus/10³ (mm³), and Column 11 is the weight per meter Plain Ends (kN), respectively.

As an example typical harmony memory matrix is shown below for a dome where the members are collected in six different groups.

$$[H] = \begin{bmatrix} 1 & 11 & 25 & 33 & 14 & 17 & 13 & 19 \\ 1 & 11 & 25 & 31 & 14 & 17 & 13 & 22 \\ 1 & 11 & 25 & 31 & 14 & 14 & 17 & 19 \\ 1 & 12 & 25 & 31 & 14 & 17 & 13 & 22 \\ 1 & 13 & 25 & 33 & 14 & 17 & 13 & 19 \\ 1 & 11 & 25 & 33 & 17 & 14 & 13 & 19 \\ 1 & 11 & 25 & 33 & 14 & 19 & 13 & 19 \\ 1 & 11 & 25 & 33 & 15 & 19 & 13 & 19 \\ 1 & 10 & 26 & 31 & 14 & 17 & 13 & 22 \\ 1 & 13 & 25 & 31 & 14 & 17 & 13 & 22 \end{bmatrix}$$

Each row of this matrix represents a potential design candidate for the dome. The numbers seen in this matrix are the sequence numbers of design variables randomly selected from discrete sets. The first row of this matrix represents the best design at that design cycle. The first column presents the ring numbers. The sequence number 1 selected by the algorithm stands for 3 rings. The second column represents the height values. The sequence number 11 selected by algorithm symbolizes 3.5 m a height for the dome. The remaining columns are the sequence numbers from pipe sections list for each group. The pipe section whose sequence number is 25 in the list which is PIPST 152 is selected

for member group 1. Sequence number 33 corresponds to PIPST 305 which is the pipe section adopted for group 2. The rest of the sections are given in columns 5, 6, 7, and 8.

4. Generate the geometrical data such as member incidences and joint coordinates, automatically using the values selected for the total number of rings and crown height as explained in Chapter 3.

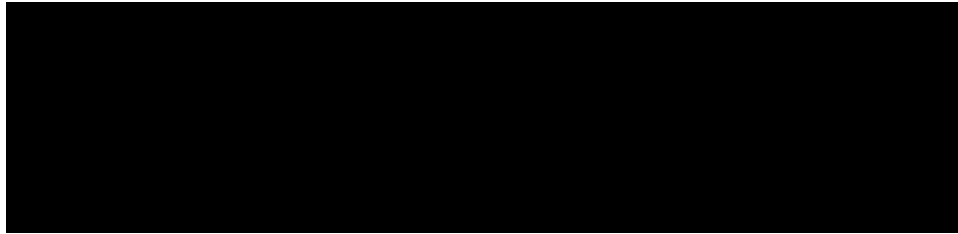
5. Carry out the nonlinear elastic critical load analysis of the steel dome with the tubular sections selected for member groups until the ultimate load factor is reached and check whether there is a loss of stability at any stage of this nonlinear analysis as explained in Chapter 2. If the loss of stability occurs then this selected design vector is taken out from harmony memory matrix and replaced by a new design vector that is selected randomly again. This replacement process is repeated until a design vector is determined that does not have instability problem. This vector is then checked whether or not it satisfies the design constraints. If it does not satisfy it is once more discarded. However, if it is slightly infeasible it is considered for the harmony memory matrix.

6. Check whether the new design vector selected should be pitch-adjusted as explained in step 3 of the harmony search method.

7. Calculate the objective function value for the newly selected design vector. If this value is better than the worst harmony vector in the harmony matrix, it is then included in the matrix while the worst one is taken out of the matrix. The harmony memory matrix is then sorted in descending order by the objective function value. If the previous example is considered once more, the harmony memory matrix includes the sequence numbers of design variables and the weight (kg) which is the objective function of the dome (Table 4.3).

Table 4.3 A harmony set of a designed dome.

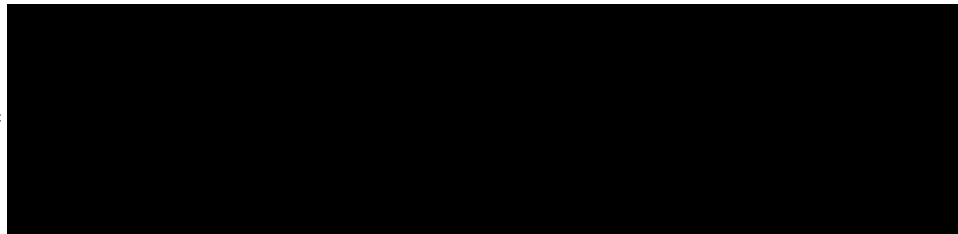
$[H]=$

A large black rectangular box redacting the content of Table 4.3, which would represent a harmony set matrix.

When the newly selected design vector, which is the 3rd row, is better than the worst harmony vector, the worst one is discarded from matrix and the new one is added as seen in Table 4.4.

Table 4.4 New harmony set of a designed dome.

$[H]=$

A large black rectangular box redacting the content of Table 4.4, which would represent the updated harmony set matrix.

8. Repeat steps 2 and 6 until the pre-selected maximum number of iterations is reached. The maximum number of iterations is selected large enough such that within this number of design cycles no further improvement is observed in the objective function.

The general flow diagram of the optimum topological design of single layer lamella domes, based upon Harmony Search Method, can be described as in following chart;

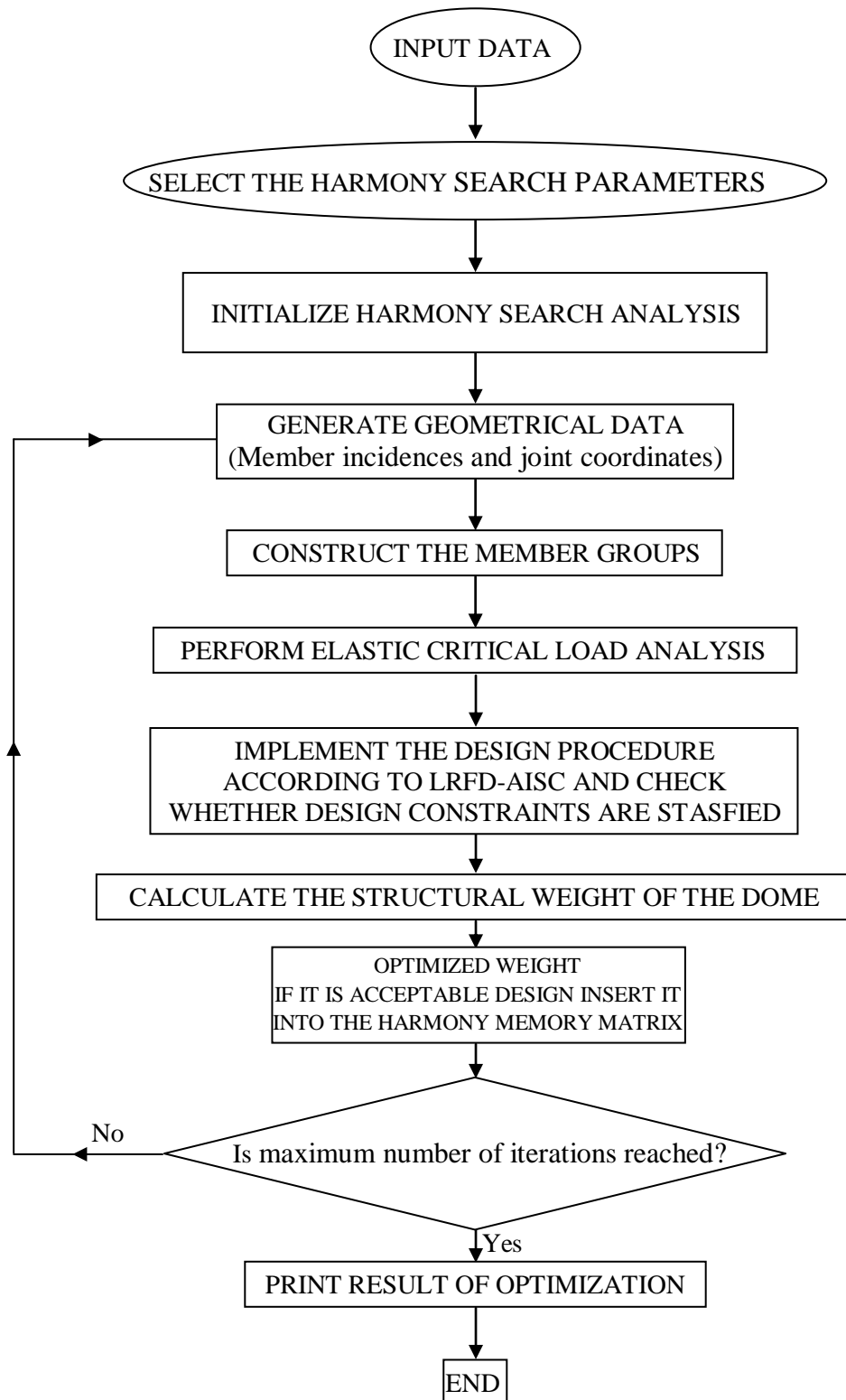


Figure 4.2 Flowchart of Harmony Search method based optimum design of algorithm.

CHAPTER 5

DESIGN EXAMPLES

The design algorithm presented is used to determine the optimum number of rings, the crown height and the circular steel hollow section designations for the single layer lamella dome shown in Figure 3.1. The preparation of the design pool, for the steel pipe sections, the height of the crown and the total number of rings, is explained in detail in the previous chapter. The modulus of elasticity for the steel is taken as 205 kN/mm^2 and the shear modulus is taken as 81 kN/mm^2 . The diameter of the dome is taken as 20 m. The limitations imposed on the joint displacements are given in Table 5.1.

Table 5.1 Displacement restrictions of the single layer lamella dome.

Joint number	Displacement restrictions (mm)		
	X-direction	Y-direction	Z-direction
1	-	-	28
2	33	33	28
3	33	33	28

Harmony memory matrix size is initially taken as 20. However, the same example is designed several times using different harmony memory matrix size which was changed from 20 to 50. In the mean time harmony memory considering rate (HMCR) and pitch-adjusting rate (PAR) are varied between 0.60 to 0.90 and 0.20 to 0.45 respectively in order to determine the most

appropriate values for the design problem under consideration. Table 5.2 shows the effect of different values of harmony search algorithm parameters on the optimum design. Different set of values yields different minimum weights. Among these the lightest dome is selected which is the fourth one in the table.

Table 5.2 The effect of Harmony Search algorithm parameters.

Analysis	HMS	HMCR	PAR	Weight (kg)	Height (m)
1	50	0.80	0.30	4214.9	3.75
2	30	0.90	0.30	4066.8	5
3	20	0.90	0.45	4038.8	5.75
4	50	0.85	0.40	4034.2	6.25

It is apparent from Table 5.2 that the selection of the above parameters is problem dependent. The total number of iterations is taken as 20000 in each design case. This number is determined after carrying out several designs with a larger number of searches. It is noticed that the result obtained within the 20000 searches remains the same even if the search continues up to 50000 for a better design. The design obtained in the last search is considered to be the optimum solution. The member grouping is decided such that the total number of groups in the dome becomes twice the total number of rings in the design problem.

The dome is considered to be subjected to three loading case as follows;

$$1. \quad P \quad (5.1)$$

$$2. \quad D + P \quad (5.2)$$

$$3. \quad D + P + W \quad (5.3)$$

where; P is the equipment load acting on crown of the dome, D is the dead load, and W is the wind load.

5.1 CASE 1 (P)

In this case dome is considered to be subjected to equipment loading of 500kN at its crown as shown in Figure 3.1. The optimum sectional designations for each group and the height obtained for the dome with different number of rings are given in Table 5.3. It is noticed in all these cases that the strength limitations are dominant in the design problem. In the optimum domes while the strength ratios were equal to 1 or very close to 1, the restricted displacements are much less than their upper bounds. Furthermore, it is clear that the lightest dome among the four optimum geometries is the one which has the least number of rings. It is apparent that the dome with a greater number of rings has more members which naturally yield a heavier structure. Hence the optimum number of rings for the lamella dome is three. All joints on the last ring are considered to be pin support for this case. The optimum dome obtained is shown in Figures 5.1 and 5.2.

Table 5.3 Optimum design for the single layer lamella dome for load case 1.

Group Number	Optimum Section Designations		
	3 rings	4 rings	5 rings
1	PIPST 127	PIPST 152	PIPST 203
2	PIPEST 89	PIPEST 89	PIPST 19
3	PIPST 64	PIPST 64	PIPST 64
4	PIPST 76	PIPST 76	PIPST 102
5	PIPST 64	PIPST 64	PIPST 64
6	PIPST 13	PIPST 76	PIPST 76
7	N.A	PIPST 64	PIPST 64
8	N.A	PIPST 13	PIPST 76
9	N.A	N.A	PIPST 64
10	N.A	N.A	PIPST 13
Optimum Height (m)	6.25	5.25	3.25
Max.Displacement (mm)	2.38	4.77	25.16
Max. Strength Ratio	0.98	1.00	1.00
Weight (kg)	4034.2	4502.1	4873.1

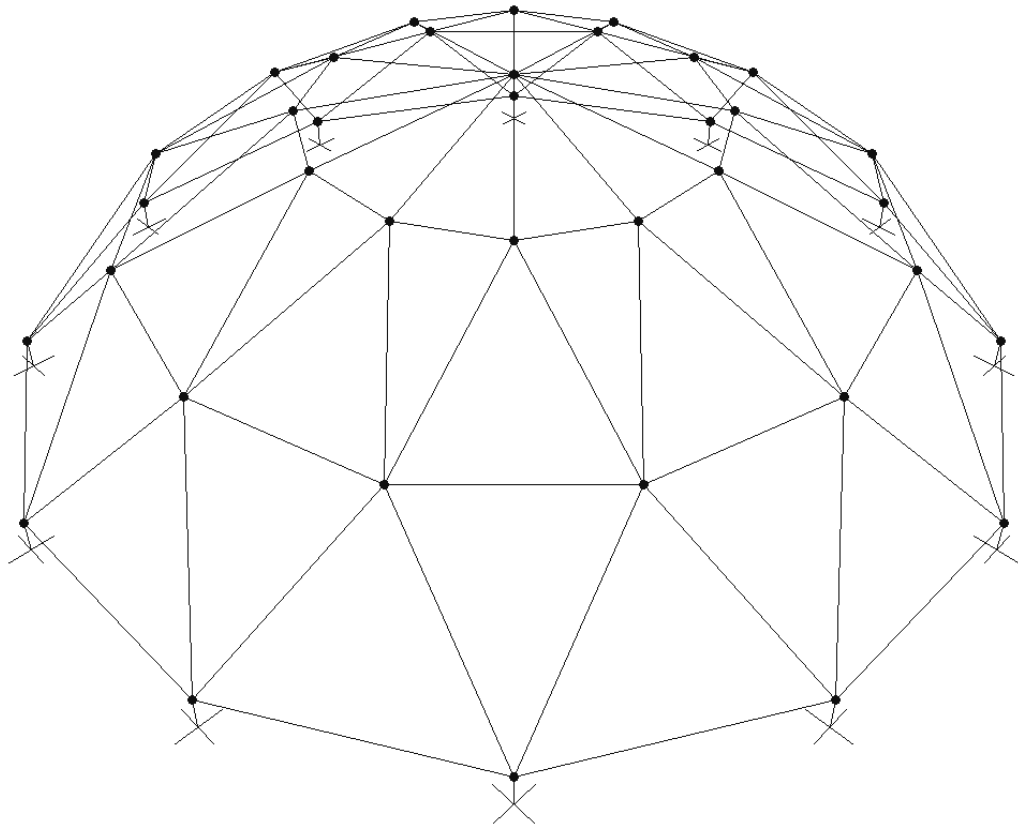


Figure 5.1 3D view of optimum single layer lamella dome.

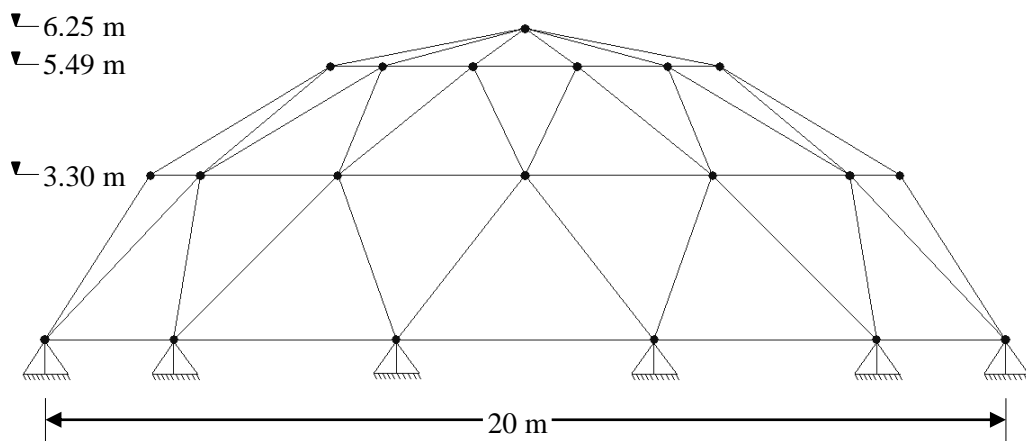


Figure 5.2 Side view of optimum single layer lamella dome.

The elastic critical load analysis of the optimum dome is shown in Table 5.4. The initial load factor is taken as 0.1 and it is increased to 1.0 with the increment of 0.1 during the elastic critical load cycles. The number of nonlinear analysis iterations required to obtain the convergence in each load factor is given in the second column of Table 5.4. It is interesting to notice that number of iterations vary from 2 iterations to 16 iterations which is the largest allowed number of iteration during elastic critical load cycles.

Table 5.4 Elastic Critical Load Factor Iterations for optimum designed dome for Case 1.

Load Factor	Number of Nonlinear Analysis Iterations
0.1	7
0.2	11
0.3	16
0.4	15
0.5	16
0.6	2
0.7	16
0.8	4
0.9	7
1.0	2

Optimum single layer lamella dome with 4 rings for the load Case 1 is shown in Figures 5.3 and 5.4.

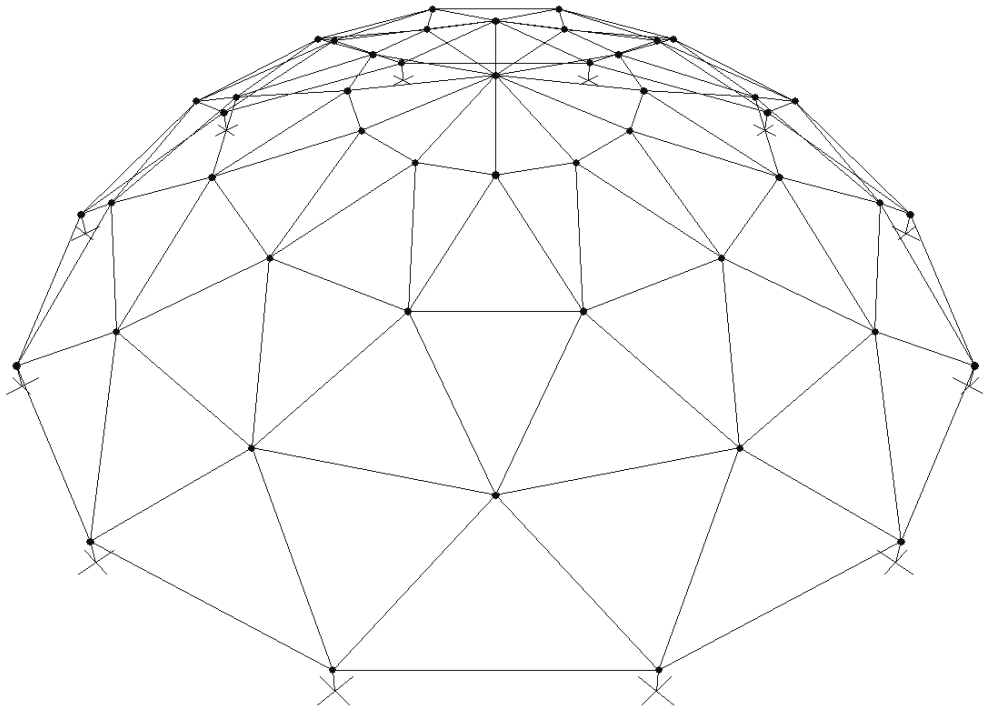


Figure 5.3 3D view of optimum single layer lamella dome with 4 rings.

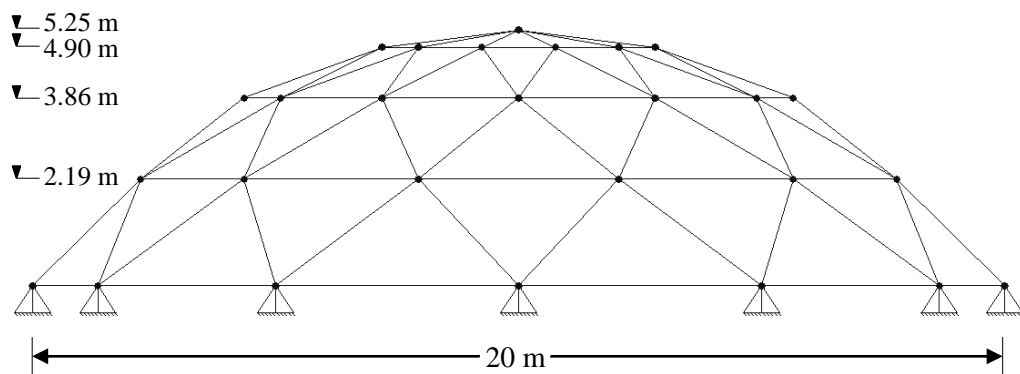


Figure 5.4 Side view of optimum single layer lamella dome with 4 rings.

Figure 5.5 and 5.6 illustrate the optimum design for single layer lamella dome with 5 rings for the load Case 1.

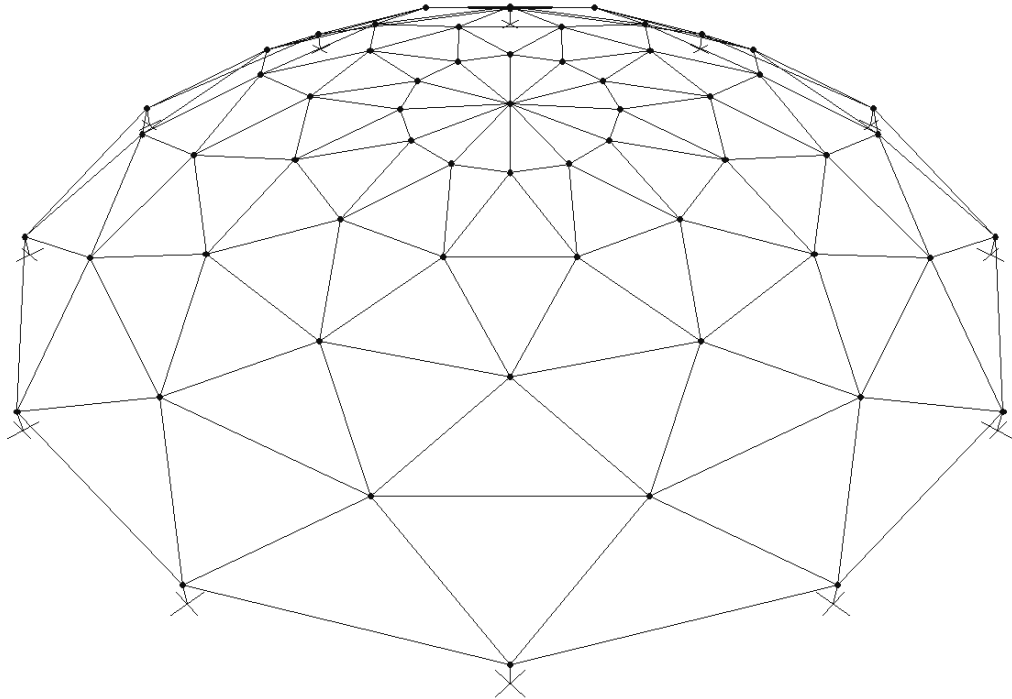


Figure 5.5 3D view of optimum single layer lamella dome with 5 rings.

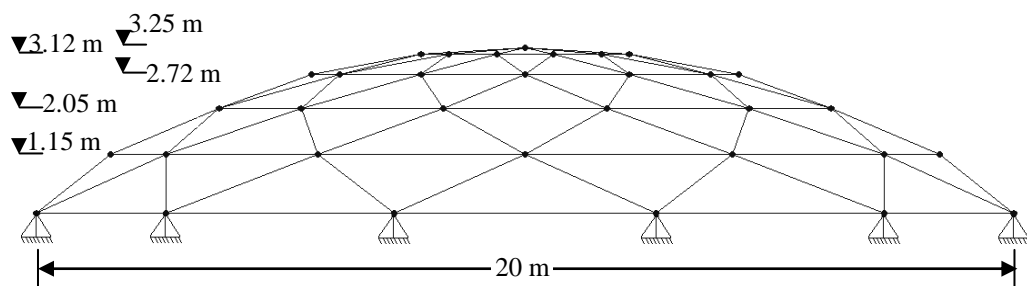


Figure 5.6 Side view of optimum single layer lamella dome with 5 rings.

The same dome is designed once again for only one pin supported joint on the last ring for the same loading case. The joint 31 for the dome with 3 rings, the joint 44 for the dome with 4 rings and the joint 55 for the dome with 5 rings on the last ring is considered to be pin supported and all the other joints on the same ring are considered to be roller-supported. The optimum solutions obtained for this case are given in Table 5.5.

Table 5.5 Optimum design of single layer lamella dome with 3 rings according to different support conditions.

Group Number	Optimum Section Designations		
	3 rings	4 rings	5 rings
1	PIPST 152	PIPST 152	PIPST 203
2	PIPST 305	PIPST 305	PIPEST 305
3	PIPST 76	PIPST 64	PIPEST 64
4	PIPST 89	PIPST 254	PIPST 76
5	PIPST 64	PIPST 76	PIPST 254
6	PIPST 102	PIPST 89	PIPST 76
7	N.A	PIPST 152	PIPEST 51
8	N.A	PIPST 89	PIPST 76
9	N.A	N.A	PIPST 203
10	N.A	N.A	PIPST 127
Optimum Height(m)	3.5	4.25	3.75
Max.Displacement(mm)	12.1	10.23	20.524
Max. Strength Ratio	1.00	1.00	1.00
Weight (kg)	6348.6	9713.3	13279

This system is much heavier than the one with all joints pinned on the last ring because harmony search method selects different steel pipe sections for groups 1, 2, 3, 4, and 6 for 3 rings dome, for groups 2, 4, 5, 6, 7, and 8 for 4 rings dome and for groups 2, 3, 4, 5, 7, 9, and 10 for 5 rings dome for this case. It is apparent from the Table 5.5 that strength constraints are dominant in the design problem and the optimum number of rings for the lamella dome is three (same

as in the previous case). It has to be noted that optimum heights in this case are different from the previous case.

If the lightest system of this case is taken into account, during the optimum design cycles, the first load factor required 4 nonlinear analysis iterations and all the other remaining load factors required 2 nonlinear analysis iterations to obtain the convergence in the axial forces.

5.2 CASE 2 (D + P)

In this case, 3 rings dome, which has the optimum ring number according to Case 1, is considered to be subjected to a combination of dead load and equipment load as presented in Figure 5.7. Equipment load of 500 kN is applied only on the crown of the dome. The sandwich type aluminium cladding is used. The load of this cladding (including frame elements to be used for the girts) is taken as 200 N/m^2 . All joints on the last ring are considered to be pin support for this case.

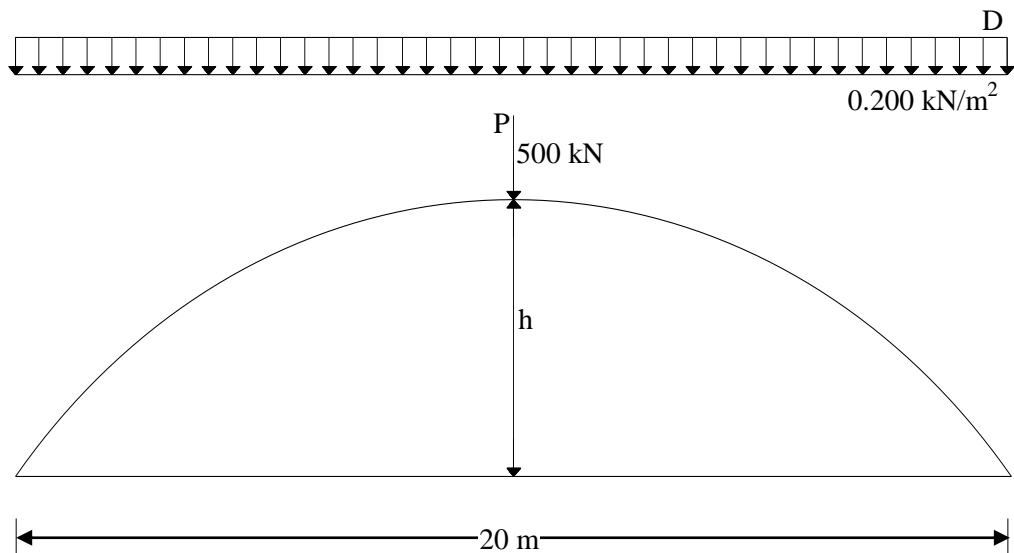


Figure 5.7 Load Case 2 (Dead Load + Equipment Load).

Dead load is converted into equivalent point load for each joint for the sake of simplicity. For this conversion distributed load is multiplied by projected area

of the dome and then this result is divided by joint number of the dome which gives the load acting on each joint. The load value at each joint is given in Table 5.6.

Table 5.6 Loads Acting on Joints for Case 2 (D + P).

Joint Number	Loads Acting on Joints (kN)
1	501.6982
2 - 37	1.6982

The optimum sectional designations obtained by the harmony search based algorithm is demonstrated in Table 5.7. It can be noticed from the table that strength constraint is dominant for this design case.

Table 5.7 Optimum design of single layer lamella dome with 3 rings for load case 2.

Group Number	Optimum Section Designations
	3 rings
1	PIPST 127
2	PIPST 254
3	PIPST 76
4	PIPST 76
5	PIPST 89
6	PIPST 13
Optimum Height (h) (m)	4.5
Max. Displacement (mm)	4.18
Max. Strength Ratio	0.99
Weight (kg)	5456.2

The optimum weight obtained from this case is heavier than the first case in which the single layer lamella dome is subjected to only 500 kN equipment load at its crown. This design is %35.25 heavier than the former case which has the optimum weight of 4034.2 kg. The reason is that, the harmony search algorithm assigns heavy sections to the some group members when the applied loads acting on joints are increased. In the current case, algorithm chooses heavier sections for group 2, 3 and 5 compared to the former case. In addition to this, optimum height of the dome is changed and some differences for the number of nonlinear analysis iterations are observed for optimum design in this case as illustrated in Table 5.8.

Table 5.8 Elastic Critical Load Factor Iterations for optimum design of Case 2.

Load Factor	Number of Nonlinear Analysis Iterations
0.1	15
0.2	15
0.3	3
0.4	3
0.5	2
0.6	11
0.7	3
0.8	8
0.9	16
1.0	3

The optimum design of single layer lamella dome for this case is demonstrated in Figures 5.8 and 5.9. It can be easily discerned from these figures that the

height of the dome is 4.5 m which is 1.75 m less than the former dome which has the 6.25 m optimum height mentioned in load case 1.

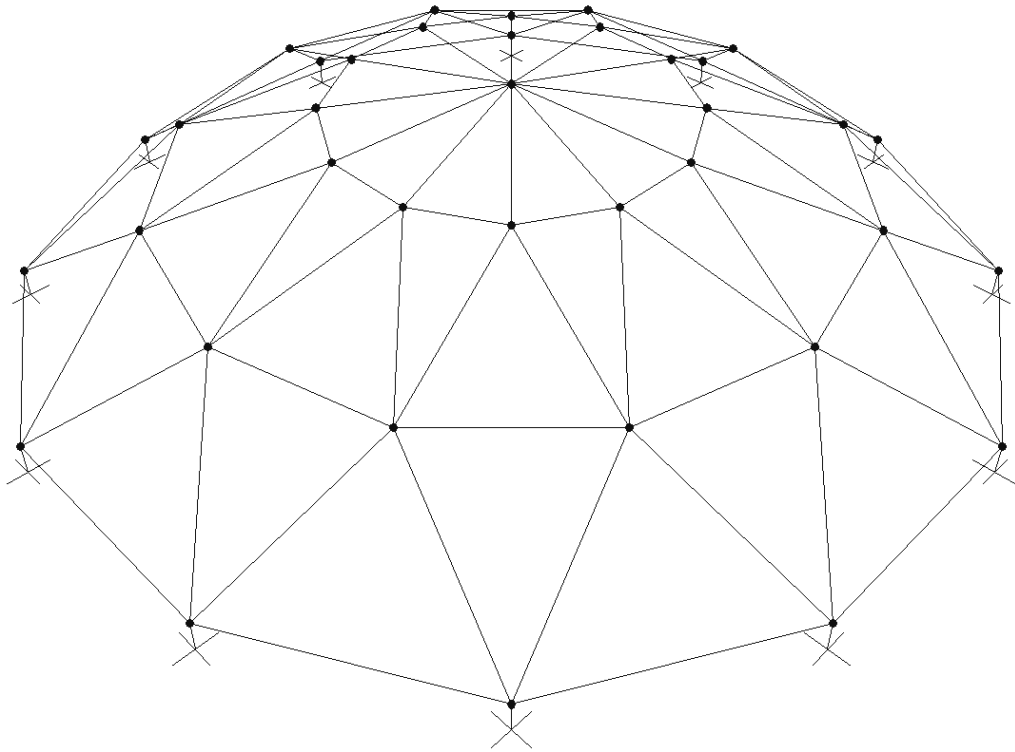


Figure 5.8 3D view of optimum single layer lamella dome for Case 2.

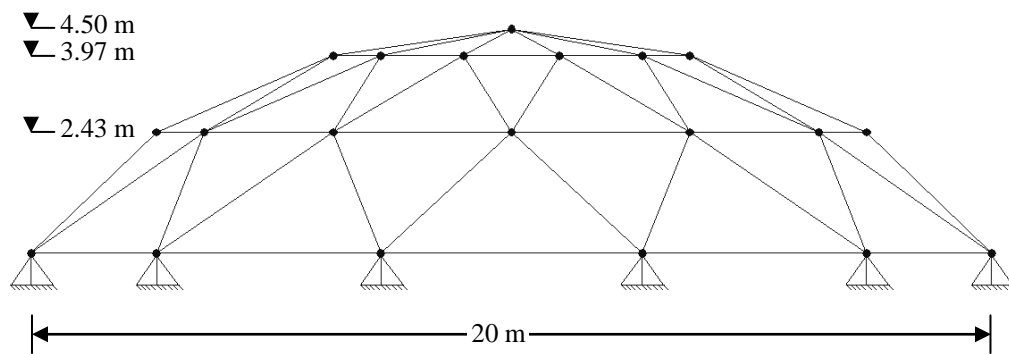


Figure 5.9 Side view of optimum single layer lamella dome for Case 2.

5.3 CASE 3 (D + P + W)

In this case, the dome with 3 rings is designed for the combination of dead load, equipment load acting only on crown of the dome, and the wind load calculated below. The design procedure of wind load (analytical procedure) explained in part 6.5.3 of ASCE 7-05 is followed.

Basic Wind Speed V is taken from Figure 6-1 of ASCE 7-05.

$$V = 40 \text{ m/s (90 mph)}$$

Wind Directionality Factor K_d is taken from Table 6.4 of ASCE 7-05.

$$K_d = 0.85 \text{ (for arched roofs)}$$

Importance Factor I for the building is determined as 1.15 from Table 1.1 of ASCE 7-05.

$$I = 1.15 \text{ (for building category III)}$$

Exposure Category is assumed as C from the definitions given in part 6.5.6 of ASCE 7-05.

Velocity Pressure Exposure Coefficient K_z is taken from Table 6.3 of ASCE 7-05.

The mean height of the roof is 13.125 m. (43.061 feet).

$$K_z = 1.055 \text{ (for exposure C and 43 ft height)}$$

Topographic Factor K_{zt} is calculated from $K_{zt} = (1 + K_1K_2K_3)^2$ where K_1 , K_2 , and K_3 are taken from Figure 6-4 of ASCE 7-05.

It is assumed that there are a 2-D ridge with $H/Lh = 0.30$, 3-D escarpment with $x/Lh = 1.00$ and 2-D ridge with $z/Lh = 0.40$ in the general topology, where;

H : Height of the hill or escarpment relative to the upwind terrain , in meter,

Lh : Distance upwind of crest to where the difference in the ground elevation is half the height of the hill or escarpment, in meter,

K_1 : Factor to account for shape of topographic feature and maximum speed-up effect,

K_2 : Factor to account for reduction in speed-up with distance upwind or downwind of crest,

K_3 : Factor to account for reduction in speed-up with height above local terrain,

x : Distance (upwind or downwind) from the crest to the building site, in meter,

z : Height above local ground level, in meter,

$K_1 = 0.43$, $K_2 = 0.33$, $K_3 = 0.30$ (from Figure 6-4 of ASCE 7-05)

$$K_{zt} = (1 + 0.43 \times 0.33 \times 0.30)^2 = 1.087$$

Gust Effect Factor G is taken as 0.85 directly by assuming the structure as rigid from part 6.5.8 of ASCE 7-05.

$$G = 0.85$$

Enclosure Classification is assumed as enclosed, since all lateral and upper parts of the building are closed and subjected to wind pressure directly.

Velocity Pressure q_z is calculated by using the equation given in part 6.5.10 of ASCE 7-05.

$$q_z = 0.613 * K_z * K_{zt} * K_d * V^2 * I \quad (N/m^2) \quad (5.4)$$

$$q_z = 0.613 * 1.055 * 1.087 * 0.85 * 40^2 * 1.15 \quad (5.5)$$

$$q_z = 1099.5 \text{ kN/m}^2$$

Internal Pressure Coefficients GC_{pi} are found as +0.18 and -0.18 for enclosed buildings from Figure 6-5 of ASCE 7-05. Two signed values (positive and negative) are used according to the code. Plus and minus signs signify pressures acting towards and away from the internal surfaces, respectively.

External Pressure Coefficients C_p are found from Figure 6-6 of ASCE 7-05. The dome is assumed to be separated into three parts as shown in Figure 5.2, such as windward quarter, center half and leeward quarter. Three different external pressure coefficients for these three parts of the dome are calculated with respect to rise-to-span ratio. The rise-to-span ratio, r is $6.25/20=0.3125$ for the dome in which the maximum height (h) of 6.25 m is considered for being safe in wind load calculation, which is obtained from Case 1 with different algorithm parameters rather than optimum solution.

$$C_p = 2.75r - 0.7 = 2.75 * 0.3125 - 0.7 = 0.16 \text{ (for windward quarter)} \quad (5.6)$$

$$C_p = -0.7 - r = -0.7 - 0.3125 = -1.0125 \text{ (for center half)} \quad (5.7)$$

$$C_p = -0.5 \text{ (for leeward quarter)} \quad (5.8)$$

Main Force Resisting Systems

Design wind pressure is calculated from Equation 6.17 of ASCE 7-05:

$$p = qGC_p - q_i(GC_{pi}) \text{ (N / m}^2\text{)} \quad (5.9)$$

where;

$q = q_h$ for roofs, evaluated at height h ,

$q_i = q_h$ for roofs of enclosed buildings,

G : Gust effect factor,

C_p : External pressure coefficient from Figure 6-6 or Figure 6-8 of ASCE 7-05,

(GC_{pi}) : Internal pressure coefficient from Figure 6-5 of ASCE 7-05.

For windward quarter

$$p = 1099.5 \times 0.85 \times (0.16) - 1099.5 \times (\pm 0.18) = \begin{cases} -48.378 \text{ N/m}^2 \\ 347.442 \text{ N/m}^2 \end{cases}$$

For center half

$$p = 1099.5 \times 0.85 \times (-1.0125) - 1099.5 \times (\pm 0.18) = \begin{cases} -1144.1672 \text{ N/m}^2 \\ -748.3472 \text{ N/m}^2 \end{cases}$$

For leeward quarter

$$p = 1099.5 \times 0.85 \times (-0.50) - 1099.5 \times (\pm 0.18) = \begin{cases} -665.1975 \text{ N/m}^2 \\ -269.3775 \text{ N/m}^2 \end{cases}$$

As a result of wind pressure procedure, a positive pressure is detected acting on the windward quarter. This means, wind effects create negative pressure (suction) on the other parts of the dome.

The pieces of optimum design of single layer lamella dome with 3 rings shown in Figure 5.10 and the schematically shown of these pieces are demonstrated in Table 5.9 as below;

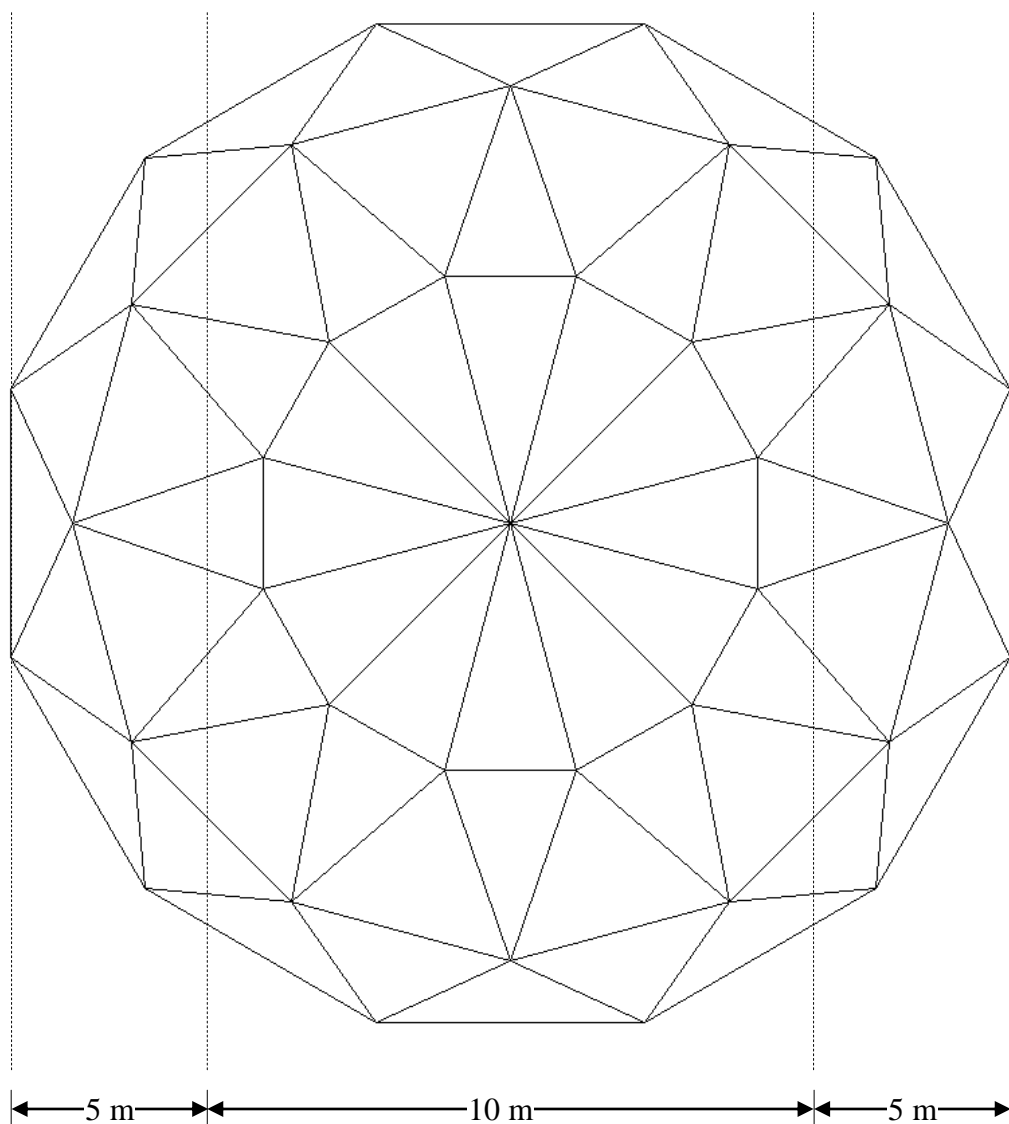


Figure 5.10 Pieces of single layer lamella dome with 3 rings.

Table 5.9 Schematic display of the pieces of the dome with 3 rings.

Whole Structure	Number of Total Joints	: 37
	Number of Total Members	: 96
	Total (Curved) Area	: 415.796 m ²
	Projected Area	: 314.160 m ²
Piece 1	Piece 2	Piece 3
Number of Joints : 7	Number of Joints : 23	Number of Joints : 7
Total Area : 82.41 m ²	Total Area : 191.32 m ²	Total Area : 82.41 m ²
Projected Area : 61.42 m ²	Projected Area : 250.984 m ²	Projected Area : 61.42 m ²

5.3.1 Load Combinations

5.3.1.1 D + P + W (internal pressure coefficient is taken as positive)

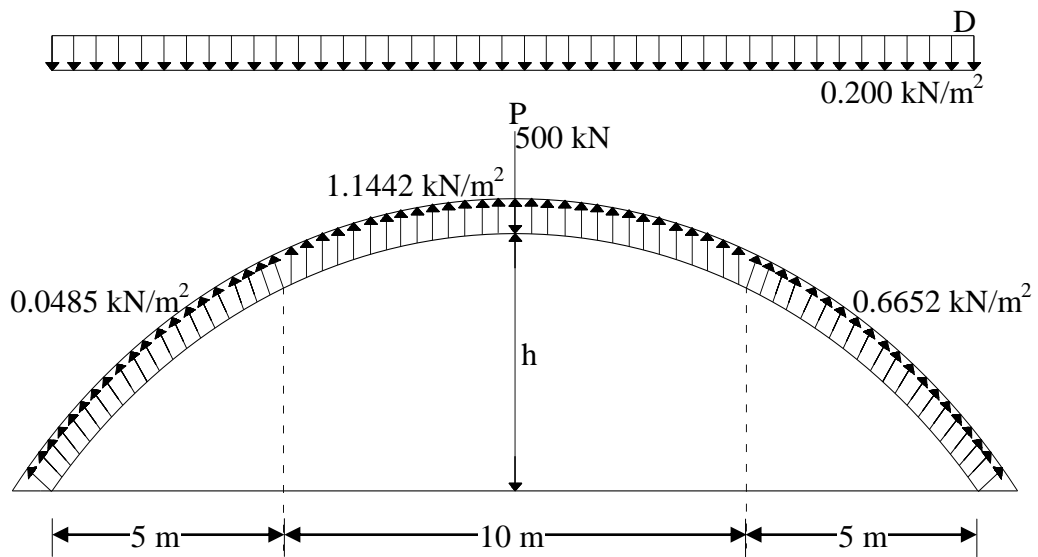


Figure 5.11 Load Case 3.1.1 (Dead Load + Equipment Load + Wind Load (internal pressure coefficient is taken as positive)).

The load combination of dead load, equipment load acting only on crown of the dome, and the wind load (internal pressure coefficient is taken as positive) is shown in Figure 5.11. The loads acting on joints are calculated as follows;

For windward quarter

$$P = (-0.200 \times 61.42 + (0.0485 \times \cos (43.17)^\circ \times 82.41)) / (7 \text{ joints}) \\ = -1.3381 \text{ kN / joint } (\downarrow)$$

$$P = ((-0.0485 \times \sin (43.17)^\circ \times 82.41)) / (7 \text{ joints}) \\ = -0.391 \text{ kN / joint } (\leftarrow)$$

For Center Half

$$P = (-0.200 \times 191.32) / (23 \text{ joints}) = -1.664 \text{ kN / joint } (\downarrow)$$

$$P = (1.1442 \times 250.984) / (23 \text{ joints}) = \frac{12.486 \text{ kN / joint } (\uparrow)}{10.822 \text{ kN / joint } (\uparrow)}$$

For Leeward Quarter

$$P = (-0.200 \times 61.42 + (0.6652 \times \cos (43.17)^\circ \times 82.41)) / (7 \text{ joints}) \\ = 3.957 \text{ kN / joint } (\uparrow)$$

$$P = ((0.6652 \times \sin (43.17)^\circ \times 82.41)) / (7 \text{ joints}) \\ = 5.358 \text{ kN / joint } (\rightarrow)$$

The results obtained for the optimum design of this loading case is given in Table 5.10.

Table 5.10 Optimum design obtained for dome with 3 rings for the case D + P + W (internal pressure coefficient is taken as positive).

Group Number	Optimum Section Designations
	3 rings
1	PIPST 127
2	PIPST 203
3	PIPST 76
4	PIPST 89
5	PIPST 102
6	PIPST 13
Optimum Height (h) (m)	4.5
Max. Displacement (mm)	4.3
Max. Strength Ratio	0.98
Weight (kg)	5412.4

The optimum dome for this loading case is a little lighter than the precedent one which has 5456.2 kg as optimum weight and is subjected to combination of dead load and equipment load at its crown. The Harmony Search algorithm selects different sections for the groups of 2, 4 and 5 for this case when it is compared with former loading case. The strength constraint is dominant and very close to one as can be seen in the above table. The optimum heights of previous design and this one are same. The elastic critical load factor iterations for optimum designed single layer lamellar dome according to this loading case are presented in Table 5.11.

Table 5.11 Elastic Critical Load Factor Iterations for optimum design of loading case D+P+W (internal pressure coefficient is taken as positive).

Load Factor	0.1	0.2	0.3	0.4	0.5	0.6	0.7	0.8	0.9	1.0
Number of Nonlinear Analysis Iterations	3	2	2	2	2	2	2	2	1	2

5.3.1.2 D + P + W (internal pressure coefficient is taken as negative)

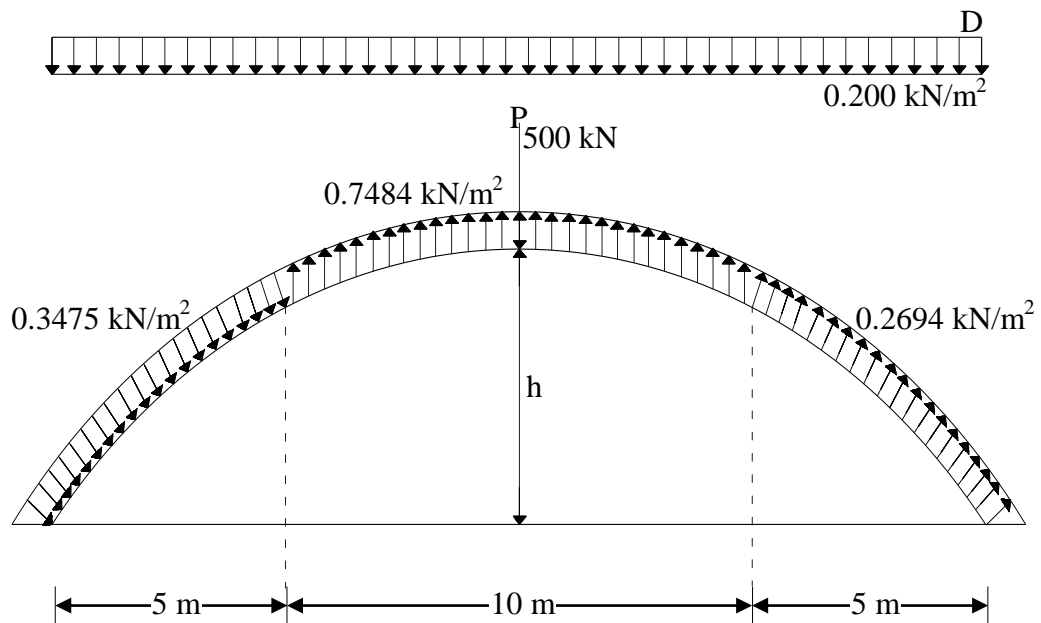


Figure 5.12 Load Case 3.1.2 (Dead Load + Equipment Load + Wind Load (internal pressure coefficient is taken as negative)).

The load combination of dead load, equipment load acting only on crown of the dome, and the wind load (internal pressure coefficient is taken as negative) is shown in Figure 5.12. The loads acting on joints are calculated as;

For windward quarter

$$P = (-0.200 \times 61.42 + (-0.3475 \times \cos (43.17)^\circ \times 82.41)) / (7 \text{ joints })$$

$$= -4.739 \text{ kN / joint } (\downarrow)$$

$$P = ((-0.3475 \times \sin (43.17)^\circ) \times 82.41) / (7 \text{ joints })$$

$$= 2.799 \text{ kN / joint } (\rightarrow)$$

For Center Half

$$P = (-0.200 \times 191.32 + 0.7484 \times 250.984) / (23 \text{ joints}) = -6.503 \text{ kN / joint } (\uparrow)$$

For Leeward Quarter

$$P = (-0.200 \times 61.42 + (0.2694 \times \cos(43.17)^\circ) \times 82.41) / (7 \text{ joints}) \\ = 0.559 \text{ kN / joint } (\uparrow)$$

$$P = ((0.2694 \times \sin(43.17)^\circ) \times 82.41) / (7 \text{ joints}) \\ = 2.169 \text{ kN / joint } (\rightarrow)$$

The results obtained for the optimum design of this loading case is given in Table 5.12.

Table 5.12 Optimum design for dome with 3 rings for D + P + W (internal pressure coefficient is taken as negative).

Group Number	Optimum Section Designations
	3 rings
1	PIPST 152
2	PIPST 203
3	PIPST 76
4	PIPST 76
5	PIPST 102
6	PIPST 13
Optimum Height (h) (m)	3.5
Max. Displacement (mm)	3.53
Max. Strength Ratio	0.98
Weight (kg)	5390.5

According to Table 5.12, the optimum dome under this loading case is lighter than the previous two cases which are D + P and D + P + W (internal pressure coefficient is taken as positive). The strength constraint is dominant and the optimum height of the dome is less than the height of previous two designs 4.5 m. The elastic critical load factor iterations for optimum designed single layer lamellar dome according to this loading case are shown in Table 5.13;

Table 5.13 Elastic Critical Load Factor Iterations for optimum design of loading case D+P+W (internal pressure coefficient is taken as positive).

<i>Load Factor</i>	0.1	0.2	0.3	0.4	0.5	0.6	0.7	0.8	0.9	1.0
<i>Number of Nonlinear Analysis Iterations</i>	6	2	2	2	1	2	7	2	1	2

The elevations of the optimum domes for all load cases are shown in Figures 5.13 - 5.15.

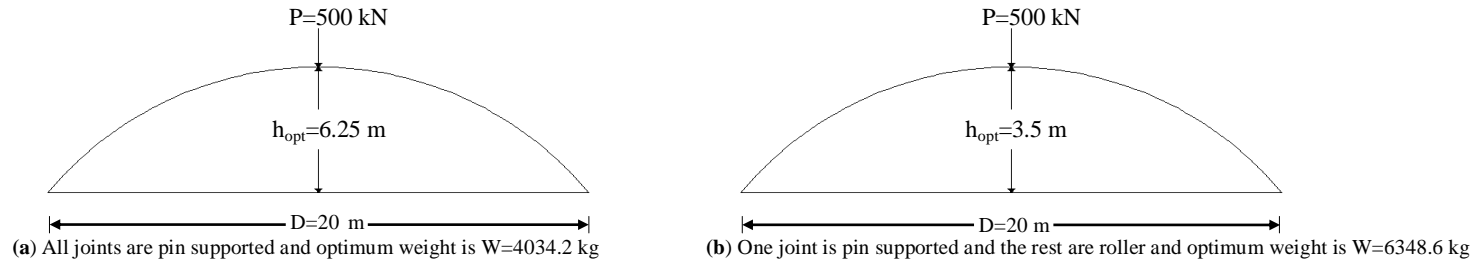


Figure 5.13 (a) and (b) Load Case 1 (P).

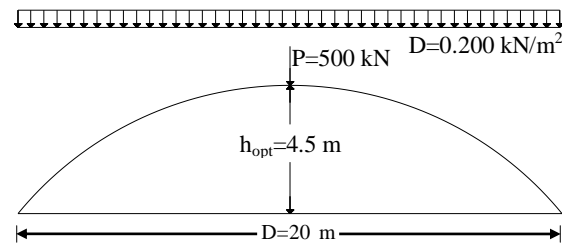


Figure 5.14 Load Case 2 (D+P). All joints are pin supported and optimum weight is $W=5456.2$ kg.

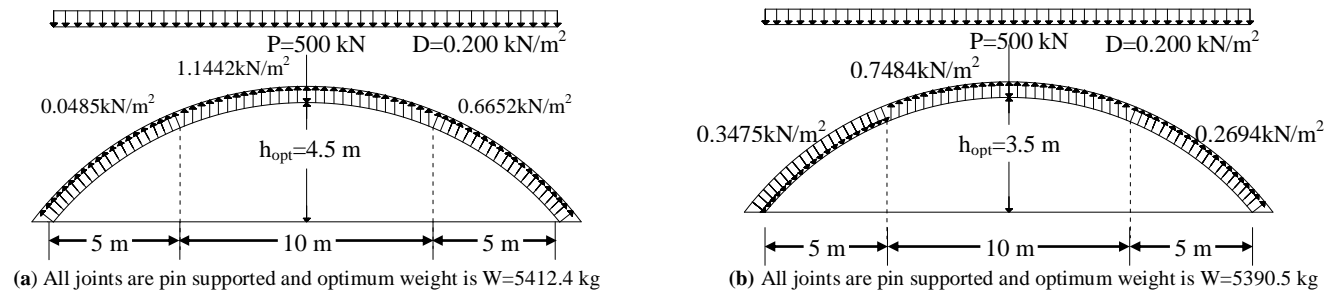


Figure 5.15 (a) Load Case 3 (D+P+W (internal pressure coefficient is taken as positive))
(b) Load Case 3 (D+P+W (internal pressure coefficient is taken as negative))

CHAPTER 6

CONCLUSIONS

In this thesis, the optimum topological design problem of geometrically nonlinear single layer lamella domes is considered. The design problem is formulated such that the total number of rings, the height of the crown, and the steel pipe section designations required for the member groups in the dome are treated as design variables. The design limitations that consist of serviceability and strength constraints are implemented from LRFD-AISC. Furthermore, the geometric nonlinearity of the dome structure is also taken into account and elastic critical load factor analysis is carried out for each candidate dome structure to make sure that the dome does not lose its stability under the external loading. The mathematical model of the programming problem obtained is discrete, complex, and highly nonlinear. The Harmony Search method which is one of the recent addition to stochastic search techniques of numerical optimization is used to obtain the solution of the design problem. It is shown in the design examples considered that the harmony search method can be used in finding the solution of optimum topology problem where the topology, shape and size of members in a structure are taken as design variable. However, three main parameters of the algorithm namely, harmony memory size HMS, harmony memory considering rate HMCR, and the pitch adjustment rate PAR are required to be selected before the harmony search method initiates its search for the optimum solution. It is shown that the appropriate values of these parameters are problem dependent and one set of values which gives good results in one design problem may not lead to a good solution in another problem. It is therefore necessary to carry out a number of runs with

different values of these parameters and determine the suitable ones that yield the lightest structure.

It is shown that the nonlinear displacements of a lamellar dome can be more than 10% of the linear displacements under the same loading. This clearly justifies that consideration of the geometrical nonlinear behavior in the optimum design of such structures is a necessity. This not only provide inclusion of the realistic behavior of these structures, but also results in further reduction in the optimum weight. Support conditions also affect the optimum design of lamellar domes. The optimum weight of the dome with roller type supports becomes 57.4% heavier than the dome where supports are all pinned.

REFERENCES

- [1] Benjamin, B.S. (1962). "*The Analysis of Braced Domes.*" Asia.
- [2] Rao, S.S. (1996). "*Engineering Optimization: Theory and Practice.*" Wiley-Interscience.
- [3] Saraç, Y. (2005). "*Optimum Design of Pin-Jointed 3-D Dome Structures Using Global Optimization Techniques.*" MSc Thesis, METU.
- [4] Arora, J.S. (Editor) (1997). "*Guide to Structural Optimization.*" ASCE.
- [5] Shapiro, J.F. (1979). "*Mathematical programming: structures and algorithms.*" Wiley.
- [6] Venkayya, V. B., Khot, N. S., and Berke, L. (1973). "*Application of Optimality Criteria Approaches to Automated Design of Large Practical Structures.*" Second Symposium Structural Optimization, AGARD-CP-123, Milan, Italy.
- [7] Goldberg, D.E. (1989). "*Genetic Algorithms in search, optimization, and machine learning.*" Addison-Wesley Publishing Company.
- [8] Holland, J.H. (1992). "*Adaption in natural and artificial systems: an introductory analysis with applications to biology, control, and artificial intelligence.*" Cambridge, Mass: MIT Press.
- [9] Rechenberg, I. (1973). "*Evolutionsstrategie, Optimierung technischer Systeme nach Prinzipien der biologischen Evolution.*" Frommann-Holzboog.

- [10] Schwefel, H.P. (1981). *Numerical Optimization of Computer Models.* Wiley.
- [11] Langdon, W.B., and Qureshi, A. (1995). *Genetic Programming-Computer Using "Natural Selection" to Generate Programs.* RN/95/76, <http://www.citeseer.ist.psu.edu/langdon95genetic.html>. Last accessed date April 20th, 2008.
- [12] Schneider, J.J., and Kirkpatrick, S. (2006). *Stochastic Optimization.* Springer.
- [13] Camp, C.V., and Bichon, B.J. (2004). *Design of Space Trusses Using Ant Colony Optimization.* Journal of Structural Engineering, 130, 741-751.
- [14] Glover, F. (1986). *Future Paths For Integer Programming and Links to Artificial Intelligence.* Comp & Oper. Res., 13, 533-549.
- [15] Aguirre-Solis, J.J. (1999). *Tabu Search Algorithm For The Open Shop Scheduling Problem With Sequence Dependent Setup Times.* The Society For Modeling and Simulation International (SCS). <http://www.scs.org/getDoc.cfm?id=2172>. Last accessed date April 16th, 2008.
- [16] Geem, Z.W., Kim, J-H., and Loganathan, G.V. (2001). *A new heuristic optimization algorithm: Harmony Search.* Simulation, 76, 60-80.
- [17] Lee, K.S., and Geem, Z.W. (2004). *A new structural optimization method based on the harmony search algorithm.* Computers and Structures, 82, 781-798.

- [18] Saka, M.P. (1990). “*Optimum Design of Pin-Jointed Steel Structures with Practical Applications.*” Journal of Structural Engineering, ASCE, 116, 10, 2599-2690.
- [19] Saka, M.P., and Ulker, M. (1992). “*Optimum design of geometrically nonlinear space trusses.*” Computer and Structures, 42, 3, 289-299.
- [20] Huyber, P. (1995). “*Super-Elliptic Geometry as a Design Tool for the Optimization of Dome Structures.*” Structural Systems and Industrial Applications, 387-399.
- [21] Saka, M.P., and Kameshki, E.S. (1998). “*Optimum design of nonlinear elastic framed domes.*” Advances in Engineering Software, 29, 7-9, 519-528.
- [22] Erbatur, F., Hasançebi, O., Tütüncü, İ., and Kılıç, H. (2000). “*Optimal design of planar and space structures with genetic algorithms.*” Computers and Structures, 75, 209-224.
- [23] Lin, S.P., and Albemani, F. (2001). “*Lattice-Dome Using a Knowledge-Based System Approach.*” Computer-Aided and Infrastructure Engineering, 16, 268-286.
- [24] Ulker, M., and Hayalioğlu, M.S. (2001). “*Optimum design of Space Trusses with Buckling Constraints by means of Spreadsheets.*” Turk J. Engin. Environ. Sci., 25, 355-367, TUBITAK.
- [25] Missoum, S., Gürdal, Z., and Gu, W. (2002). “*Optimization of nonlinear trusses using a displacement-based approach.*” Struct. Multidisc. Optim., 23, 214-221.

- [26] Khot, N.S., and Kamat, M.P. (1985). “*Minimum weight design of truss structures with geometric nonlinear behavior.*” AIAA Journal, 23, 139-144.
- [27] Yuan, X.F., and Dong, S.L. (2002). “*Nonlinear analysis and optimum design of cable domes.*” Engineering Structures, 24, 965-977.
- [28] Rajasekaran, S., Mohan, V.S., and Khamis, O. (2004). “*The optimisation of space trusses using evolution strategies with functional networks.*” Engineering with Computers, 20, 75-87.
- [29] Lingyun, W., Mei, Z., Guangming, W. and Gang, M. (2005). “*Truss optimization on shape and sizing with frequency constraints based on genetic algorithm.*” Comput. Mech., 35, 361-368.
- [30] Kitipornchai, S., Kan, W., Lam, H-F., and Albermani, F. (2005). “*Factors affecting the design and construction of Lamella suspen-dome systems.*” Journal of Constructional Steel Research, 61, 764-785.
- [31] Toğan, V., and Daloğlu, A.T. (2006). “*Optimization of 3D trusses with adaptive approach in genetic algorithms.*” Engineering Structures, 28, 1019-1027.
- [32] López, A., Puente, I., and Serna, M.A. (2007). “*Numerical model and experimental tests on single-layer latticed domes with semi-rigid joints.*” Computers and Structures, 85, 360-374.
- [33] Kameshki, E.S., and Saka, M.P. (2007). “*Optimum geometry design of nonlinear braced domes using genetic algorithm.*” Computers and Structures, 85, 71-79.

- [34] Saka, M.P. (2007). “*Optimum topological design of geometrically nonlinear single layer latticed domes using coupled genetic algorithm.*” Computers and Structures, 85, 21-22, 1635-1646.
- [35] Coates, R.C., Coutie, M.G., and Kong, F.K. (1972). “*Structural Analysis*” Nelson.
- [36] Ekhande, S.G.i Selvappalam, M., and Madugula, K.S. (1989). “*Stability Functions for Three-Dimensional Beam-Columns.*” Journal of Structural Engineering, 115, 2, 467-479.
- [37] Saka, M.P. (2007). “*Optimum Geometry Design of Geodesic Domes Using Harmony Search Algorithm.*” Advances in Structural Engineering, 10, 6, 595-606.
- [38] Manual of Steel Construction. (1991). “*LRFD, Volume 1, Structural Members, Specifications & Codes.*” American Institute of Steel Construction Inc.
- [39] Galambos, T.V, Lin, F.J., and Johnston, B.G. (1996). “*Basic Steel Design with LRFD.*” Prentice Hall.
- [40] Lee, K.S., Geem, Z.W. (2005). “*A new meta-heuristic algorithm for continuous engineering optimization: harmony search theory and practice.*” Computer methods in applied mechanics and engineering, 194, 3902-3933.